CHEMICAL VAPOUR TRANSPORT REACTIONS OF III - V COMPOUND SEMICONDUCTORS

A thesis submitted for the degree of

Doctor of Philosophy of the

University of London

by

Eleanor Joan Tarbox

Royal Holloway College,
Egham Hill,
Egham,
Surrey.

November 1977

ABSTRACT

Chemical vapour transport reactions of III-V compound semiconductors

Eleanor Joan Tarbox

The chemical vapour transport reactions of some Group III-V semiconductors with hydrogen halides have been studied by a modified entrainment method.

Enthalpies and entropies for the transport reactions in the systems: indium arsenide-hydrogen bromide, indium arsenide-hydrogen chloride and gallium arsenide-hydrogen bromide were calculated. The effect of surface kinetics on the rate of transport of gallium arsenide by hydrogen bromide gas was investigated.

Binary diffusion coefficients for hydrogen bromide and hydrogen chloride gases in hydrogen have been obtained by a study of the transport of indium in hydrogen bromide or hydrogen chloride under limiting equilibrium conditions. Using literature results for the temperature dependence of the vapour pressure of zinc, the binary diffusion coefficients of zinc atoms in helium and in argon over the temperature range 850 - 1120 K were determined. A modified entrainment method apparatus was used to monitor the evaporation of zinc in the inert gas.

ACKNOWLEDGEMENTS

The work recorded in this thesis was carried out under the supervision of Dr. A. Finch, to whom the author wishes to express her gratitude for guidance and encouragement. Sincere thanks are also due to Dr. P.J. Gardner for numerous valuable discussions.

The author also wishes to thank Dr. M.M. Faktor and his colleagues at the Post Office Research Department for their help during the tenure of this Science Research Council C.A.S.E. award.

'Science does not claim infallibility, nor does it provide ready-made solutions for all and every problem. The scientific attitude is to solve problems, and if unsuccessful, to start anew, always guided by a hypothesis and corrected by experiment.'

Professor E.H. Hutten in 'The Language of Modern Physics', 1956.

CONTENTS

Chapter 1

Introduction

Chapter 1

1.1 Introduction

Reactions between Group III-V compounds and the hydrogen halides find extensive use in the electronics industry for the deposition of thin layers of these semiconductors by chemical vapour transport.[1]

In recent years there has been an increasing interest in the vapour-phase epitaxy of semiconducting compounds[2] for the manufacture of semiconductor lasers used in optical communications systems.[3] The high frequency of optical waves (compared with electrical signals) makes them potential information carriers of extremely large bandwidth. Rapid progress is being made in production techniques for silica fibres[4] suitable for optical transmission in the 800 - 900 nm range in conjunction with semiconductor devices.

The simplest chemical vapour transport system[5] may be described by the reaction:

Solid + volatile transporting agent $\rightleftharpoons$ volatile product.

Crystal growth from the gas phase proceeds when the following reaction takes place:

Gas (disordered) $\longrightarrow$ Crystal (ordered).

all the constituents of the solid phase must be present in the gas phase. There are two main types of gas phase growth:
(a) where the constituents are volatile at the temperature of the experiment (e.g. growth of CdS) and (b) where the constituents are reacted with a third species in order to produce volatile species (e.g. growth of GaAs) - chemical vapour transport.

Indium based semiconductive compounds (InAs, InP, $In_x Ga_{1-x} P$) are becoming more important because of the recent demand for optical sources in the longer wavelength region. These electronic devices are made by means of crystal growth via chemical vapour transport reactions.

This thesis describes the investigation of several crystal growth systems and, in addition, examines the kinetics of surface processes in one of them.

In chapter 2 the experimental methods and apparatus[6] are discussed. The evaporation of water in nitrogen[7] is studied by the modified entrainment method as a validation experiment; the zinc-inert gas system is then described. When the vapour pressure of a substance is well known, its binary diffusion coefficient may be found by examining its rate of evaporation, in the modified entrainment apparatus, into an inert carrier gas. Here, the diffusion coefficients of zinc in argon and zinc in helium were calculated by this method over the temperature range 850 - 1120 K.

One of the factors which determine the rate of transport of a solid material is the rate of diffusion of the reactive species in the carrier gas. In chapter 3, the use of a chemical transport reaction to study the diffusion of hydrogen chloride and hydrogen bromide in a multicomponent gas, consisting largely of hydrogen[8], is described. From experimental transport rates, the binary diffusion coefficient of each hydrogen halide in hydrogen is obtained. Hence it is possible to calculate effective diffusion coefficients for multi-component gas mixtures used in chemical vapour transport experiments (see section 1.4).

The investigation of the reaction of indium arsenide with hydrogen chloride gas and hydrogen bromide gas is described in chapter 4. Thermodynamic parameters are calculated for the transport reactions and compared with literature values for the predicted species present.

In the modified entrainment method,[9] the condensed phase sample is contained in a silica reaction bottle which has a capillary outlet (typically 20 mm long and 2 mm diameter). This bottle is suspended in a furnace from a recording microbalance, so that changes in sample weight are recorded continuously. A stream of carrier gas or gaseous reactants flows downwards through the furnace tube and communicates with the sample through the capillary channel. The reactants and products pass through the channel by a combination of diffusion and Stephan flow (see section 1.4). The measured rate of weight loss of the sample may be related to the partial pressures inside the bottle. The theoretical model (section 1.4) that has been employed to calculate the partial pressures of the vapour species assumes that equilibrium conditions exist in the reaction bottle between the solid and gas phases. If surface kinetics determine the rate of transport, rather than the transport of the reactants through the gas phase, then the rate of weight loss of the solid will be reduced. In chapter 5 the gallium arsenide-hydrogen bromide system is examined in this context.

The experimental method described in this thesis provides direct and quantitative information about transport rates. Even if a satisfactory thermodynamic analysis of the likely participating transport reactions is not obtained, the results still enable the

crystal grower to find the optimum conditions for growth or to discard the system as unsuitable. In chapter 6 a brief study of the indium antimonide-hydrogen chloride system is reported.

1.2 Review

There are many methods currently used for the vapour deposition of Group III-V compounds:- evaporation techniques, sputtering, closed tube and open flow methods.[10]

Vapour phase growth is by far the most widely-used technique for semiconductor compounds.[2] Vapour phase epitaxy consists of oriented crystal growth of the material, which has been transported from the gas phase, onto a suitable solid substrate and offers control over thickness and crystalline perfection of the epitaxial layers produced.[11]

Tietjen and Enstrom,[12] in their review of vapour phase growth, describe an open-flow method in which a time-of-flight mass spectrometer[13] coupled to the crystal growth apparatus enabled the chemistry of the vapour phase to be studied.

Many articles have been written on the transport of gallium arsenide in hydrogen chloride and hydrogen bromide gases.[14,15,16,18,19] A review of some thermodynamic analyses and an interpretation of the kinetics of the GaAs/HCl system is given by Shaw.[17]

Less literature has been published on the indium arsenide/hydrogen halide systems. Mizino et al[20] have grown epitaxial layers of InAs on InAs substrates using the reaction of $AsCl_3$ with indium or polycrystalline InAs in a hydrogen stream. They discuss the

thermodynamic and kinetic limitations to the growth rate. The thermodynamics of the growth of indium arsenide in a bromide system was studied by Sandulova[21] by a static tensimetric method. Mullin and Hurle[22] have predicted the conditions for thermodynamic equilibrium in various ternary systems using established thermodynamic data but draw attention to the need for more accurate thermodynamic results.

Diffusion coefficients of binary mixtures of dilute gases are comprehensively compiled in a recent review by Marrero and Mason,[23] however there is no reference to hydrogen halides diffusing in hydrogen. Nesmeyanov[24] describes methods for measuring vapour pressures and gives values for the vapour pressure of various elements as a function of temperature.

1.3 Methods of obtaining thermodynamic data

The modified entrainment method used in this thesis overcomes the limitations of the Knudsen and Langmuir techniques[6] and is suitable for studying reaction equilibria involving gases as well as for measuring vapour or dissociation pressures.

The Knudsen method relies on the measurement of the rate of effusion of a vapour through a small orifice (of infinite thickness), from a container where the vapour is at its saturation pressure.

Langmuir experiments are carried out in vacuo, the rate of weight loss of the solid sample being monitored as a function of temperature.

In the M.E.M. the region over which diffusion occurs is limited to a channel of known geometry and rate of weight loss is independent of the rate of flow of the carrier gas.

1.4 Theory

1.4.1 Simple theoretical description of the modified entrainment method

The theory of the modified entrainment method has been presented fully [7,18]; here a short summary will be given.

A one-dimensional model (fig. 1.1) may be used to describe gas transport in the channel through which vapour in the bulb of the sample bottle communicates with the external gas stream. At $x = 0$ it is assumed that the vapour composition is the same as that over the surface of the condensed phase and at $x = 1$ the composition of the vapour in the channel is nearly identical to that in the external gas stream. These two approximations are valid because, in this case, the bulb diameter is large compared with the channel diameter and the gas flow rate is sufficiently large to sweep away local concentrations of vapour. The effect on $\dot{w}$ of varying flow rate has been studied.[7]

Consider first the evaporation of a single species A in a stream of inert gas Z. The increase in molar volume, on evaporation of species A, generates a Stefan flow in the channel which sweeps both species upwards. Diffusion fluxes are caused by the partial pressure gradients of A and Z and a zero nett flow of species Z results. The flow equations may be written in the following form[7] (assuming that the total pressure along the channel is essentially constant):

$$J_A = \frac{Up_A}{RT} - \frac{D}{RT}\frac{dp_A}{dx} = \frac{\dot{w}}{M_A c} \qquad (1.1)$$

$$J_Z = \frac{Up_Z}{RT} - \frac{D}{RT}\frac{dp_Z}{dx} = 0 \qquad (1.2)$$

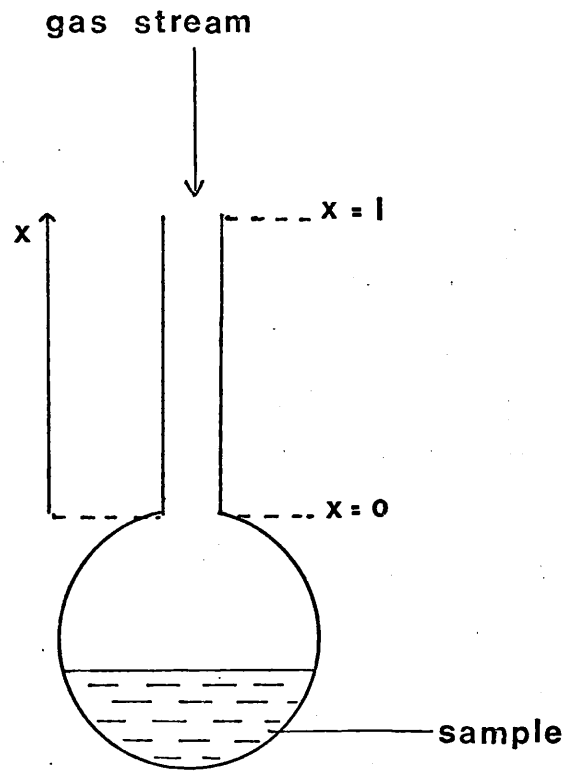

FIG. 1.1 Reaction bottle.

where D is the binary diffusion coefficient, U is the Stefan velocity, $\dot{w}$ is the measured rate of weight loss, M_A the molecular mass of species A in the vapour and c the cross-sectional area of the channel.

Addition of equations (1.1) and (1.2) causes the diffusion terms to cancel:

$$J_A = \frac{UP}{RT} \qquad (1.3)$$

where P is the total pressure. Substituting equation (1.3) into equation (1.1) to eliminate U, and integrating from x = 0 to x = l. (At x = l, $p_A = 0$; at x = 0, $p_A = p_A^o$ the saturated vapour pressure of species A.) Hence:

$$p_A^o = P[1 - e^{-\xi}] \qquad (1.4)$$

where $\xi = \frac{J_A RTl}{DP} = \frac{\dot{w}RTl}{DM_A Pc}$ is the 'transport function'.

For small rates of weight loss, the exponential in equation (1.4) may be approximated to obtain:

$$p_A^o \simeq \dot{w}RTl/DM_A c \qquad (1.5)$$

It may be assumed that T/D is a constant provided that measurements of weight loss are taken over a restricted temperature range (for example in the evaporation of water in nitrogen experiment). In this case a plot of $Rln\dot{w}$ vs. 1/T has a slope of $-\Delta H_{vap}$ and an intercept at 1/T = 0 of $\Delta S_{vap} - Rln(RTl/DM_A c)$, since:

$$Rlnp_A^o = -\Delta H_{vap}/T + \Delta S_{vap}$$

where ΔH_{vap} and ΔS_{vap} are the enthalpy and entropy changes of evaporation of substance A.

It becomes necessary, however, to correct for the temperature dependence of the diffusion coefficient when measurements are made over a wide temperature range.

Expression (1.6) holds,

$$D = \frac{D_o P_o}{P} \left(T/T_o\right)^{1+s} \qquad (1.6)$$

where D_o is the value of D at a reference temperature T_o and pressure P_o (usually 1 atmosphere) and s lies between 0.5 and 1.0 (frequently near 0.8).

Hence, for small rates of weight loss, a plot of $R\ln(\dot{w}/T^s)$ vs. $1/T$ has a slope of $-\Delta H_{vap}$ and an intercept at $1/T = 0$ of $\Delta S_{vap} - R\ln\left[\frac{1RPT_O^{1+s}}{D_O M_A^c}\right]$.

This method can be used to calculate values for the enthalpy and entropy changes of evaporation (see Chapter 2) and gives results that are independent of the rate of flow of the external gas stream. Results obtained in this way are often slightly uncertain because of the lack of data on diffusion coefficients and their variation with temperature.

A simple heterogeneous reaction is now considered:

$$In(c) + HX(g) \leftrightarrows InX(g) + \tfrac{1}{2}H_2(g) \qquad (1.7)$$

where X is a halogen. The equilibrium constant for reaction (1.7) can be expressed as a ratio of equilibrium vapour pressures:

$$K_p = \frac{p^oInX(p^oH_2)^{0.5}}{p^oHX} \qquad (1.8)$$

The same arguments may be used here as for the evaporation of a single species in an inert gas. Assuming that $p^1_{InX} = 0$ and $\xi_{InX} \leqslant 1$ due to the sweeping effect of the gas stream, the following equations result:

$$p^{o}_{InX} \simeq 2\ \xi_{InX} P \tag{1.9}$$

$$p^{o}_{HX} \simeq P(\varepsilon - 2\ \xi_{HX}) \tag{1.10}$$

$$p^{o}_{H_2} = P - p^{o}_{InX} - p^{o}_{HX} \tag{1.11}$$

where ξ_i is the transport function for species i, defined as in (1.12):

$$\xi_i = \frac{\dot{w} RT l}{2 D_{i/m} P M_c} \tag{1.12}$$

(M is the atomic weight of indium and $D_{i/m}$ the effective diffusion coefficient of species i in the multicomponent gas mixture).

The fraction of reactive species in the free stream is defined as:

$$\frac{p^{l}_{HX}}{P} = \varepsilon \tag{1.13}$$

If $\varepsilon \ll 1$ and $\xi \simeq \varepsilon$ (for the In/HBr system: T = 1068 K, $\varepsilon = 0.05$ and $\xi = 0.02$) then equation (1.8) may be simplified:

$$K_p \simeq 2 \xi_{InX} \sqrt{P} / (\varepsilon - 2 \xi_{HX}) \tag{1.14}$$

In the experiments described in chapter 3 the reactions are found to have gone to completion, K_p is large and so from (1.14) $\xi_{HX} \simeq \varepsilon / 2$. From equation (1.12) the diffusion coefficient of the reactant HX in the gas mixture is simply:

$$D_{HX/H_2} = \dot{w} RT l / PM \varepsilon c \tag{1.15}$$

The rate of weight loss is limited by the rate of diffusion of HX down the channel of the sample bottle (p^{o}_{HX} is effectively zero).

To allow for the temperature dependence of D, equation (1.16) must be included in this analysis

$$D(T) = D_o(T/273.15)^{1+s} \qquad (1.16)$$

(ignoring in this equation the pressure dependence of D) where D_o is a constant (the diffusion coefficient at 273.15 K) and s is approximately 0.8.

At very low values of ε the gas mixture is sufficiently dilute for the following to be true:

$$D_{HCl/m} \simeq D_{HCl/H_2}$$

However, at our experimental values of ε (0.05) this approximation fails by a factor of about 2. A second order approximation[8] to multicomponent diffusion shows that:

$$D_{HCl/H_2} = (1 + a_{HCl}\varepsilon + b_{HCl}\xi_{HCl})D_{HCl/m}$$

$$= \gamma D_{HCl/m} \qquad (1.17)$$

$$\text{where } a_{HCl} = \frac{D_{HCl/H_2}}{D_{HCl/InCl}} - \tfrac{1}{2} \qquad (1.18)$$

$$\text{and } b_{HCl} = \left[\frac{D_{HCl/H_2}}{D_{HCl/InCl}} - 1\right]\left[\frac{D_{H_2/HCl}}{D_{H_2/InCl}} - 1\right] - \tfrac{1}{2} \qquad (1.19)$$

(Similarly for HBr)

The coefficients a_{HX} and b_{HX} can either be estimated using Graham's Law[25]:

$$D_{i/j}/D_{i/k} = (M_k/M_j)^{0.5} \qquad (1.20)$$

or they may be found by experiment (see chapter 3).

Also, $p^{(o)}_{HX}/p = \varepsilon - 2\gamma_{HX}\,\xi_{HX}$. When $K_p \gg 1$, then $p^{o}_{HX} \simeq 0$ so:

$$\varepsilon \simeq 2\,\gamma_{HX}\,\xi_{HX}$$

Equation (1.15) now becomes:

$$D_{HX/H_2} = \frac{\dot{w}RTl}{PMc}\left[\frac{b_{HX}}{-(1+a_{HX}\varepsilon) + \sqrt{(1+a_{HX}\varepsilon)^2 + 2b_{HX}\varepsilon}}\right] \qquad (1.21)$$

A general expression for the equilibrium constant in a system with one dominant reaction has been derived[7]:-

$$K_p = \xi / (\varepsilon - \xi) \qquad (1.22)$$

where $\varepsilon = p_{HX}/P$ and ξ, the transport function, is given by:

$$\xi = \frac{\dot{w}RTl}{MPcD}$$

$\varepsilon \ll 1$ and $\xi \simeq \varepsilon$.

$$\text{Thus} \quad \dot{w} = \frac{MPcD}{RTl}\,(Kp\ \varepsilon\ /(1 + Kp)) \qquad (1.23)$$

At high temperatures K_p becomes large (for $\Delta H^{o} > 0$) and $\dot{w}$ is limited by D_{HX/H_2}. This phenomenon is observed in the transport experiments described in chapters 4 and 5.

1.4.2. Kinetics of heterogeneous reactions

In the previous section it has been assumed that equilibrium conditions exist inside the silica reaction bottle. This assumption is valid if: (a) the channel is sufficiently resistive or (b) the sample area is sufficiently large to compensate quickly for the weight lost. If these constraints are relaxed then the partial pressures are determined by surface kinetics.

A brief outline of the theory[26] will be given here; in Chapter 5 its application to CVT results is discussed.

In the sublimation of a solid M, the rate of weight loss from a bottle having an oversized channel is given by:

$$\frac{\dot{w}^*}{M_M} = k_f A - k_r A P_M^* \qquad (1.24)$$

where A is the sample area, M_M is the molecular weight of M, k_f and k_r are simple rate constants, $\dot{w}^*$ is the rate of weight loss under non-equilibrium conditions and P_M^* is the non-equilibrium, steady state, partial pressure of M in the capsule.

Using the theory from the previous section and assuming that $k_r = k_f$ then:

$$\left(\frac{DPc}{RTl}\right) \frac{1}{k_r A P_M^o} \ln\left(\frac{P}{P-P_M^*}\right) = 1 - \frac{P_M^*}{P_M^o} \qquad (1.25)$$

where P_M^o is the equilibrium partial pressure of M in the capsule and $1-(P_M^*/P_M^o)$ represents the extent of the departure from equilibrium.

A condensation coefficient,[27] α_L, may be defined as the fraction of molecules striking the surface which condense onto it and $Z\alpha_L$ may be substituted for k_r in equation (1.25)

$$k_r = Z\alpha_L \qquad (1.26)$$

where $Z = \dfrac{1}{(2\pi MRT)^{\frac{1}{2}}}$

The value of (P_M^*/P_M^o) will decrease with increasing cross-sectional area of the channel or decreasing sample surface area, A, or on decreasing the value of α_L.

Considering the reaction:

$$M(c) + HX(g) \quad \leftrightharpoons \quad MX(g) + \tfrac{1}{2}H_2(g)$$

The forward and reverse rates may be described by the following expressions, if the reaction proceeds by a single path:

$$J_f = k_f \, p_{MX}^{x} \; p_{H_2}^{y/2} \; p_{HX}^{z} \tag{1.27}$$

$$J_r = k_r \, p_{MX}^{x+1} \; p_{H_2}^{(y+1)/2} \; p_{HX}^{z-1} \tag{1.28}$$

At equilibrium $J_f = J_r$ so

$$K = k_f/k_r = p_{MX} p_{H_2}^{\frac{1}{2}} \; p_{HX}^{-1} \tag{1.29}$$

If the reaction is hindered by the absorption of HX then $x = -1$, $y = 1$ and $z = 0$. So J_f and J_r are given by:

$$J_f = \frac{k_f \sqrt{p_{H_2}}}{p_{MX}} \quad , \quad J_r = \frac{k_r p_{H_2}}{p_{HX}}$$

and $$K \simeq \frac{2 \xi^* \sqrt{P}}{\varepsilon} \quad \left(1 - \frac{2c(\xi^*)^2 P}{k_f \varepsilon \sqrt{P}}\right)$$

$$= \frac{2 \xi^* \sqrt{P}}{\varepsilon} \quad \left(1 - \frac{2 \xi^* \sqrt{P}}{\varepsilon} \; \frac{\xi^* c}{k_f}\right)$$

Hence $$K = K^* \left(1 - \frac{K^* J}{k_f}\right) \tag{1.30}$$

The correction term K^*J/k_f is only important if J approaches k_f/K^* (and here $K^* \ll \sqrt{P}$).

1.5 References

1. M.M. Faktor, I. Garrett, 'Crystal Growth from the vapour', Chapman and Hall, London.

2. B.E. Barry, Thin Solid Films, 39, 35 (1976).

3. 'Optical Fibre Technology', editor D. Gloge, IEEE Press, New York.

4. P.W. Black, Electrical Communication, 51(1), 4(1976).

5. H. Schafer, 'Chemical Transport Reactions', Academic Press, New York and London (1964).

6. R.H. Moss, Ph.D. Thesis,University of London (1975).

7. D. Battat, M.M. Faktor, I. Garrett, R.H. Moss, J. Chem. Soc. Faraday Trans. I, 70, 2267 (1974).

8. D. Battat, M.M. Faktor, I. Garrett, R.H. Moss, J. Chem. Soc. Faraday Trans. I, 70, 2293 (1974).

9. M.M. Faktor, I. Garrett, J. Crystal Growth, 38, 213 (1977).

10. 'Crystal Growth Theory and Techniques', 1, editor C.H.L. Goodman Plenum Press (1974).

11. A. Resiman, T.O. Sedgwick, Phase Diagrams, 4, 1 (1976).

12. J.J. Tietjen, R.E. Enstrom, Solid State Technol., 15 (10), 42 (1972).

13. V.S. Ban, J. Crystal Growth, 17, 19 (1972).

14. D.J. Kirwan, J. Electrochem. Soc., 117(12), 1572 (1970).

15. A. Boucher, L. Hollan, 117(7), 932 (1970).

16. G. Bougnot et al., Mat. Res. Bull., 6,137 (1971).

17. D.W. Shaw, J. Crystal Growth, 31, 130 (1975).

18. D. Battat, M.M. Faktor, I. Garrett, R.H. Moss, J. Chem. Soc. Faraday Trans. I, 70, 2302 (1974).

19. M.M. Faktor, I. Garrett, M. Lyons, R.H. Moss, J. Chem. Soc. Faraday Trans. I, 73, 1446 (1977).

20. O. Mizuno, H. Wantanabe, D. Shinoda, Jap. J. Appl. Phys., 14(2), 184 (1975).

21. A.V. Sandulova et al., Russ. J. Phys. Chem., 47(3), 429 (1973).

22. J.B. Mullin, D.T.J. Hurle, J. Luminescence, 7, 176 (1973).

23. T.R. Marrero, E.A. Mason, J. Chem. Phys. Ref. Data, 1(1), 3(1972).

24. A.N. Nesmeyanov, 'Vapour Pressure of the Chemical Elements', Elsevier Publ. Co. Ltd. (1963).

25. T. Graham, Phil. Trans. Roy. Soc., 136, 573 (1846).

26. M.M. Faktor, I. Garrett, M.H. Lyons, R.H. Moss, unpublished work.

27. G.M. Rosenblatt, J. Chem. Phys., 64(10), 3942 (1976).

Chapter 2

Evaporation of water in nitrogen and evaporation of zinc in helium ard argon experiments

Chapter 2

2.1 Introduction

The modified entrainment method has been used to study heterogeneous equilibria in various systems.[1,2] The method was first validated[3] by comparing vapour pressure measurements on water and lead with previously reported data.

The evaporation of water and zinc experiments described in this chapter were designed to test the apparatus over two temperature ranges, 300–323K and 850–1120K respectively. The experimental results were correlated with well-established literature data.[4,5,6]

2.2 Experimental system

The experimental system has been described previously.[3,7,8] A general diagram of the apparatus is given in figure 2.1.

The solid or liquid sample to be transported was placed in a light-weight reaction bottle over which the transporting gas flowed. A stoppered pyrex bottle (fig. 2.2) was used for the experiments with water but later investigations were carried out using a stopperless silica bottle (fig. 2.3). The dimensions of the capillary on top of the bottle were measured accurately with a travelling microscope and a correction applied for the opening out of the channel into the bottle (Appendix 1).

The bottle containing the sample was suspended from loop A (maximum pan capacity 1.0 g), or loop B (maximum pan capacity 2.5 g) of a Cahn R G electrobalance by means of a long silica fibre. The changing weight of the sample, under isothermal conditions, was plotted on a chart recorder (Bryans 28000).

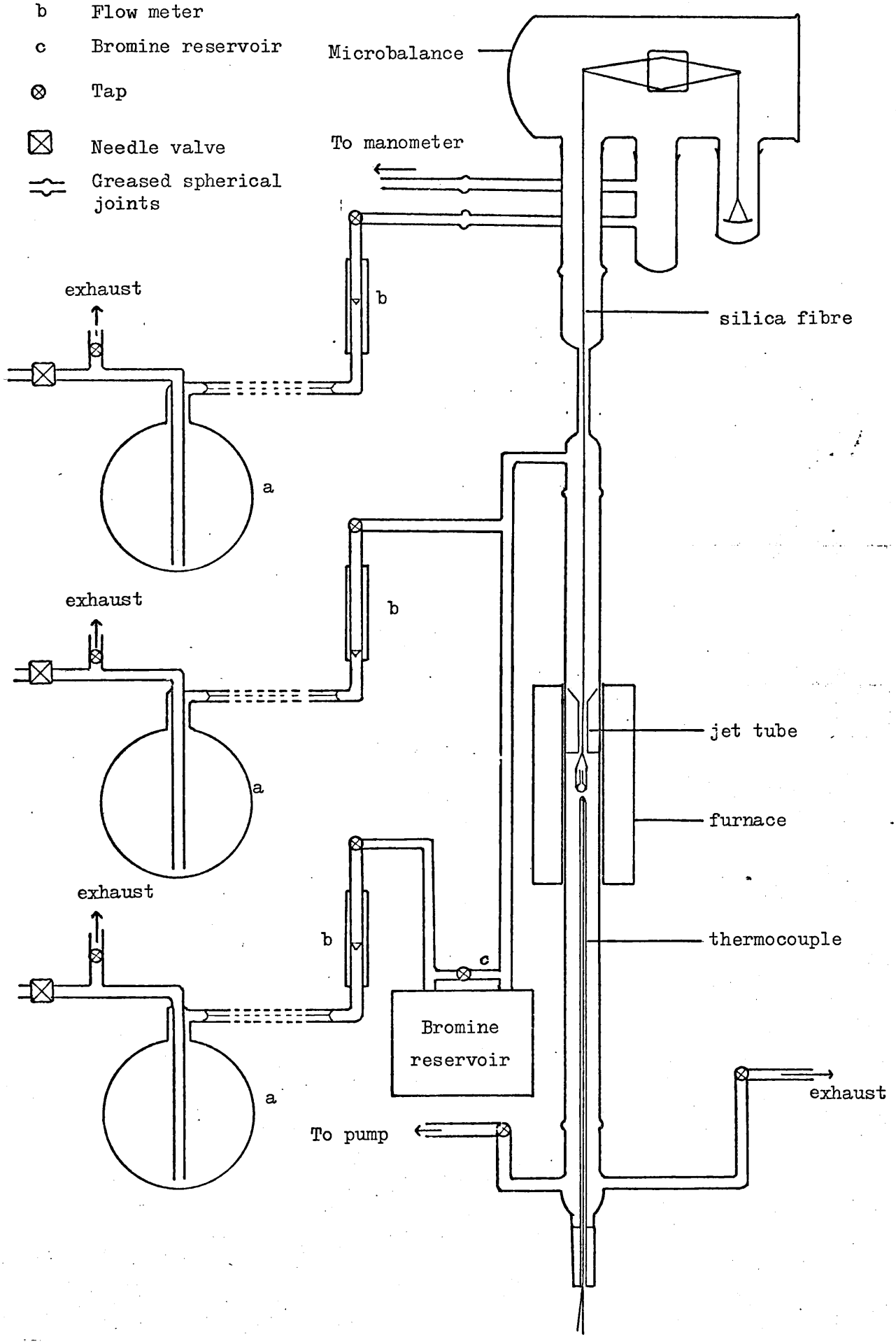

FIG. 2.1 Experimental system

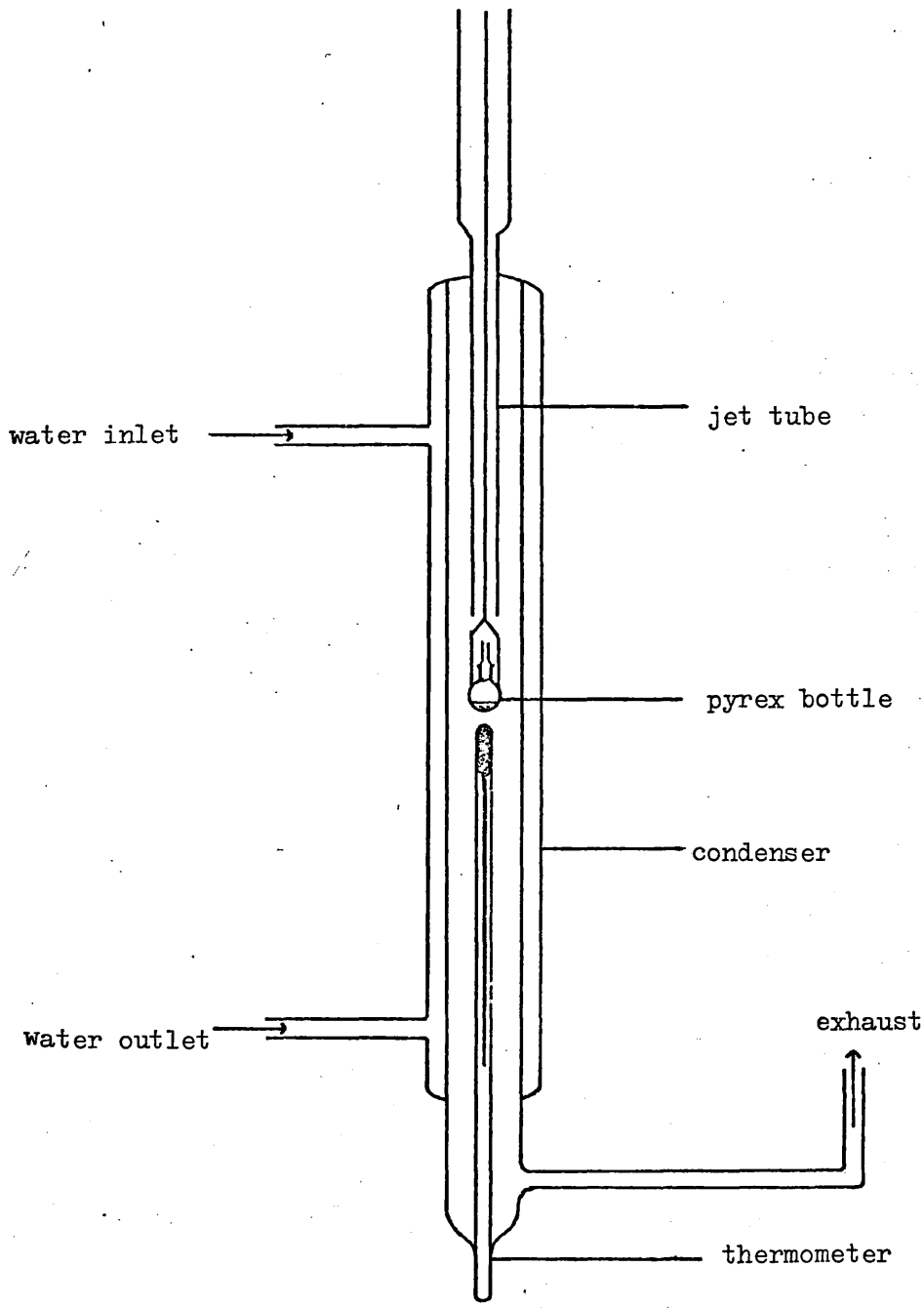

FIG. 2.2 Diagram of the stoppered pyrex bottle and the condenser used for the evaporation of water in nitrogen experiments

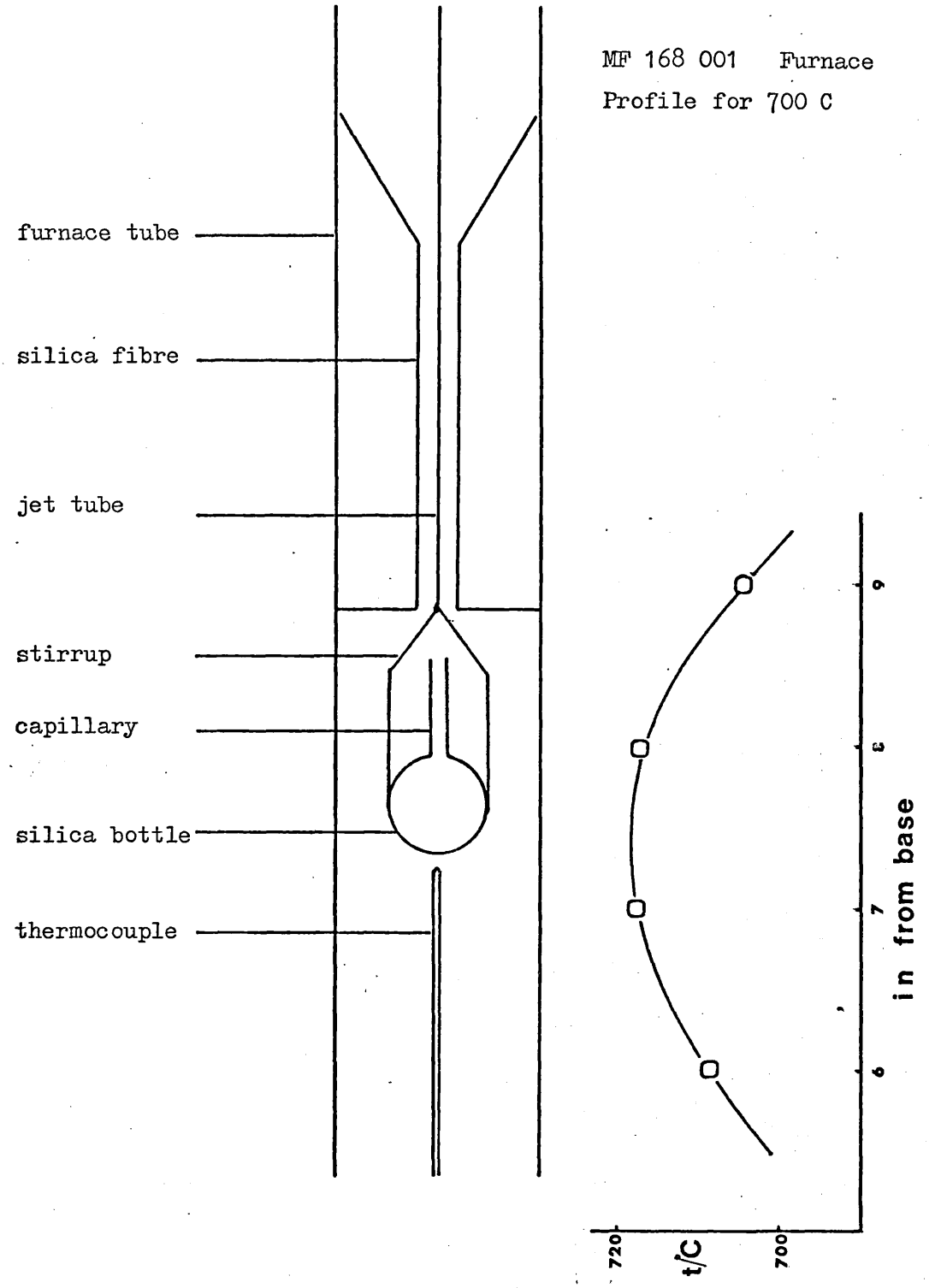

FIG. 2.3 Scale diagram of silica bottle and furnace tube for high temperature experiments, including a furnace profile.

Gases were dried by passing through cylinders packed with molecular sieves: B.D.H. type 4A, 1/16" pellets; or for acidic gases, Union Carbide AW 300 1/16. Hydrogen was purified with a palladium diffuser unit (Johnson Matthey and Co. Ltd., model H28/1). Gas flows were controlled by Mechanism metering valves (Negretti and Zambra Ltd., type BS-LMV-L-V-4) and a monel, twin needle valve (Nupro, type M-4MGD-TFE) for hydrogen chloride gas. Flow rates were measured with Meterate RS1 flow meters fitted with ruby floats. The function of the upper gas inlet was to keep the balance in a non-corrosive atmosphere, while reactive gases were introduced via a lower inlet below a constriction. Typical pressures in the system were 3 to 5 torr in excess of atmospheric pressure.

The sample could be heated in either of two ranges: (i) 0-50°C using a water-jacketted tube connected to a cooler circulator unit (Grant LC10), or (ii) 300-1100°C with a two zone, 825 watt, 100 volt, 12 inch tube furnace (Severn Science Ltd.). The temperature of the reaction bottle was measured with a mercury-in-glass thermometer, for the lower range, the bulb of the thermometer being positioned close to the bottle (fig. 2.2). For higher temperatures, a Pt/Pt - 13% Rh thermocouple, sheathed in thin-walled silica tube was placed 2 to 3 mm below the bottle. The potential difference across the thermocouple was monitored using a digital panel meter displaying mV output to two decimal places. A cold junction correction having been applied, temperatures in Kelvin were determined from N.B.S. reference tables. The thermocouple wire supplied by Johnson Matthey Metals Ltd., produces an e.m.f. that will not deviate from the standard table by more than the equivalent of 1°C at the Gold Point. Both the sample and the

thermocouple bead were situated within the plateau of the furnace profile for that temperature (see fig. 2.3).

It has been shown[3] that the gas velocity may be increased, with a subsequent reduction of turbulence, by the introduction of a jet-tube above the bottle (fig. 2.3). The rate of weight loss due to evaporation was also shown to be independent of the flow rate except at very low values.[3]

Before commencing an experiment, the apparatus was always evacuated (typically to 5×10^{-2} torr) and flushed several times with the carrier-gas to be used. In the case of hydrogen, it was then thoroughly tested for leaks with a gas leak detector (Gow-mac Instrument Company, model 21-212).

2.3 Evaporation of water

2.3.1 Experimental

The sample, deionised distilled water, was contained in a pyrex bottle (fig. 2.2) weighing 1.26 g and the balance calibrated for operation using loop B. The inert gas for this experiment was nitrogen (BOC oxygen free, 99.9% minimum purity) the flow rate being typically $(1.25 \pm 0.03) \times 10^{-3}$ $dm^3 s^{-1}$, except for the seven results at 320.75K where the flow rate was varied from $(0.3$ to $2.3) \times 10^{-3}$ $dm^3 s^{-1}$. A Meterate calibration chart was used to calculate flow rates. The sample temperature was measured with a mercury-in-glass thermometer ($-10^{\circ}C$ to $50^{\circ}C$, $0.1^{\circ}C$ intervals). The thermometer was calibrated, whilst totally immersed in a water bath, against a total immersion thermometer (N.P.L. 8876, $-5^{\circ}C$ to $50^{\circ}C$). Agreement to within $0.1^{\circ}C$ was observed and the stem correction found to be negligible.

2.3.2 Results

The experimental results are given in table 2.1 as rates of weight loss, $\dot{w}$, at various temperatures, T. Using the diffusion coefficients, D(T), for water in nitrogen from Schwertz and Brow,[9] the transport function, ξ , was calculated using:

$\xi = \dot{w}RTl/DPM_{H_2O}c$ where l is the length of the channel and c the cross-sectional area.

Then from the equation:

$$p^{\circ}_{H_2O} = P_{TOT}[1 - e^{-\xi}] \qquad (1.4)$$

$Rln\,(p^{\circ}_{H_2O}/Pa)$ was found and plotted against $10^3K/T$ in figure 2.5.

A least squares analysis of the results yielded equation (2.1).

$$Rln(p^{\circ}_{H_2O}/Pa) = (-43.51 \pm 0.84)10^3/T + (215.50 \pm 2.68) \qquad (2.1)$$

Then, using $Rln(p^{\circ}_{H_2O}/P) = -\Delta H^{\circ}_{vap}/T + \Delta S^{\circ}_{vap}$, values of ΔH°_{vap} and ΔS°_{vap}, at the mean operating temperature of 311.15K, were found:-

$\Delta H^{\circ}_{vap} = 43.51 \pm 0.84$ kJ mol^{-1} and

$\Delta S^{\circ}_{vap} = 119.68 \pm 2.68$ J $mol^{-1}K^{-1}$

2.3.3 Discussion

The seven results recorded at 320.75K are plotted in figure 2.4 and show that $\dot{w}$ is independent of flow rate[3] over the range (0.3 to 2.3) x 10^{-3} dm^3s^{-1}. However, the effect of atmospheric pressure variations was not considered in these experiments. Fluctuations in atmospheric pressure can make a significant difference to calculations of $Rlnp^{\circ}_{H_2O}$. An 8% drop in total pressure, for example, gives a similar change in $p^{\circ}_{H_2O}$, ($p^{\circ}_{H_2O}$ being proportional to P_{TOT}).

Table 2.1

Evaporation of water, loop B – rates of weight loss, $\dot{w}$, at temperatures T and calculated values of vapour pressure, $p^{o}_{H_2O}$, using literature diffusion coefficients, D.

T/K	10^{11} $\dot{w}$/kg s^{-1}	$10^{4}D/m^{2}s^{-1}$	$R\ln(p^{o}_{H_2O}/Pa)$
322.65	19.3750	0.2897	80.3672
322.65	19.2260	0.2897	80.3083
321.75	20.3540	0.2877	80.7739
321.65	20.7500	0.2875	80.9230
320.75	17.3148	0.2855	79.5723
320.75	17.3611	0.2855	79.5929
320.75	18.2963	0.2855	79.9957
320.75	17.8889	0.2855	79.8230
320.75	18.1667	0.2855	79.9412
320.75	17.3519	0.2855	79.5888
320.75	17.5000	0.2855	79.6542
320.35	17.1850	0.2845	79.5318
319.35	16.2000	0.2822	79.1149
318.35	15.5710	0.2801	78.8419
317.15	14.5690	0.2775	78.3684
317.05	15.1040	0.2773	78.6519
314.95	12.4620	0.2724	77.2377
313.75	11.5060	0.2702	76.6433
313.25	11.4140	0.2688	76.6084
311.55	10.4170	0.2648	75.9614
310.35	9.5098	0.2620	75.2920
309.55	8.6140	0.2604	74.5319
308.15	8.5050	0.2573	74.4896
306.75	7.4390	0.2541	73.4813
305.55	7.6170	0.2513	73.7283
304.25	6.7500	0.2483	72.8200
304.05	6.4733	0.2480	72.4874
303.75	7.1320	0.2475	73.2753
302.65	5.9460	0.2448	71.8695
302.65	5.3778	0.2448	71.0571
301.95	5.0740	0.2434	70.6135
301.75	5.6040	0.2427	71.4362
299.65	4.6070	0.2382	69.9429

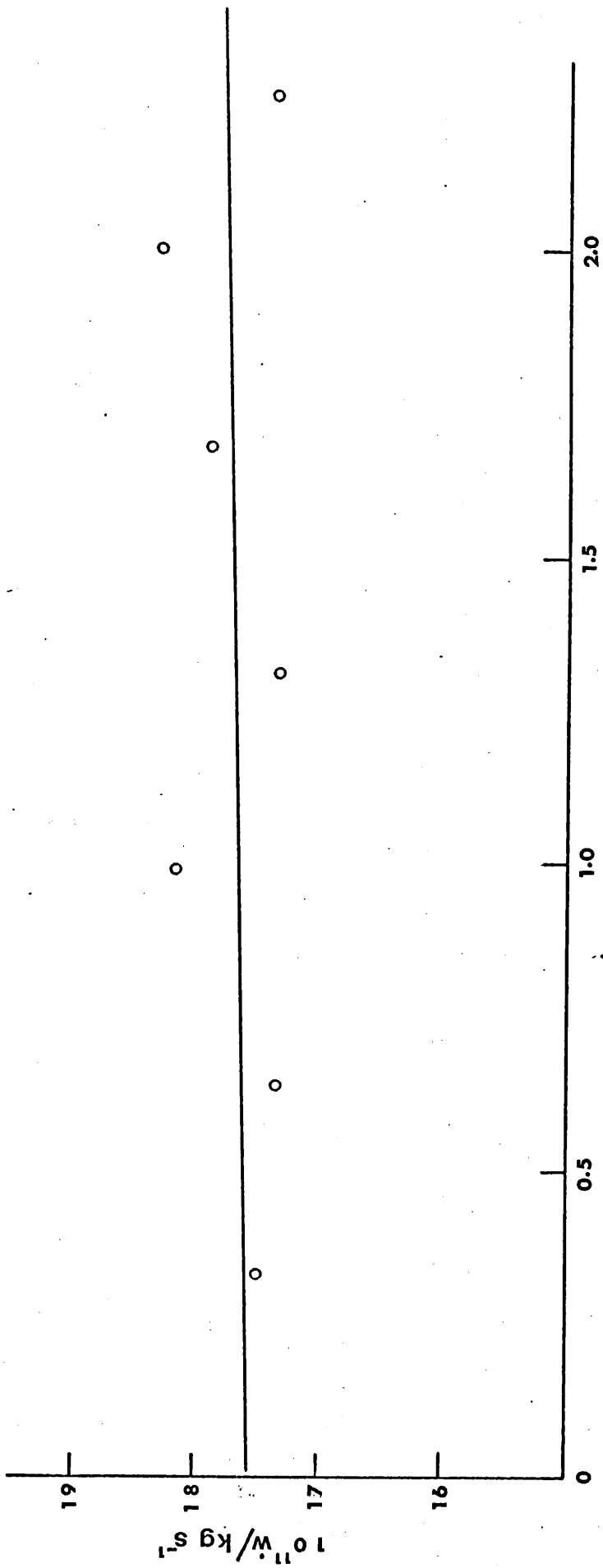

FIG. 2.4 Effect of nitrogen flow rate, $\dot{y}$, on rate of evaporation of water, $\dot{w}$.
T = 320.75 K, P = 760 Torr.

The value obtained for ΔH^{o}_{vap} is in excellent agreement with the literature values[4,5] of 43.54 and 43.55 kJ mol^{-1} at a mean operating temperature of 311.2K. However, the experimental value for ΔS^{o}_{vap} is too high by 2.4 J $mol^{-1}K^{-1}$.

Consistently high values of $\dot{w}$ were recorded over the range of temperatures investigated, this indicated the possibility of a leak round the stopper in the bottle. The next section describes how this supposition was tested.

2.4 Evaporation of water experiments - investigation of leaking stopper

2.4.1 Experimental

A pyrex, stoppered bottle weighing approximately 0.66 g was charged with deionised distilled water and suspended from loop A (maximum capacity 1.0 g) of the electrobalance. Flow rates of nitrogen were kept between 1.2×10^{-3} and 1.3×10^{-3} dm^3 s^{-1} and the atmospheric pressure was recorded for each run, the excess pressure in the apparatus being approximately 3 torr.

The stopper was pushed firmly into the bottle for the first eight runs, subsequent runs being conducted with the stopper lightly greased with silicone high vacuum grease.

2.4.2 Results

Tables 2.2 and 2.3 give the weight losses recorded at each temperature, the total pressure in the apparatus and the diffusion coefficients from Schwertz and Brow. Following the same procedure as in section 2.3.2, values of $R\ln p^{o}_{H_2O}$ were calculated (using the total pressure as measured) and plotted vs. $10^3 K/T$ in figure 2.5. Experimental and literature vapour pressures are shown in table 2.4.

Table 2.2

Evaporation of water, loop A, stopper pushed in firmly - rates of weight loss, $\dot{w}$, at temperatures T and calculated values of vapour pressure, $p^{o}_{H_2O}$, using literature diffusion coefficients, D.

T/K	P_{TOT}/Torr	$10^{11}\dot{w}$/kg s^{-1}	$10^{4}D/m^{2}s^{-1}$	$R\ln(p^{o}_{H_2O}/Pa)$
322.45	753.06	16.476	0.2895	80.934
319.95	757.79	14.682	0.2840	80.148
318.55	761.19	13.688	0.2808	79.667
315.35	761.19	11.099	0.2735	78.169
311.15	753.06	8.852	0.2643	76.553
309.25	761.44	7.642	0.2600	75.475
305.15	761.85	6.032	0.2507	73.771
299.60	762.10	4.276	0.2383	71.261

Table 2.3

Evaporation of water loop A, greased stopper

T/K	P_{TOT}/Torr	$10^{11}\dot{w}$/kg s^{-1}	$10^{4}D/m^{2}s^{-1}$	$R\ln(p^{o}_{H_2O}/Pa)$
323.15	763.48	11.369	0.2912	78.059
322.35	756.77	10.900	0.2893	77.758
320.15	763.98	9.657	0.2843	76.895
319.25	752.86	9.721	0.2822	76.977
318.15	769.67	8.667	0.2798	76.120
317.05	757.38	8.433	0.2775	75.935
315.35	758.24	7.448	0.2735	75.022
313.35	752.30	6.771	0.2688	74.346
312.45	757.38	6.392	0.2671	73.916
308.65	752.30	5.144	0.2586	72.331
306.15	753.37	4.401	0.2530	71.181
304.75	757.13	4.017	0.2498	70.509
303.15	756.62	3.652	0.2463	69.807
302.65	758.29	3.585	0.2452	69.680
300.15	756.87	3.095	0.2397	68.600
299.35	760.68	2.839	0.2377	67.943

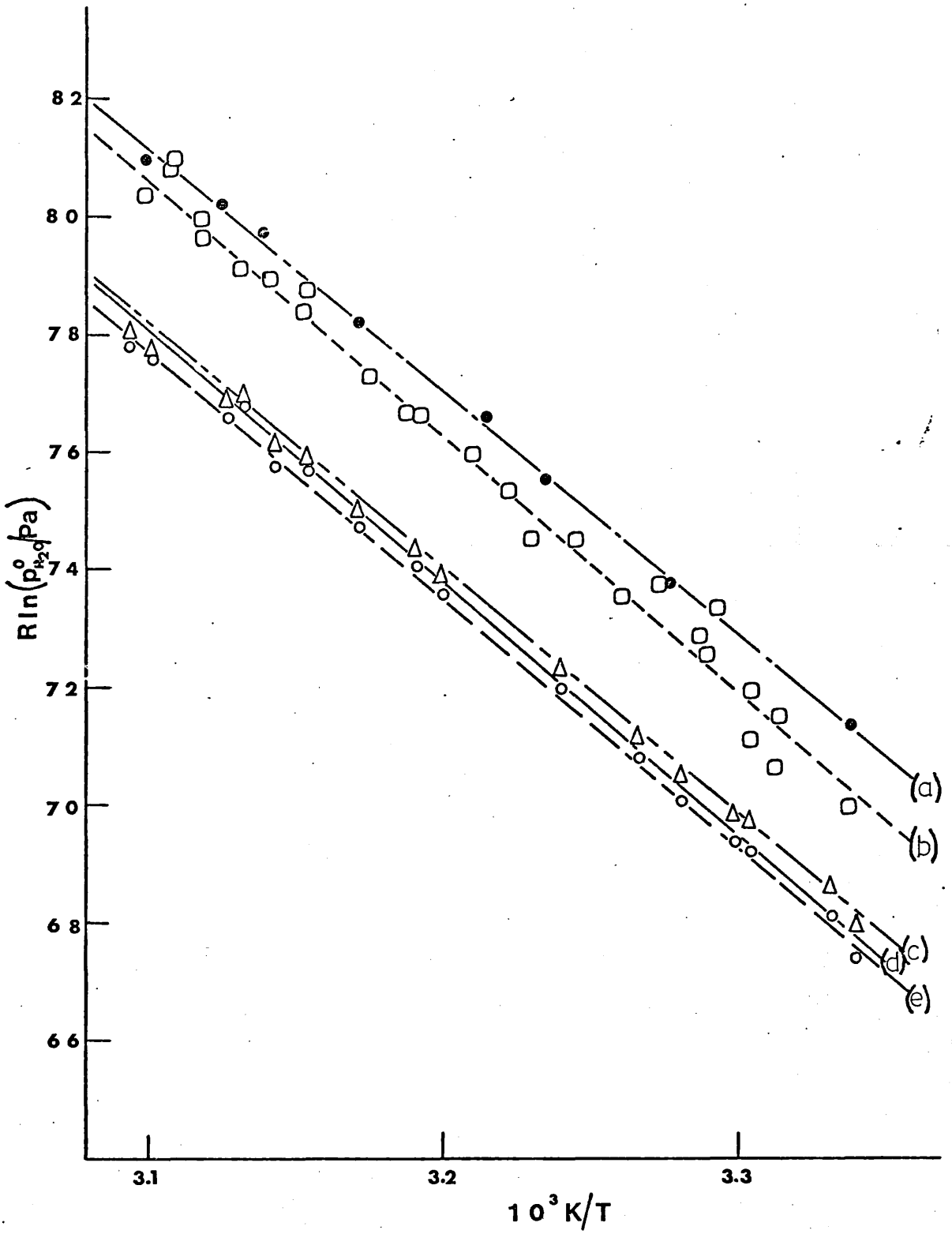

FIG. 2.5 Evaporation of water in nitrogen:-

● (a) Loop A, leaking, stoppered bottle.
□ (b) Loop B, leaking, stoppered bottle.
△ (c) Loop A, greased stopper, D values from ref. 9.
(d) Literature values[4,5]
○ (e) Loop A, greased stopper, D values from ref. 10.

Table 2.4

Evaporation of water - experimental and literature vapour pressures at various temperatures.

	$p^{\circ}_{H_2O}$/Pa(50°C)	$p^{\circ}_{H_2O}$/Pa(40°C)	$p^{\circ}_{H_2O}$/Pa(25°C)
Stopper pushed in firmly	17847.5	10893.0	4881.3
Stopper greased	12175.6	7488.0	3397.2
Ambrose and Lawrenson[4]	12345.0	7381.2	3168.6
Wexler[5]	12344.8	7381.3	3168.7

2.4.3 Discussion

The vapour pressures obtained from the non-greased bottle indicate a leak. Although the experimental line from the greased stopper results lies very close to the literature line (fig. 2.5), there is a sufficient difference in slope to make a significant error in ΔH°_{vap} and ΔS°_{vap} (ΔH°_{vap} being 2.7 kJ mol^{-1} too low and ΔS°_{vap} 8.4 J $mol^{-1}K^{-1}$ too low).

More recent data on diffusion coefficients in the vapour phase was found in a paper by O'Connell.[10] Using these values, the greased stopper results given in table 2.3 were recalculated (table 2.5).

These results are plotted in figure 2.5; a least squares analysis gave: $\Delta H^{\circ}_{vap} = 42.04 \pm 0.54$ kJ mol^{-1} and $\Delta S^{\circ}_{vap} = 112.23 \pm 1.73$ J $mol^{-1}K^{-1}$. (Literature values[4,5] : $\Delta H^{\circ}_{vap} = 43.56$ kJ mol^{-1}

Table 2.5

Evaporation of water, greased stopper - vapour pressures calculated using O'Connell's diffusion coefficients.

T/K	$10^4 D/m^2 s^{-1}$	$R\ln(p^\circ_{H_2O}/Pa)$
323.15	0.3005	77.778
322.35	0.2990	77.533
320.15	0.2950	76.562
319.25	0.2930	76.756
318.15	0.2910	75.709
317.05	0.2889	75.643
315.35	0.2857	74.693
313.35	0.2818	74.050
312.45	0.2800	73.567
308.65	0.2729	71.978
306.15	0.2680	70.786
304.75	0.2652	70.054
303.15	0.2622	69.334
302.65	0.2612	69.184
300.15	0.2567	68.075
299.35	0.2550	67.361

and $\Delta S^\circ_{vap} = 117.31$ J mol^{-1}K^{-1}). The O'Connell D values not only gave a closer fit to the literature line but also improved the values of ΔH°_{vap} and ΔS°_{vap}.

At higher temperatures the observed rate of weight losses were too low and this was thought to be due to the cooling effect of the gas stream. An investigation revealed that at high

temperatures (above 40°C) larger flow rates lowered the rate of weight loss. The gas stream is cooler than the bottle at high temperatures since it flows through a jet tube separated from the condenser walls by about 10 mm (fig. 2.2). A temperature change of only 1.5°C is required to bring these points onto the literature line.

2.4.4 Conclusion

From figure 2.5 it is clear that the stoppered pyrex bottle leaks. The vapour pressures obtained from the greased stopper experiments are in good agreement with the literature values[4,5] compared with recent experiments.[3] However, because of a slight error in slope (figure 2.5) probably caused by a cooling effect, the values of ΔH^{o}_{vap} and ΔS^{o}_{vap} are slightly inaccurate.

2.5 Evaporation of Zinc in Helium and Argon

2.5.1 Experimental

The sample, zinc wire (Goodfellow Metals Ltd. 99.99 + % purity), was wiped with methanol, cut into pieces with a surgical blade and placed in a small silica bottle (fig. 2.3). The dimensions of this 0.52 g bottle were noted and an appropriate capillary correction made (see Appendix 1). The bottle was suspended from the more-sensitive loop A of the electrobalance.

The inert gas used flowed into the system both through the balance chamber and below it. Typical flow rates were $(1.02 \pm 0.08) \times 10^{-3}$ $dm^3 s^{-1}$ for argon and $(1.18 \pm 0.04) \times 10^{-3}$ $dm^3 s^{-1}$ for helium. The excess pressure in the system was 3 to 5 torr. The water content of the exhaust gas stream was measured frequently with a dewmeter (Roberts and Armstrong Engineers Ltd). The apparatus was purged with hydrogen at 900°C at intervals during both experiments to eliminate surface contamination from the zinc sample.

2.5.2 Results

The water content of the gas stream was found to be 25 ppm in helium and 100 ppm in argon. The possibility of zinc oxide formation is discussed in section 2.5.3.

Experimental rates of weight loss are given in tables 2.6 and 2.7, the precision of $\dot{w}$ being 0.04% for zinc in helium and 0.18% for zinc in argon. The plots of ln $\dot{w}$ vs. $10^3 K/T$ (fig. 2.6) are linear except at low temperatures where recorded weight losses are lower than expected.

The vapour pressure of zinc as a function of temperature is well known,[6] see equation (2.2).

$$\log_{10}(p/\text{torr}) = -7.9190 - 5330.735/T - 1.61644 \times 10^{-3}T + 5.59972 \log_{10}T \qquad (2.2)$$

For the water evaporation experiments, well-established values of D(T) were inserted into the transport equation and values of $p^{o}_{H_2O}(T)$ derived and compared with literature values. In these experiments the reverse procedure was adopted i.e. $p^{o}_{Zn}(T)$ was assumed to be accurately known and values of D(T) for zinc in argon or helium obtained by substitution into the same equations.

The temperature dependence of D is given by:

$$D = D_o \left(\frac{T}{T_o}\right)^{1+s} \qquad (1.6)$$

where D_o is the value of D at a temperature T_o and one atmosphere pressure. The value of s is usually between 0.5 and 1.0, frequently near 0.8.[3] The graphs of lnD vs. lnT (fig. 2.7) have a slope of (1+s). Values of s were obtained from the linear portions of the plots by least squares analysis and are given in table 2.8.

Table 2.6

Evaporation of zinc in helium - rates of weight loss, $\dot{w}$, at temperatures T and calculated values of diffusion coefficients using literature vapour pressures.

T/K	$10^{10}\dot{w}$/kg s^{-1}	$10^{4}D/m^{2}s^{-1}$
1060.15	188.2692	5.7409
1060.15	185.9615	5.6705
1059.65	185.9615	5.7089
1059.15	186.9231	5.7772
1053.65	169.1379	5.6300
1053.15	168.1035	5.6335
1053.15	167.9310	5.6277
1052.35	166.7241	5.6478
1037.25	132.8571	5.5192
1036.95	132.8571	5.5417
1036.95	132.4286	5.5238
1036.95	130.8571	5.4583
1036.95	130.0000	5.4225
1035.55	128.6667	5.4694
1034.75	127.7333	5.4890
1034.25	125.3333	5.4225
1019.95	100.4211	5.2807
1018.65	99.1579	5.3081
1017.35	98.2000	5.3517
997.45	71.8462	5.1630
997.15	70.5714	5.0929
977.35	52.3158	5.0077
976.90	51.5790	4.9694

Table 2.6 (continued)

T/K	$10^{10}\dot{w}$/kg s^{-1}	$10^{4}D/m^{2}s^{-1}$
960.45	39.5790	4.8535
959.55	39.5200	4.9117
947.90	32.1000	4.7552
947.45	31.6480	4.7205
939.95	28.1778	4.7145
939.15	28.2000	4.7769
928.40	22.4914	4.5073
928.05	22.4000	4.5139
917.90	19.2195	4.5528
917.90	18.9714	4.4940
911.55	16.8851	4.4353
908.90	16.3575	4.4874
897.65	13.1525	4.3499
897.15	13.0098	4.3391
893.05	11.9879	4.2863
893.05	11.9152	4.2603
887.15	10.6919	4.2286
886.85	10.6703	4.2419
881.15	9.6195	4.2224
880.75	9.4100	4.1594
866.95	7.2519	4.0948
866.35	7.0963	4.0506
858.85	6.4483	4.2201
858.85	6.3742	4.1716
858.85	6.3355	4.1462
847.65	4.7756	3.8501
847.65	4.7707	3.8462

Table 2.7

Evaporation of zinc in argon - rates of weight loss, $\dot{w}$, at temperatures T and calculated diffusion coefficients using literature vapour pressures.

T/K	$10^{10}\dot{w}$/kg s^{-1}	$10^{4}D/m^{2}s^{-1}$
1119.95	134.5833	1.7729
1099.85	94.0385	1.6606
1078.95	67.5172	1.5930
1060.35	50.1539	1.5231
1060.05	50.7895	1.5486
1048.95	42.8696	1.5186
1036.65	34.5965	1.4491
1035.85	34.2759	1.4514
1026.95	29.9394	1.4314
1016.45	25.4103	1.4023
1016.15	25.2821	1.4010
1007.40	22.2222	1.3888
998.15	18.6200	1.3255
998.15	18.2692	1.3005
989.65	16.9464	1.3595
976.40	12.7763	1.2401
969.05	11.4419	1.2357
949.25	8.1000	1.1754
943.45	7.8952	1.2517
928.55	5.6012	1.1197
924.15	5.5281	1.1850
919.65	4.8750	1.1230

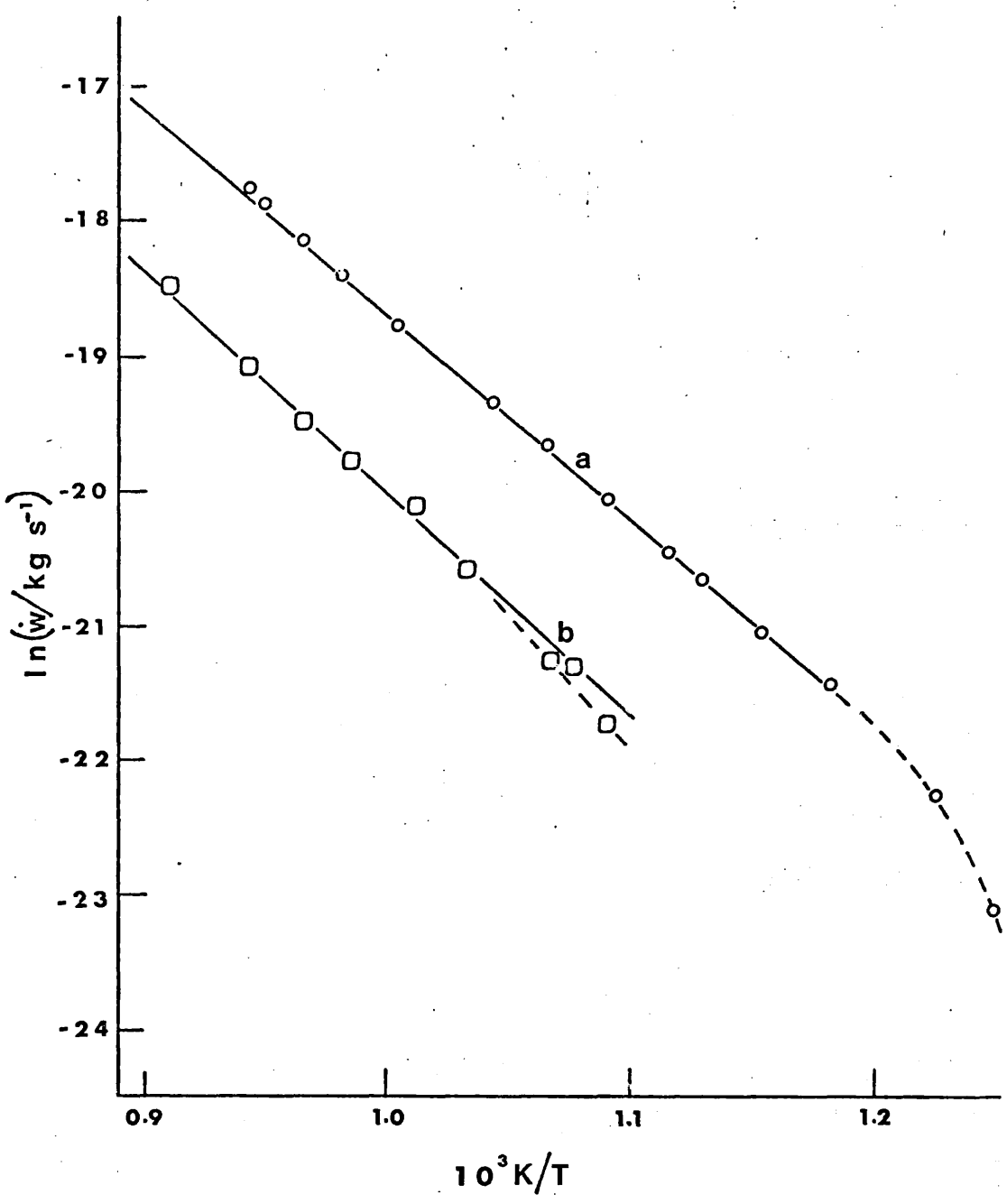

FIG. 2.6 Evaporation of zinc in (a) helium and (b) argon.

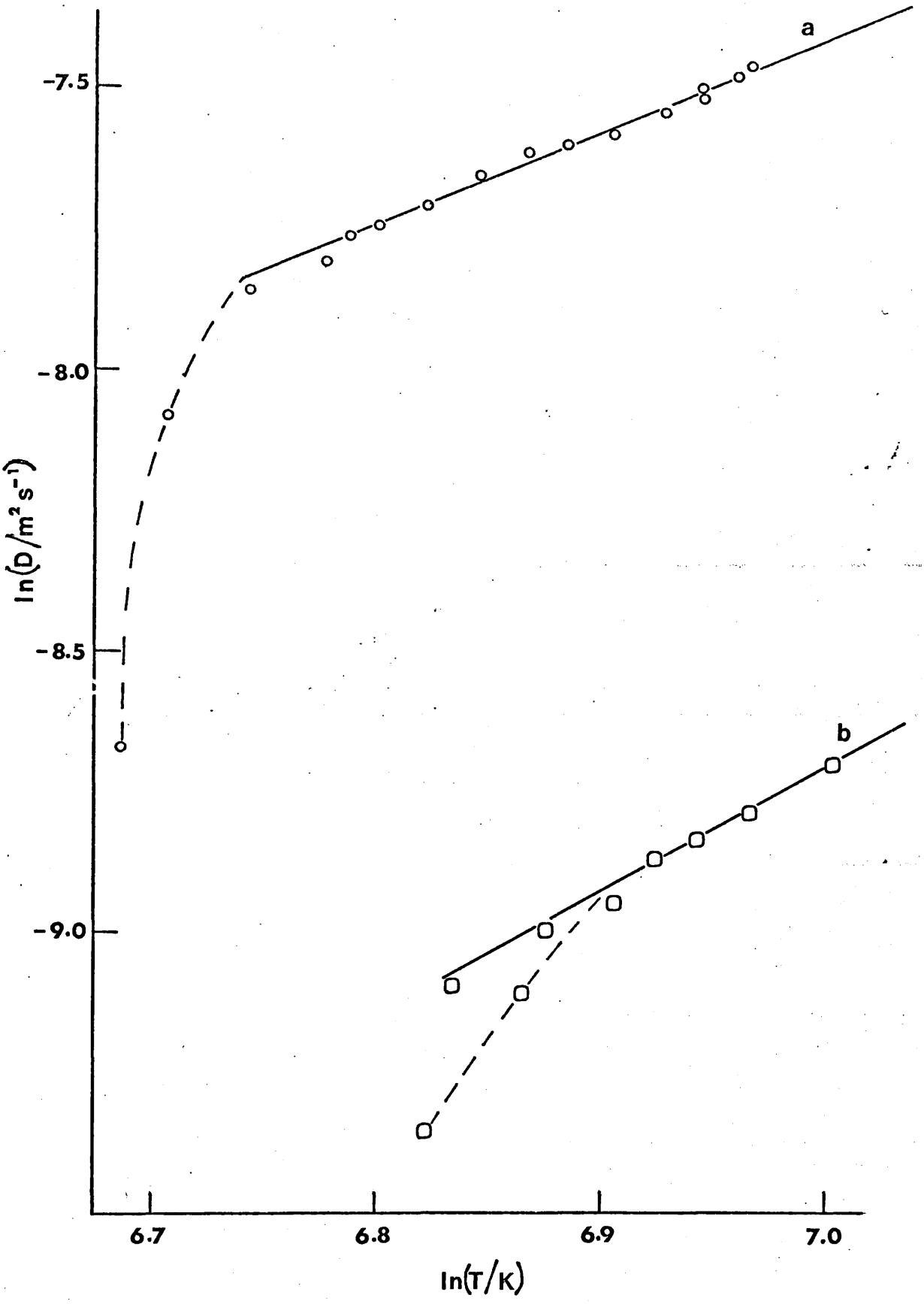

FIG. 2.7 Evaporation of zinc in (a) helium and (b) argon. Temperature dependence of diffusion coefficients.

Table 2.8

System	s	ref.
zinc/helium	0.629 ± 0.025	this work
zinc/argon	1.203 ± 0.089	this work
zinc/hydrogen	0.71 ± 0.04	8

2.5.3 Discussion

It is clear from the results obtained that the following equilibrium should be investigated:

$$ZnO(c) + H_2(g) \rightleftharpoons Zn(c) + H_2O(g)$$

ΔG° for this reaction is given by[11]:

$$\Delta G^\circ = 26850.0 + 11.38\ T \log_{10} T - 46.35T \qquad (2.3)$$

Equation (2.4) can now be used to determine the direction of spontaneity of the reaction.

$$\Delta G = \Delta G^\circ + RT \ln \left(\frac{a_{Zn}\ p_{H_2O}}{a_{ZnO}\ p_{H_2}} \right) \qquad (2.4)$$

When hydrogen, containing about 20 ppm of water, is flowing over the sample:

$p_{H_2O}/p_{H_2} \simeq 2.6 \times 10^{-5}$ and the activities are: $a_{Zn} = a_{ZnO} = 1$

Table 2.9 gives values of ΔG° and ΔG at various temperatures T.

Table 2.9

T/K	ΔG°/kJ mol^{-1}	ΔG/kJ mol^{-1}
400	84.3	49.0
700	71.4	9.6
770	68.8	0.8
780	68.5	-0.4
800	67.8	-2.9
1000	61.1	-27.1

Above 777K any zinc oxide formed on the surface of the zinc is reduced by the hydrogen atmosphere. So, in the zinc/argon and zinc/helium experiments, purging the system with hydrogen at 900°C effectively reduced any zinc oxide present. With no hydrogen in the system, any water present pushes the equilibrium to the left.

$$ZnO(c) + H_2(g) \rightleftharpoons Zn(c) + H_2O(g)$$

Hence the depression of $\dot{w}$ at lower temperatures may be attributed to the formation of an oxide layer on the surface of the sample. In the evaporation of zinc in hydrogen experiment [8] the graph is linear over the entire temperature range investigated. Oxide formation is prevented in this case by the presence of a highly reducing atmosphere.

The value of the numerical coefficient s obtained from the evaporation of zinc in helium experiment lies within the predicted range.

For zinc in argon however, the result is rather too high, this is probably due to interference by the zinc oxide layer.

Graphical representations of $R\ln(\dot{w}/T^s)$ and $R\ln(p^o_{Zn}/Pa)$ against inverse temperature both yield ΔH_{vap} from their gradients. Figure 2.8 illustrates the close agreement between this work and literature data.[6] It may be concluded from this evidence that the calculated values of s appear to be acceptable.

The diffusion coefficients derived from these experiments are compared with those of Nickolaev and Aleksovskii[12] and also with values calculated by Arnold[13] in figure 2.9. Their results, at elevated temperatures, seem to be compatible with this work although their values of s for zinc in argon are 0.67 and 0.66 respectively.

The final values obtained for the binary diffusion coefficients of zinc in helium and zinc in argon, as a function of temperature, are given in the following equations:

$$D_{Zn/He}(T) = 0.625 \times 10^{-4} \left(\frac{T}{273.15}\right)^{1.629 \pm 0.025} \ m^2 s^{-1} \qquad (2.5)$$

$$D_{Zn/Ar}(T) = 0.077 \times 10^{-4} \left(\frac{T}{273.15}\right)^{2.203 \pm 0.089} \ m^2 s^{-1} \qquad (2.6)$$

The error in D^o being unrealistic because of the necessary extrapolation. [The results reported in the literature[14] are calculated from earlier experiments during which the silica bottle was leaking round the stopper].

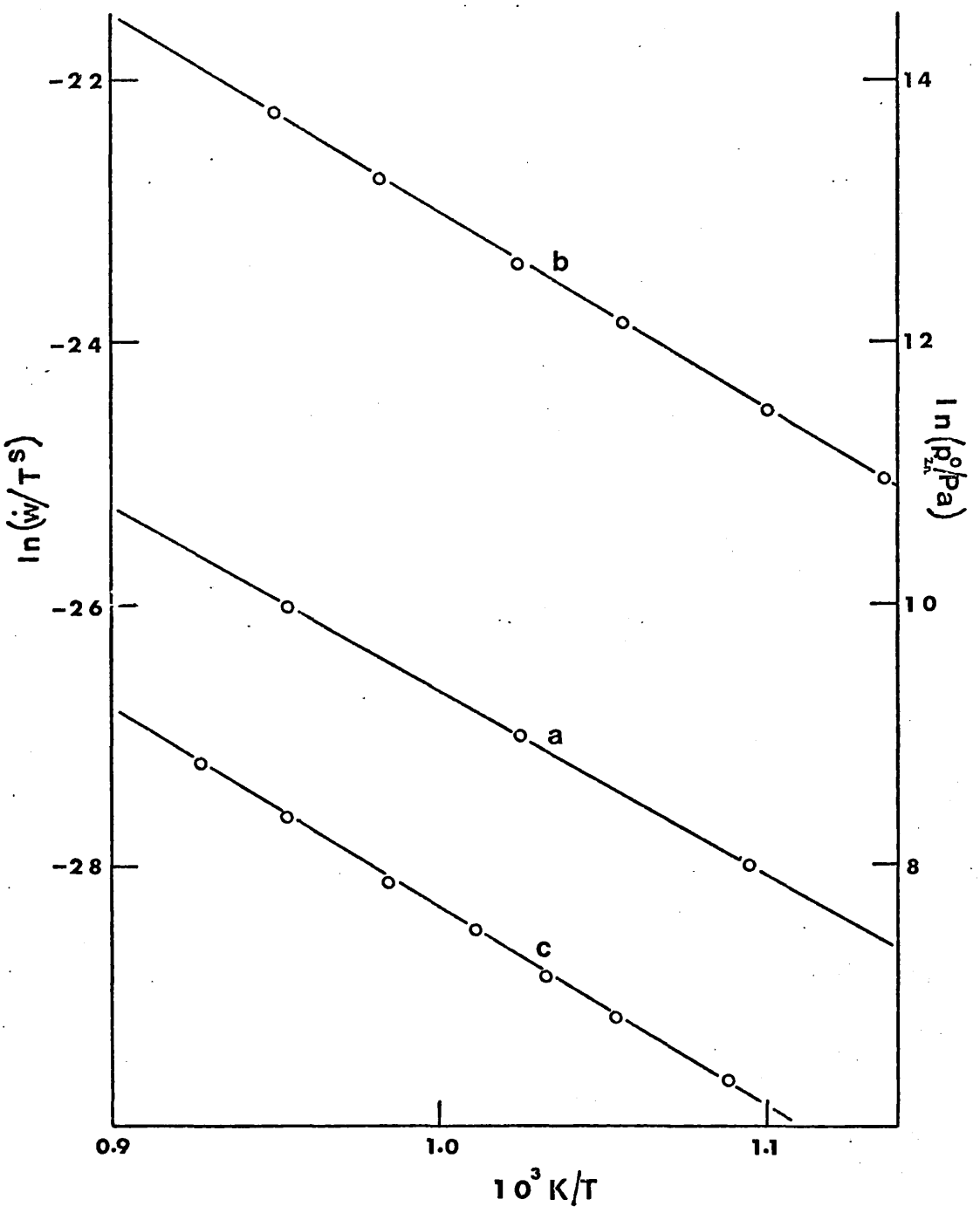

FIG. 2.8 Comparison between: (a) literature[6] values of vapour pressure zinc vs. inverse temperature and experimental evaporation results (b) zinc/helium and (c) zinc/argon; all of the lines yield ΔH_{vap} from their gradients.

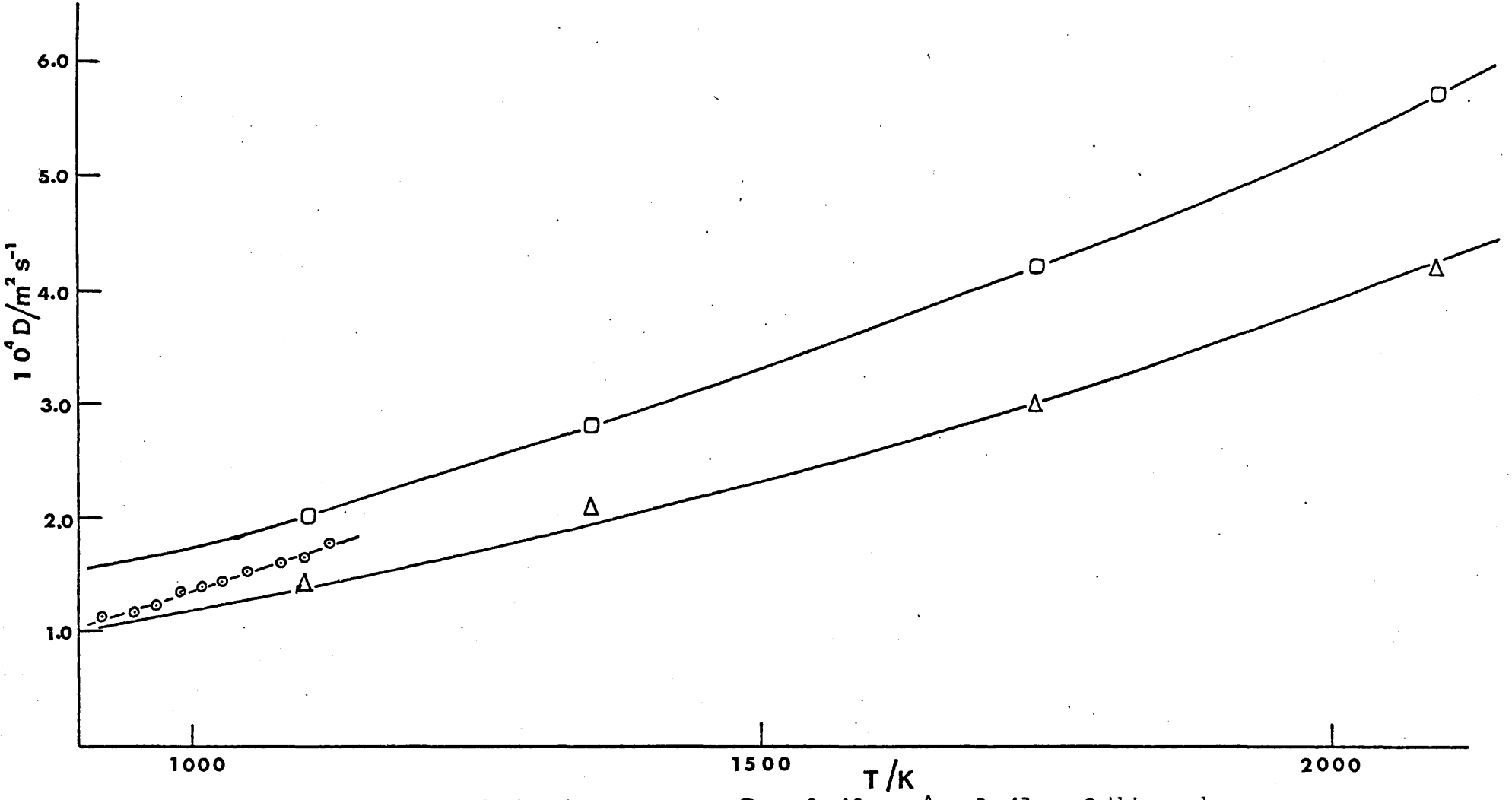

FIG. 2.9 Diffusion coefficient of zinc in argon. □ ref. 12, Δ ref. 13, ⊙ this work.

2.6 References

1. D. Battat, M.M. Faktor, I. Garrett, R.H. Moss, J. Chem. Soc. Faraday Trans. I, 70, 2280 (1974).

2. D. Battat, M.M. Faktor, I. Garrett, R.H. Moss, J. Chem. Soc. Faraday Trans. I, 70, 2302 (1974).

3. D. Battat, M.M. Faktor, I. Garrett, R.H. Moss, J. Chem. Soc. Faraday Trans. I, 70, 2267 (1974).

4. D. Ambrose, I.J. Lawrenson, J. Chem. Thermodynamics, 4(5), 755 (1972); Nat. Phys. Lab. UK Div. Chem. Stand. Rep. No.24 (1973).

5. A. Wexler, J. Res. Nat. Bur. Stand., 80A(5-6), 775-85 (1976).

6. A.N. Nesmeyanov, 'Vapour Pressure of the Chemical Elements', Elsevier Publ. Co. Ltd. (1963).

7. R.H. Moss, Ph.D. Thesis, University of London (1975).

8. S.W. Yardley, unpublished work.

9. F.A. Schwertz, J.E. Brow, J. Chem. Phys., 19, 640 (1951).

10. J.P. O'Connell, M.D. Gillespie, W.D. Krostek, J.M. Prausnite, J. Phys. Chem., 73, 2000 (1969).

11. O. Kubaschewski, E.L. Evans, C.B. Alcock, 'Metallurgical Thermochemistry', Pergamon Press (1967).

12. G.I. Nikolaev, V.B. Aleksovskii, Soviet Physics - Tech. Phys., 9(4), 575 (1964).

13. J.H. Arnold, Ind. Eng. Chem., 22, 1091 (1930).

14. M.M. Faktor, I. Garrett, J. Crystal Growth, 38, 213 (1977).

Chapter 3

Indium-hydrogen chloride and indium-hydrogen bromide systems

Chapter 3

3.1 Introduction

Hydrogen halides are frequently used as transporting agents in the growth of Group III-V semiconductors by chemical vapour transport. The rate of diffusion of the hydrogen halides in hydrogen, the carrier gas, is one of the factors determining the rate of transport of these electronic materials. Reactive gas concentrations also affect transport rates and must be precisely known; for this reason the flowmeters were calibrated.

The modified entrainment method (see section 1.4) may be used to study gaseous interdiffusion when the equilibrium constant for the transport reaction is extreme. In this case the rate of weight loss is limited by the rate of diffusion of the hydrogen halide down the channel of the bottle. Using a second-order approximation[1] to the theory of multicomponent diffusion, the binary diffusion coefficient of hydrogen halide in hydrogen may be calculated from experimental transport rates.

Experiments involving the transport of indium in a hydrogen halide, described in this chapter, were designed to obtain realistic values for the binary diffusion coefficients of hydrogen halides in hydrogen. These data were necessary for the analysis of future transport experiments (chapter 4).

3.2 Calibration of hydrogen flowmeters

The calibration curve for the hydrogen flowmeters, supplied by Meterate (fig. 3.1), was checked by a water displacement method.

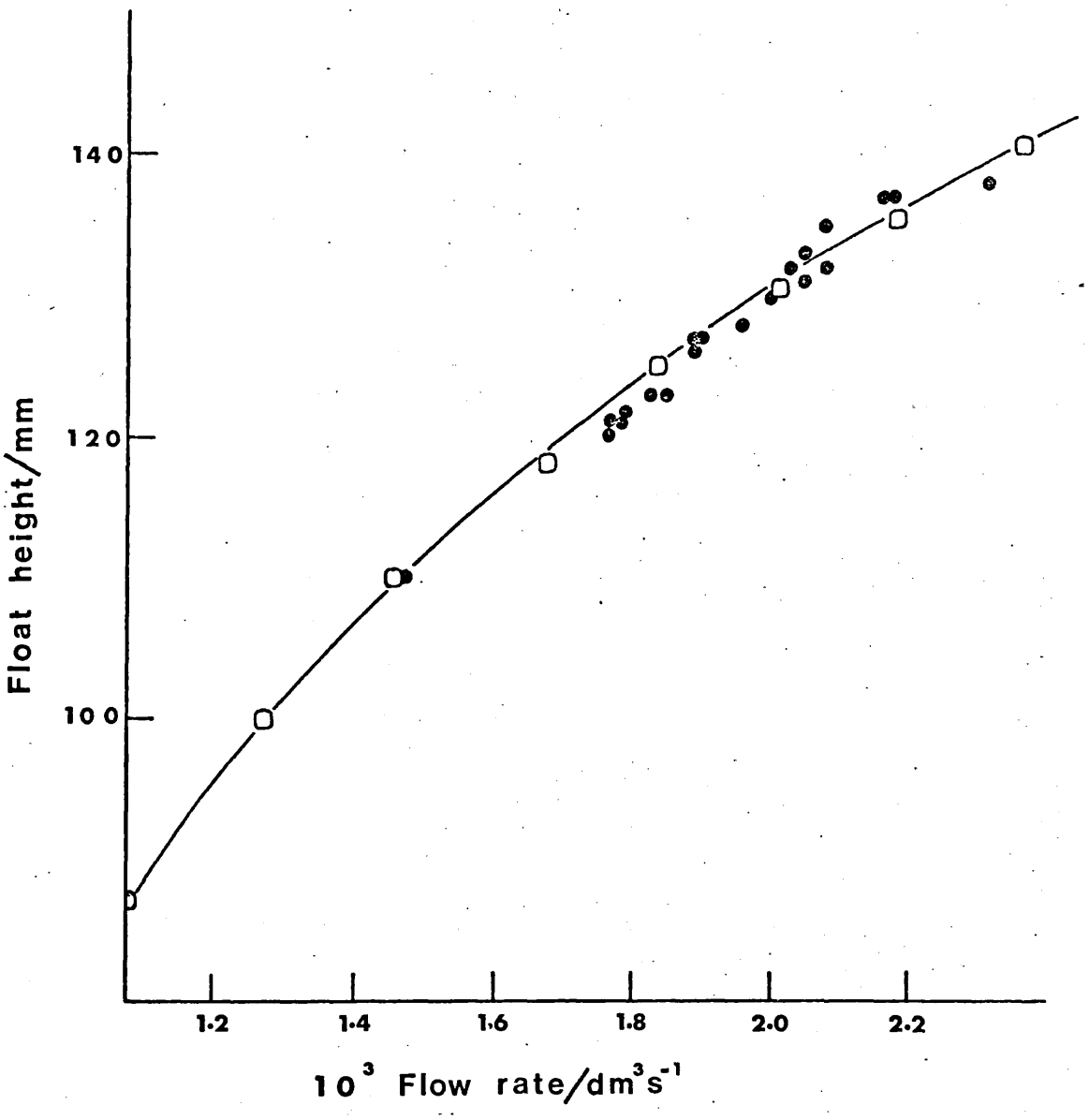

FIG. 3.1 Calibration curve for RS1 Flowmeter using a Ruby float and hydrogen gas (25°C), □ . ● water displacement method.

Hydrogen (BOC, high purity, 99.99% minimum purity) was passed through a flowmeter and collected in an inverted volumetric flask (1 dm^3); the water displaced had previously been saturated with hydrogen. Flow rates were measured at various float heights on both flowmeters and the pressure in the system noted. Approximately eighty results were recorded and plotted on the calibration graph supplied with the flowmeter.

Although the results were not sufficiently precise to warrant detailed statistical analysis, they confirmed satisfactorily the calibration curve in the region of interest (see fig. 3.1). The effect of varying back-pressure on flow rate was also investigated. In the $2.0 \times 10^{-3} dm^3 s^{-1}$ flow rate region, a 30 torr increase in back-pressure created a 3% increase in flow rate for the same float height.

3.3 Calibration of hydrogen chloride flowmeter

3.3.1 Summary of experimental techniques

The initial hydrogen chloride (Matheson gas products, technical grade, 99.0% purity) calibration[2] was effected by condensing hydrogen chloride in two 77K traps. The gas was dissolved cautiously in water and the resulting solution titrated against standardised sodium hydroxide using phenolphthalein indicator. The results of this procedure were considered unsatisfactory on two accounts: a) results obtained using this calibration curve were in disagreement with other similar work,[3] and b) the effect of back-pressure was ignored.

A second experiment was subsequently designed. The hydrogen and hydrogen chloride flowmeters were connected in parallel to an outlet and the gases passed through a Drechsel bottle via a coarse sintered-glass frit. The float heights were set to the experimental values normally utilised, i.e. in the range 90–130 mm for the hydrogen flowmeters (in these calibration experiments nitrogen was used as the carrier gas) and between 5 and 80 mm for the hydrogen chloride flowmeter. In order to maintain a constant back-pressure, gases were passed through a second Drechsel bottle (in parallel with the first and containing an equivalent amount of liquid). At a noted time, the gas flow direction was switched to the absorption train via a multi-way tap and the time taken to neutralise a solution of sodium hydroxide of known molarity, containing a few drops of indicator, was noted (typically 15–20 min). Fifty seven results were obtained at different hydrogen chloride float heights and back-pressures, the latter being dependent on the volume of liquid in the Drechsel bottles. The hydrogen chloride content of the gas stream was found to be greater than in the previous method but the scatter of the results was considerable as the effect of an unsteady back-pressure was to change the hydrogen chloride content of the gas stream.

In a further experiment various modifications were tried. The back-pressure generated by the resistance of the sintered frits was compensated for by a water pump which sucked gas through a line of three Drechsel bottles. All three bottles contained sodium hydroxide solution but it was found (by back titration with normal

hydrochloric acid) that all the hydrogen chloride gas was absorbed by the first two. In later experiments an electric pump replaced the water pump to give a more stable pressure in the system. Sixty six results were recorded but they were still irreproducible.

In the final experiment, two glass absorption-columns were filled with glass beads (fig. 3.2) such that their resistance to gas flow was the same. Sodium hydroxide solution of known concentration, containing a few drops of indicator, was run through the first column from a dropping funnel for a set time, while the hydrogen/hydrogen chloride mixture was flowing upwards. The gas flow was then switched to the equilibration column (set up in parallel) and the first column washed thoroughly with distilled water. The partially neutralised sodium hydroxide solution was then mixed with the washings and back-titrated against hydrochloric acid. The precision of the results was improved by shutting off one of the hydrogen flowmeters (see fig. 2.1), to increase the concentration of hydrogen chloride in the gas, and also by replacing most of the polythene tubing with glass. Back-pressure was successfully controlled with a teflon-keyed needle valve.

3.3.2 Results of absorption column method

More than two hundred results were recorded but only the later, more precise results, were analysed (table 3.1). Figure 3.3 suggests that the ruby float in the flowmeter was sticking to the side-walls in places. A least squares fit to the lower float height points (12-24 mm) yielded the following equation:

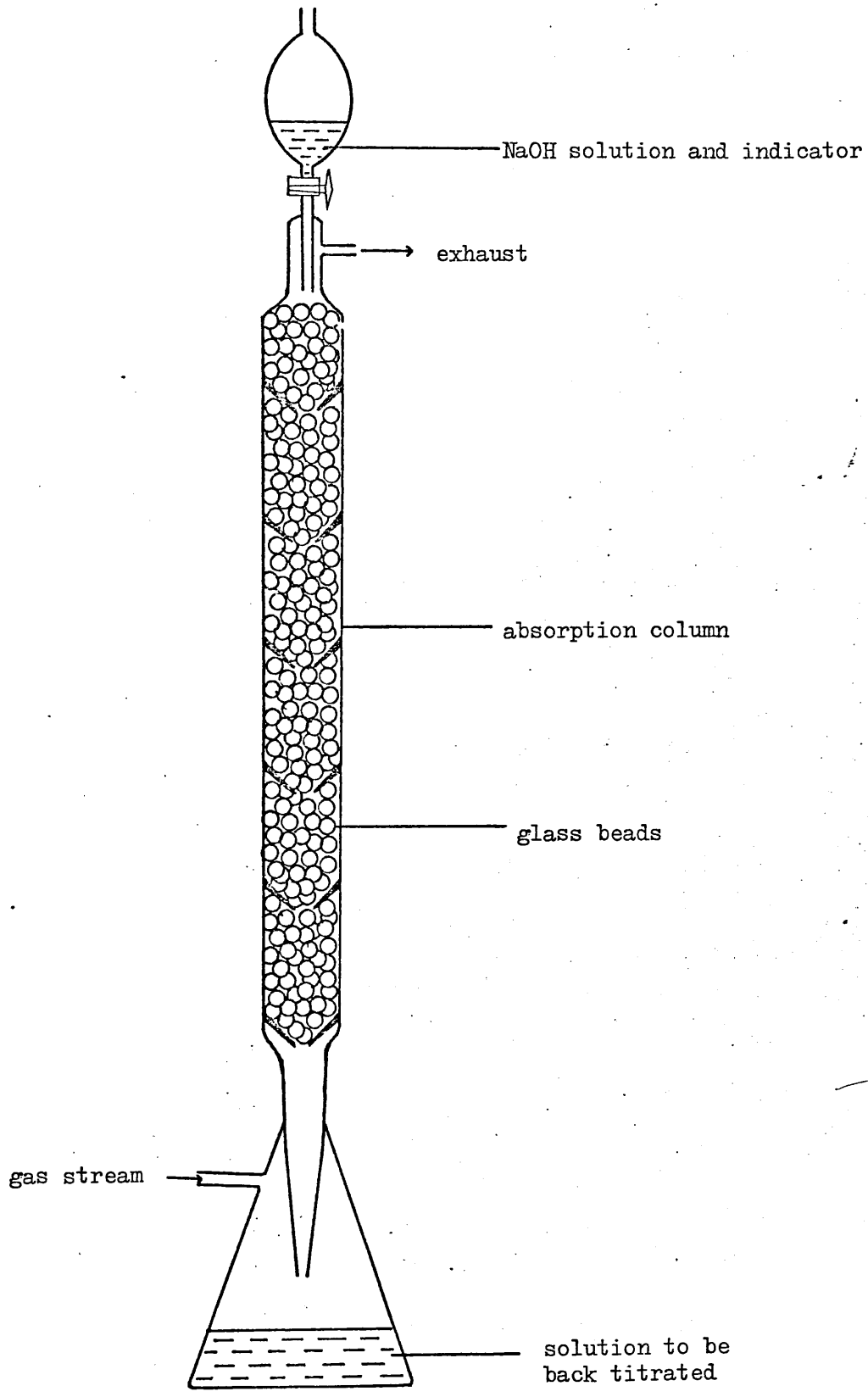

FIG. 3.2 Glass absorption column used in the calibration of the gas stream for HCl and HBr content.

Table 3.1

Calibration results for HCl flowmeter - flow rates, y, at float heights, x.

x/mm	$10^4 y/dm^3 s^{-1}$	x/mm	$10^4 y/dm^3 s^{-1}$
12	1.657	24	2.327
12	1.588	24	2.362
12	1.638	27	2.305
12	1.617	27	2.340
15	1.657	27	2.238
15	1.798	28	2.318
15	1.729	28	2.355
15	1.810	30	2.413
15	1.651	30	2.737
16	1.800	30	2.714
17	1.953	30	2.739
17	1.977	32	2.561
17	2.011	32	2.519
18	2.034	32	2.519
18	1.966	33	2.815
19	2.105	33	2.791
19	2.233	33	2.737
19	2.145	33	2.840
19	2.145	34	2.935
19	2.232	34	2.956
19	2.223	35	3.061
20	2.232	37	3.091
20	2.240	37	3.206
21	2.200	37	3.116
21	2.183	38	3.131
21	2.168	38	3.154
21	2.091	40	3.712
21	2.243	40	3.681
22	2.252	40	3.686
22	2.279	40	3.802
23	2.252	42	3.642
		44	3.878

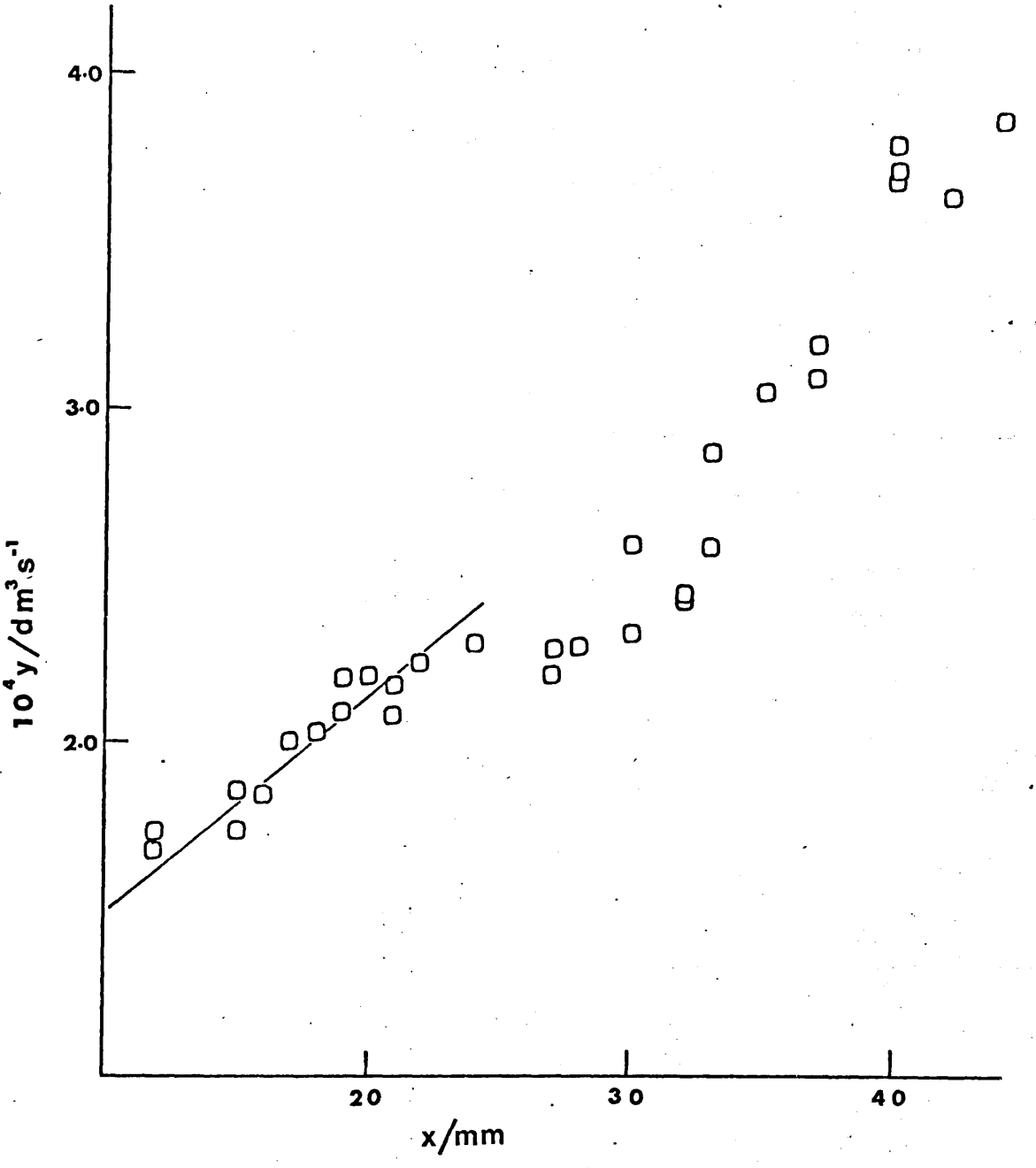

FIG. 3.3 Calibration curve for HCl flowmeter.
Flow rates, y, at float heights x.

$$y/dm^3s^{-1} = 6.6796 \times 10^{-6} (x/mm) + 8.096 \times 10^{-5}$$

where y is the flow rate in dm^3s^{-1} and x is the float height in mm. For the 40 mm float height point, the average of four results was taken. Table 3.2 summarises the results.

Table 3.2

Values of epsilon calculated from flow rates, y, at float heights, x.

x/mm			$10^4\ y/dm^3s^{-1}$			
H_2	H_2	HCl	H_2	H_2	HCl	$\varepsilon = \frac{p_{HCl}}{p_{TOT}}$
130	128	10	19.85	19.14	1.48 ± 0.08	0.0365
130	128	19	19.85	19.14	2.08 ± 0.08	0.0506
130	128	40	19.85	19.14	3.72 ± 0.06	0.0871

3.4 Calibration for hydrogen bromide

3.4.1 Experimental

To provide for the introduction of hydrogen bromide as the reactive gas, a bromine reservoir was incorporated into the lower hydrogen gas inlet (fig. 3.4). (The bromine reacts with the hydrogen in the furnace tube to produce hydrogen bromide). Acid-resistant molecular sieves (Union Carbide, AW 300 1/16") were placed in the reservoir and heated to 150°C at 10^{-2} Torr. Bromine

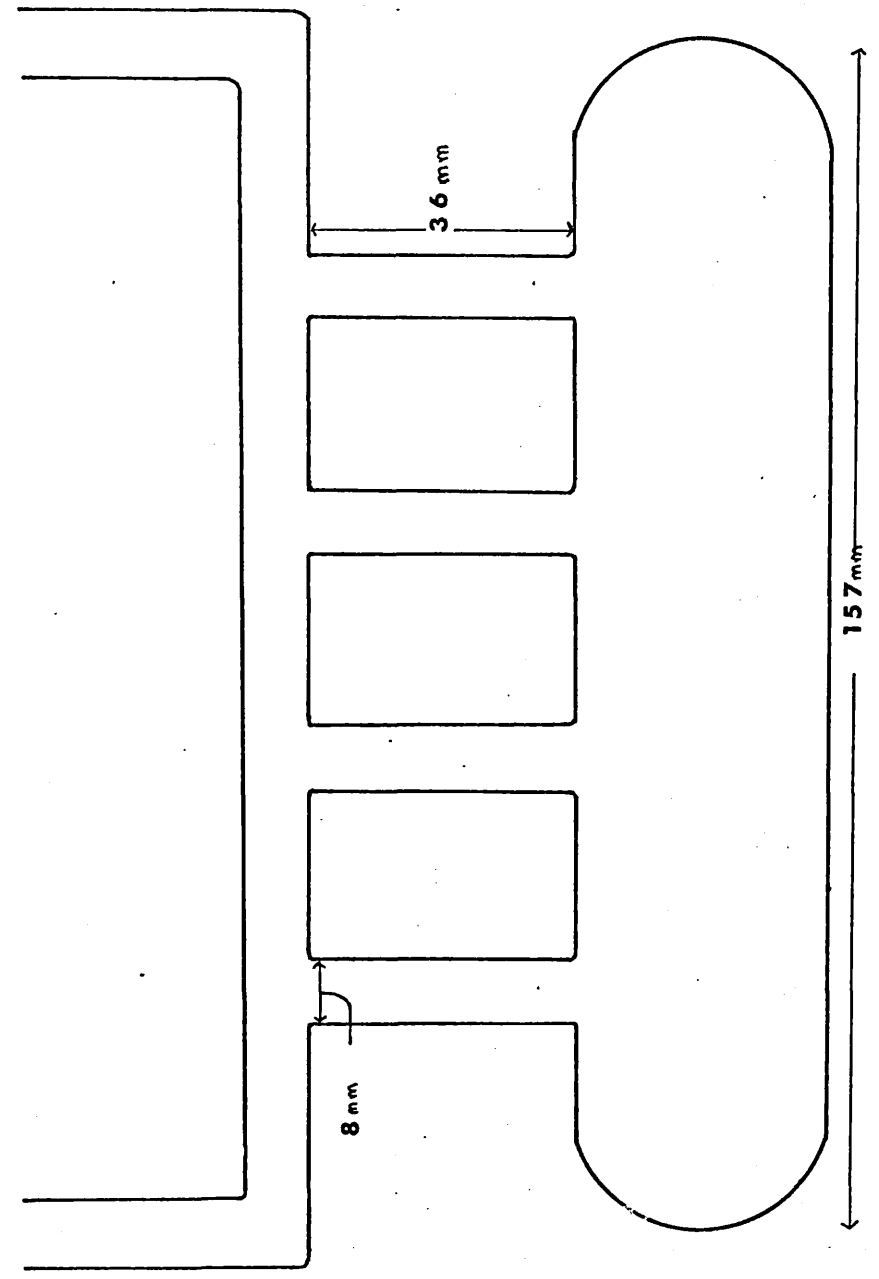

FIG. 3.4 Bromine reservoir.

(BDH, Aristar grade) was then introduced into the reservoir via a dropping funnel. The absorption-column method was used for the calibration of the hydrogen bromide content of the gas stream (see section 3.3.1). In this case, however, the furnace had to be used to effect the conversion to hydrogen bromide and so all the ancillary glassware was in place (see fig. 2.1). The flow of gas was such that an excess of hydrogen passed through the balance chamber, via the upper inlet, to reduce the risk of corrosion.

The temperature stability of the water bath (Grant, SX 10) used to heat the bromine reservoir was checked with a platinum resistance thermometer. At temperatures below 40°C the bath temperature was steady, to within 0.01°C, for several hours. To reduce evaporation losses a layer of plastic spheres was put on the surface of the water.

3.4.2 Results

The temperature of the furnace was varied between 1080K and 680K. With the bath temperature at 29.8°C, incomplete conversion to HBr occurred and free bromine was observed in the absorption-columns at furnace temperatures below 720K (this bleached the phenolphthalein indicator). For the higher concentration of hydrogen bromide this effect was observed at 730K.

With the water bath around the bromine reservoir set at 29.8°C ε ($pHBr/P_{TOT}$) was found to be 0.0354 ± 0.0005 (mean and one standard deviation of mean of 30 experiments). At a bath temperature of 39.4°C, $\varepsilon = 0.0591 \pm 0.0006$ (mean and one standard deviation of mean of 39 experiments). These results are summarised in table 3.3.

Table 3.3

Values of ε at bath temperatures t, hydrogen float heights x, and flow rates y.

t/°C	x/mm H_2	x/mm H_2	$10^4 y/dm^3 s^{-1}$ H_2	$10^4 y/dm^3 s^{-1}$ H_2	ε
29.8	131	110	20.2	14.6	0.0354
39.4	131	110	20.2	14.6	0.0591

3.4.3 Discussion

Values for the equilibrium constant, Kp, for the reaction: $H_2(g) + Br_2(g) \leftrightharpoons 2HBr(g)$ can be calculated using literature data[4] (see table 3.4); the forward reaction appears to be more favourable at lower temperatures.

The steady state reaction of H_2 and Br_2 has been studied in a flow system[5] in the temperature range 600–1470 K. An equation was given for the temperature dependence for the rate of combination of H_2 and Br_2. Values calculated from this equation (table 3.4) show that at lower temperatures the formation of hydrogen bromide is kinetically limited.

Table 3.4

Values for the equilibrium constant, Kp, at temperatures T and the rate of combination of H_2 and Br_2, k exp.

T/K	Kp	$k_{exp}/dm^3\ mol^{-1}\ s^{-1}$
500	9×10^{11}	1.2×10^{-6}
800	8×10^{7}	5.3
1100	1×10^{6}	5.6×10^{3}

3.5 Indium-hydrogen chloride and indium-hydrogen bromide systems

3.5.1 Experimental

The apparatus has been described in detail in section 2.2. Indium shot (Halewood Chemicals Ltd., nominal purity 99.999%) was cut into pieces with a surgical blade and loaded into the silica bottle with the 2 mm diameter channel (Appendix 1 gives dimensions). The carrier gas, hydrogen (BOC, 99.99% minimum purity) was passed through the palladium diffuser. The hydrogen chloride (Matheson Gas Products, 99.0% purity) was used in three concentrations:

ε = 0.0365, 0.0506 and 0.0871 (see section 3.3.2).

When transporting indium in hydrogen bromide, the hydrogen chloride inlet was shut off (see fig. 2.1). Using the bromine reservoir, as described in section 3.4, ε values of 0.0354 and 0.0591 were reproduced.

Loop A of the electrobalance was used for both experiments and the rate of weight loss from the sample bottle, $\dot{w}$, measured as a function of temperature and hydrogen halide concentration.

Table 3.5

Transport of indium by hydrogen chloride gas ($\varepsilon = 0.0871$) - rates of weight loss, $\dot{w}$, at temperatures T and pressures in the system P.

P/Torr	T/K	$10^{10}\dot{w}$/kg s^{-1}
761.16	1161.15	82.712
742.62	1151.25	82.957
742.62	1151.25	82.348
743.89	1120.25	73.704
743.89	1120.25	73.385
759.38	1080.85	79.758
748.46	1063.05	80.656
748.46	1063.05	80.492
742.62	1040.75	70.286
742.62	1040.75	69.643
748.46	1020.15	71.666
748.46	1020.15	69.014
759.38	990.15	74.773
741.35	981.55	63.032
741.35	981.55	62.065
748.46	950.15	64.868
748.46	950.15	62.645
743.89	909.15	58.242
743.89	909.15	57.879

Table 3.6

Transport of indium by hydrogen chloride gas ($\varepsilon = 0.0506$) - rates of weight loss, $\dot{w}$, at temperatures T and pressures in the system P.

P/Torr	T/K	$10^{10}\dot{w}$/kg s^{-1}
776.14	1235.25	60.188
776.14	1235.25	59.875
775.89	1216.15	62.774
775.89	1216.15	62.387
775.89	1181.15	57.529
775.89	1181.15	57.000
761.16	1161.15	58.970
742.62	1151.25	59.879
742.62	1151.25	59.563
775.89	1120.90	60.438
743.89	1120.25	59.030
743.89	1120.25	53.778
765.22	1101.85	58.061
765.22	1101.85	54.389
759.38	1080.85	55.714
748.46	1063.05	54.222
765.22	1051.25	55.714
765.22	1051.25	52.000
742.62	1040.75	55.143
742.62	1040.75	54.111
748.46	1020.15	50.308
763.70	1008.40	51.895
763.70	1008.40	51.158
759.38	990.15	52.105
763.70	969.25	51.158
763.70	969.25	49.897
748.46	950.15	50.974
748.46	950.15	49.500
763.70	939.05	49.500
763.70	939.05	49.436
776.40	920.45	46.619
776.40	920.45	44.818
743.89	909.15	46.381
743.89	909.15	46.306

Table 3.7

Transport of indium by hydrogen chloride gas ($\varepsilon = 0.0365$) - rates of weight loss, $\dot{w}$, at temperatures T and pressures in the system P.

P/Torr	T/K	10^{10} $\dot{w}$/kg s^{-1}
761.16	1257.55	50.103
761.16	1257.55	47.700
761.16	1216.00	49.487
742.62	1151.25	50.103
743.89	1120.25	44.409
743.89	1120.25	44.227
759.38	1080.45	47.095
748.46	1063.05	45.429
748.46	1063.05	44.455
742.62	1040.75	39.240
742.62	1040.75	38.157
748.46	1020.15	41.702
748.46	1020.15	40.612
748.46	950.15	38.980
748.46	950.15	38.235

3.5.2 Results for the indium-hydrogen chloride system

The rates of weight loss, $\dot{w}$, recorded at various temperatures T and three values of ε are given in tables 3.5 to 3.7. In the temperature range investigated (909-1258 K), the resulting ln $\dot{w}$ vs. 10^3 K/T graphs (fig. 3.5) were linear.

Using the simplified formula given in section 1.4:

$$D = \dot{w}RTl/PM\varepsilon A \qquad (1.15)$$

a value of $D_{HX,m}$, the diffusion coefficient of hydrogen halide in the gas mixture (m), was calculated for each experimental point and the results plotted as lnD vs. lnT in figure 3.6. Fitting the points from each line to the expression

$$D(T) = D^{o}(T/273.15)^{1+s} \qquad (1.16)$$

where D^{o} (the diffusion coefficient at $0^{o}C$) is a constant and s is approximately 0.8,[1] the following results were obtained (table 3.8).

Table 3.8

$D^{o}_{HCl,m}$ and s results at respective values of ε .

ε	$10^4 D^{o}/m^2 s^{-1}$	s
0.0871	0.131 ± 0.255	1.365 ± 0.155
0.0506	0.331 ± 0.289	0.846 ± 0.070
0.0365	0.340 ± 0.662	0.903 ± 0.154

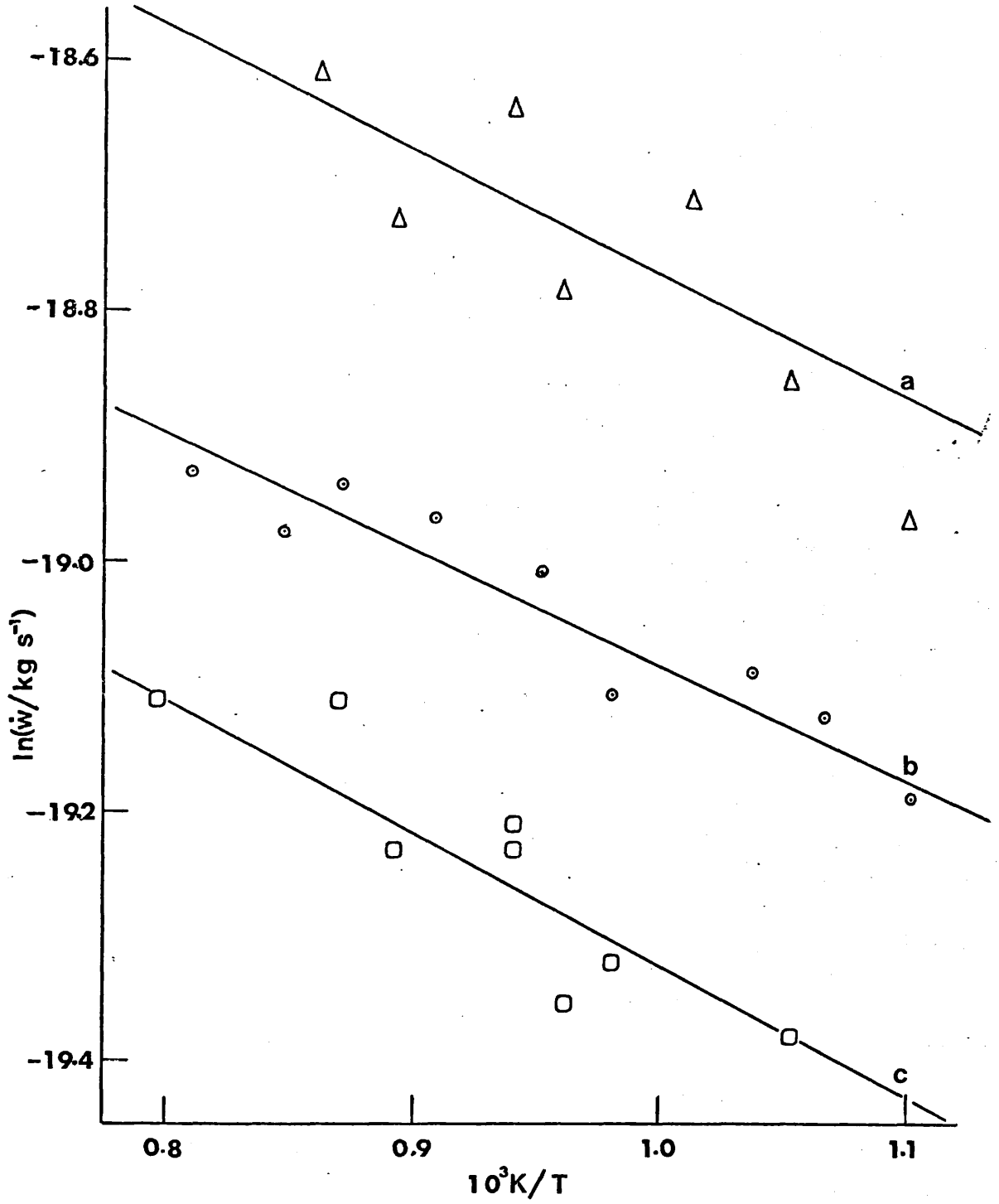

FIG. 3.5 Transport of indium by hydrogen chloride gas, experimental results.

(a) $\varepsilon = 0.0871$, (b) $\varepsilon = 0.0506$ and (c) $\varepsilon = 0.0365$.

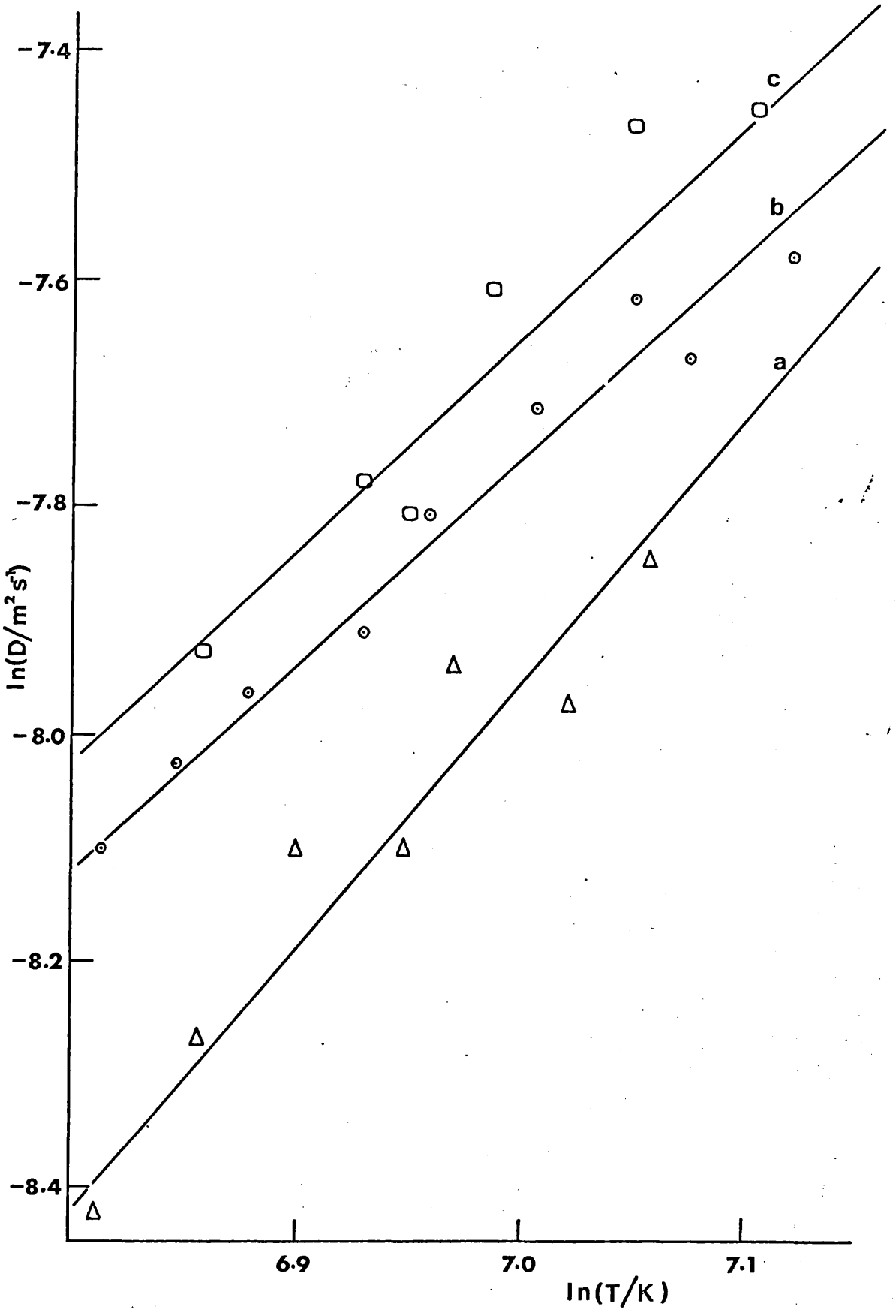

FIG. 3.6 Variation of D_{HCl,H_2} with temperature: diffusion coefficients independent of concentration.
(a) $\varepsilon = 0.0871$, (b) $\varepsilon = 0.0506$ and (c) $\varepsilon = 0.0365$.

The uncertainties in D^{o} and s are calculated by applying the following equations to the lnD vs. lnT graphs:

$$\text{Error in slope} = \left(\frac{\Sigma \delta^{2}}{(n-2)\left(\Sigma x^{2} - \frac{(\Sigma x)^{2}}{n}\right)} \right)^{\frac{1}{2}} \qquad (3.1)$$

$$\text{Error in intercept} = \left(\frac{\Sigma x^{2} \, \Sigma \delta^{2}}{(n-2)(n\Sigma x^{2} - (\Sigma x)^{2})} \right)^{\frac{1}{2}} \qquad (3.2)$$

where δ is the residual in lnD, x = lnT and n is the number of results.

These experiments were carried out in the temperature range 900–1250 K, the values of D^{o} (at 273.15 K) were obtained by back extrapolation of the 'least squares fits' to the lnD vs. lnT graphs. Any uncertainty in the slopes or intercepts of the lines is magnified by this extrapolation. More errors were introduced by the inaccuracy of the HCl float height setting. With no flow controller on the flowmeters it was not possible to maintain a precise value of ε, especially when using low HCl float heights. The uncertainty in ε for these experiments is estimated to be $\pm$ 10%.

The value of D^{o} increases as ε decreases because this simple analysis (see section 1.4) ignores the presence of minority components (in this case InCl). A second-order approximation to multicomponent diffusion[1] shows that the diffusion coefficient of the hydrogen halide in the gas mixture should be replaced by a binary coefficient $D_{HX,\,H_2}$ (where HX = HCl or HBr) divided by a composition-dependent factor γ_{HX}:

$$\gamma_{HX} = 1 + a_{HX}\varepsilon + b_{HX}\,\xi_{HX}. \qquad (1.17)$$

The coefficients a_{HX} and b_{HX} may be estimated using the following theoretical expressions:

$$a_{HX} = \frac{D_{HX,\,H_2}}{D_{HX,InX}} - \tfrac{1}{2} \qquad (1.18)$$

$$b_{HX} = \left(\frac{D_{HX,\,H_2}}{D_{HX,InX}} - 1\right)\left(\frac{D_{H_2,\,HX}}{D_{H_2,InX}} - 1\right) - \tfrac{1}{2} \qquad (1.19)$$

or obtained from this experiment.

The simplified formula for D, equation (1.15), may now be re-written as:

$$D_{HX,H_2} = \frac{\dot{w}RT1}{PMA}\left[\frac{b_{HX}}{-(1+a_{HX}\varepsilon)+\sqrt{(1+a_{HX}\varepsilon)^2+2b_{HX}\varepsilon}}\right] \qquad (1.21)$$

$$= D^{o}(T/273.15)^{1+s}$$

A computer programme was written to find the values of a_{HX} and b_{HX} which produced D_{HX,H_2} results giving the best fit to the experimental data (fig. 3.7). These values of a_{HX} and b_{HX} were compared with those calculated using Graham's Law[6]:

$$D_{ij}/D_{ik} = (M_k/M_j)^{\frac{1}{2}} \qquad (1.20)$$

to calculate the ratios of the diffusion coefficients appearing in the theoretical expressions for a_{HX} and b_{HX} (equations 1.18 and 1.19). The results are summarised in table 3.9.

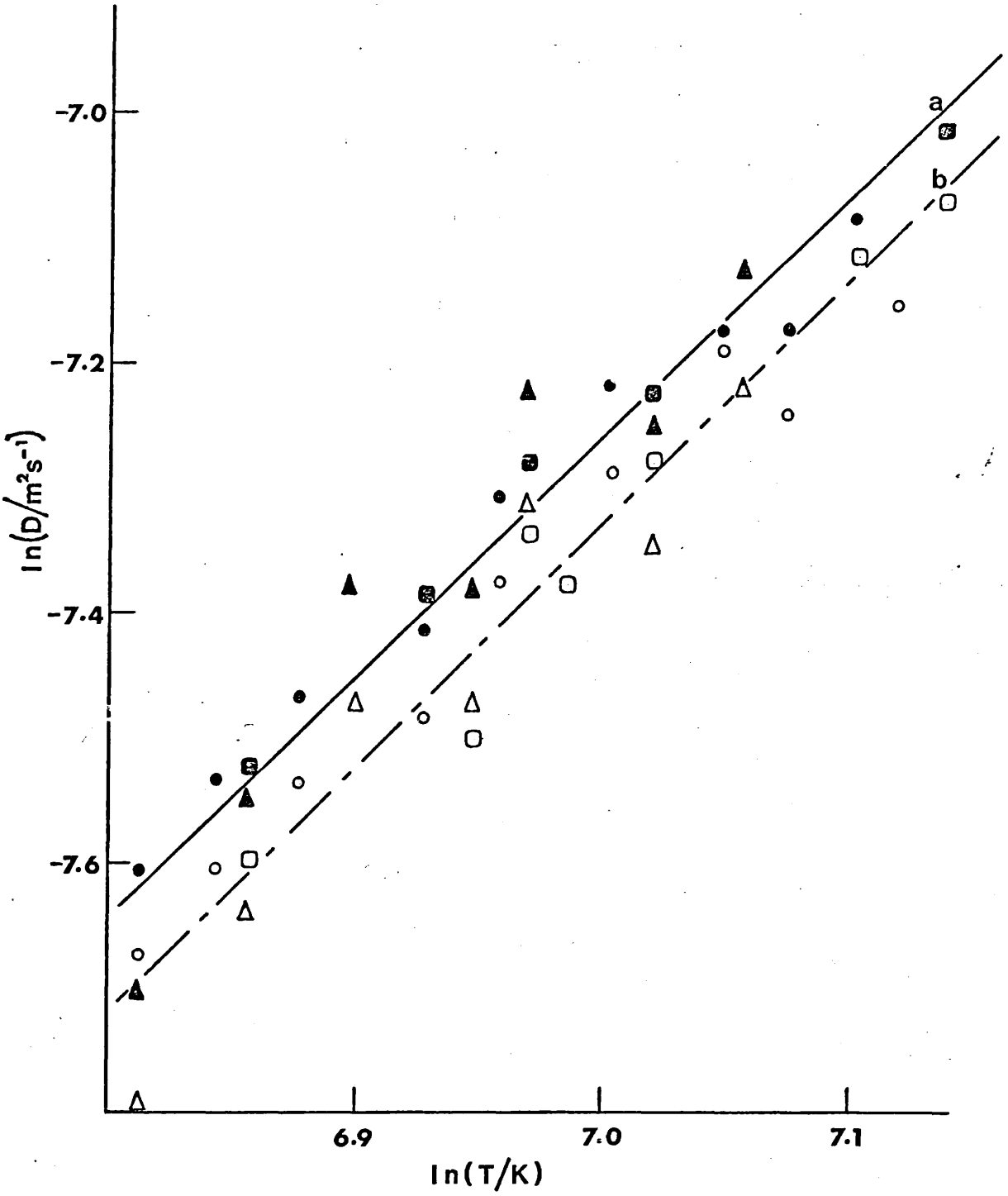

FIG. 3.7 Variation of D_{HCl,H_2} with temperature: diffusion coefficients dependent on concentration. 'Least squares' fit ▲, $\varepsilon = 0.0871$; ●, $\varepsilon = 0.0506$; ■, $\varepsilon = 0.0365$,(a).
'Graham's law' fit Δ, $\varepsilon = 0.0871$; o, $\varepsilon = 0.0506$; □, $\varepsilon = 0.0365$,(b).

Table 3.9

'Least squares fit' to experimental results (fig. 3.7) - gives values for D^{o}_{HCl,H_2} (the diffusion coefficient of HCl in hydrogen at $0^{o}C$) and for the numerical coefficient, s, using the second-order approximation to multicomponent diffusion.

Graham's Law approach	Minimum 'least-squares' deviation
$a_{HCl} = 8.134$, $b_{HCl} = 7.364$	$a_{HCl} = 10.134$, $b_{HCl} = 8.364$
Slope (lnD vs. lnT = 1.990 ± 0.067	Slope (lnD vs. lnT) = 1.964 ± 0.064
Intercept = -21.253 ± 0.464	Intercept = -20.998 ± 0.446
$D^{o}_{HCl,H_2} = (0.415 \pm 0.347) \times 10^{-4}$	$D^{o}_{HCl,H_2} = (0.462 \pm 0.372) \times 10^{-4}$
$s = 0.990 \pm 0.067$	$s = 0.964 \pm 0.064$

3.5.3 Results of the transport of indium in hydrogen bromide

The rates of weight loss, $\dot{w}$, recorded at various temperatures T and two values of ε are given in tables 3.10 and 3.11. In the temperature range investigated (894 - 1214 K), the resulting ln $\dot{w}$ vs. 10^3 K/T graphs (fig. 3.8) were linear.

Values of the diffusion coefficient, $D_{HBr,m}$, of hydrogen bromide in the gas mixture were calculated for each experimental point (as in section 3.5.2) and the results plotted as lnD vs. lnT in figure 3.9. Fitting the points from each line to equation (1.16), the results in table 3.12 were obtained.

Table 3.10

Transport of indium by hydrogen bromide gas ($\epsilon = 0.0591$) - rates of weight loss, $\dot{w}$, at temperatures T and pressures in the system P.

P/Torr	T/K	$10^{10}\dot{w}$/kg s^{-1}
742.11	1214.15	54.167
742.11	1213.85	54.778
742.11	1180.05	53.556
742.11	1179.65	53.722
736.27	1139.45	51.368
736.27	1139.15	51.737
736.27	1138.30	51.789
745.16	1119.25	51.000
745.16	1119.25	50.769
745.16	1080.15	49.487
745.16	1079.65	49.800
742.11	1062.95	49.300
742.11	1062.15	49.200
745.16	1040.75	47.333
745.16	1039.95	48.000
742.11	1008.40	49.200
742.11	1008.40	48.150
745.16	978.55	45.762
745.16	977.65	45.952
736.27	939.65	45.581
736.27	939.65	44.591
745.16	921.05	43.955
745.16	920.55	44.571
745.16	920.55	44.136
742.11	895.05	43.364
742.11	895.05	42.478

Table 3.11

Transport of indium by hydrogen bromide gas ($\varepsilon = 0.0354$) - rates of weight loss, $\dot{w}$, at temperatures T and pressures in the system P.

P/Torr	T/K	10^{10} $\dot{w}$/kg s^{-1}
736.52	1181.75	37.539
736.52	1178.65	38.039
736.52	1140.55	37.585
736.52	1139.25	36.717
736.52	1118.05	36.370
736.52	1117.65	37.269
736.52	1081.75	36.185
736.52	1080.90	35.926
736.52	1062.75	33.778
735.76	1042.15	34.069
735.76	1042.15	34.000
736.52	1008.40	34.357
736.52	1008.40	33.793
735.76	980.85	32.966
735.76	980.40	31.581
735.76	951.25	31.867
735.76	950.55	32.000
736.52	920.95	32.033
736.52	919.95	31.742
736.52	910.95	30.281
735.76	894.15	30.839
735.76	894.15	29.969

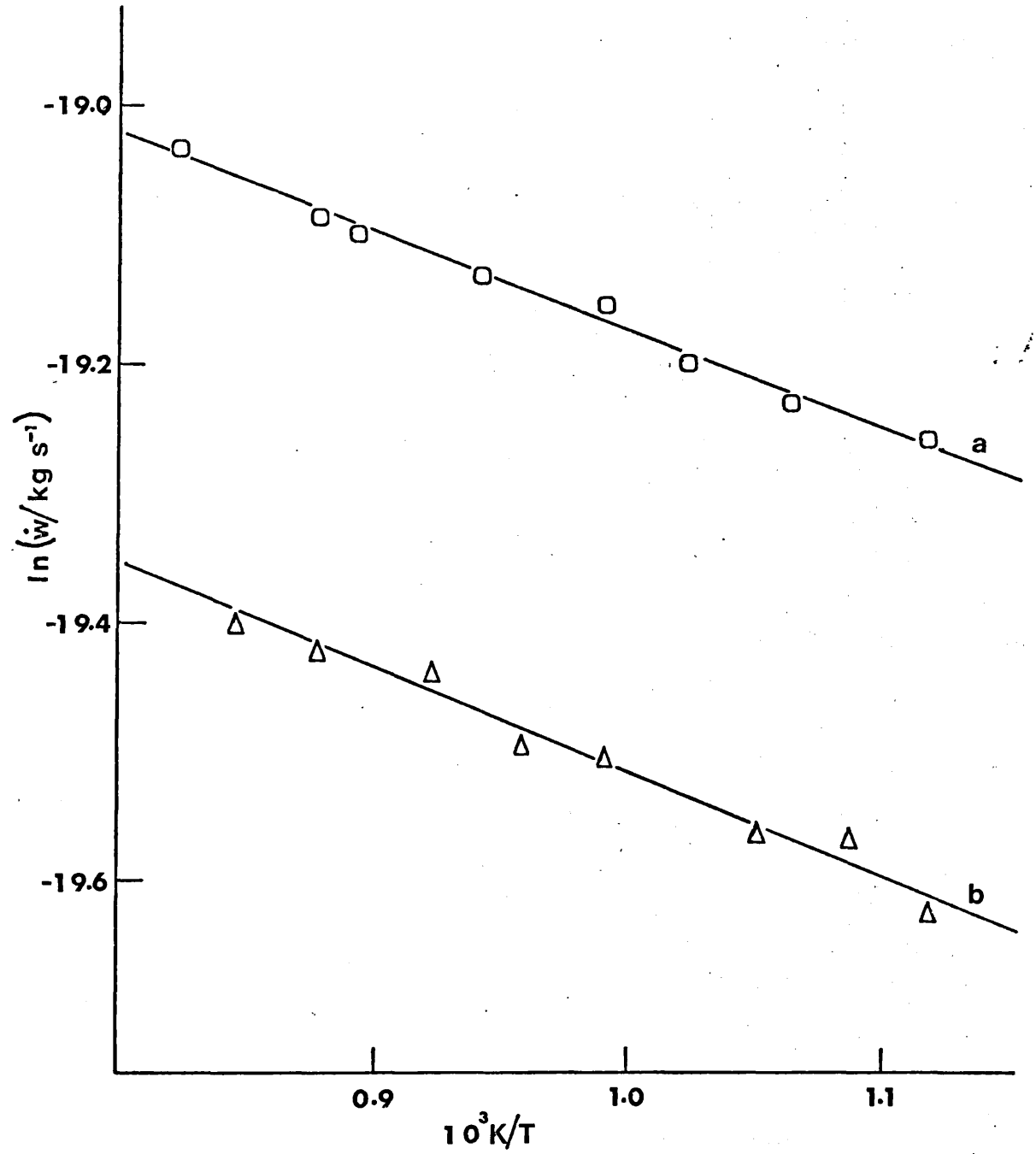

FIG. 3.8 Transport of indium by hydrogen bromide gas, experimental results.
(a) $\varepsilon = 0.0591$ and (b) $\varepsilon = 0.0354$.

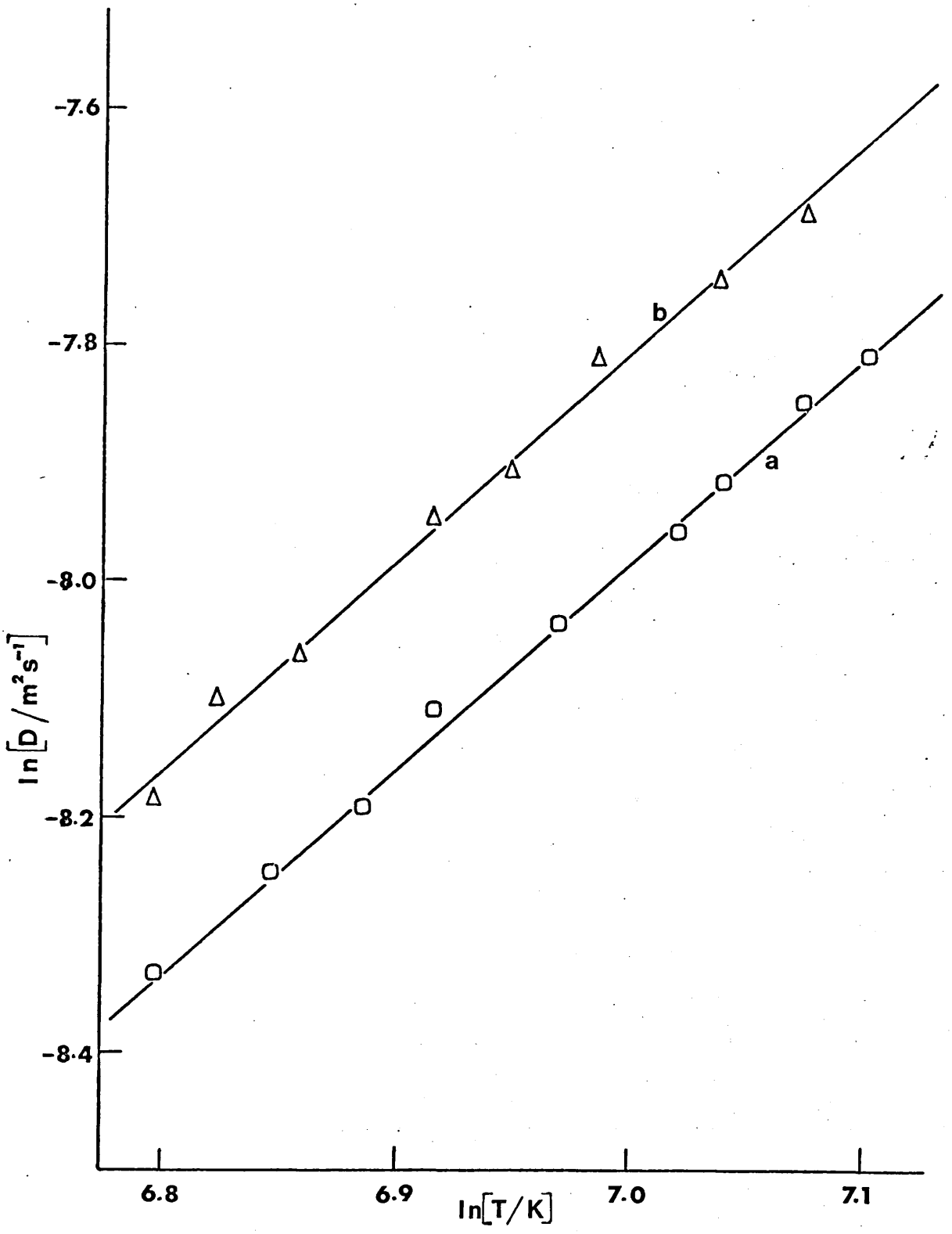

FIG. 3.9 Variation of D_{HBr,H_2} with temperature: Diffusion coefficients independent of concentration. (a) $\varepsilon = 0.0591$ and (b) $\varepsilon = 0.0354$.

Table 3.12

Values of $D^{o}_{HBr,m}$ and s at two different hydrogen bromide concentrations, ε .

ε	$10^4 D^o/m^2 s^{-1}$	s
0.0591	0.295 ± 0.106	0.761 ± 0.029
0.0354	0.335 ± 0.187	0.800 ± 0.045

The errors in D^{o} and s are significantly smaller than those for the previous experiment (table 3.8).

The computer programme written for the previous experiment (section 3.5.2) was adapted for the analysis of these hydrogen bromide results. Similar theoretical expressions (equations 1.18 and 1.19) were used to calculate a_{HBr} and b_{HBr} and the results are tabulated below (table 3.13).

Table 3.13

'Least squares fit' to experimental results (fig. 3.10) - gives values for D^{o}_{HBr,H_2} (the diffusion coefficient of HBr in hydrogen at 0°C) and for the numerical coefficient, s, using the second-order approximation to multicomponent diffusion.

Graham's Law approach	Minimum least squares deviation
$a_{HBr} = 9.33$, $b_{HBr} = 4.37$	$a_{HBr} = 10.83$, $b_{HBr} = 4.87$
Slope (lnD vs. lnT) $= 1.770 \pm 0.027$	Slope (lnD vs. lnT) $= 1.777 \pm 0.025$
Intercept $= -19.874 \pm 0.190$	Intercept $= -19.879 \pm 0.172$
$D^{o}_{HBr,H_2} = (0.479 \pm 0.165) \times 10^{-4}$	$D^{o}_{HBr,H_2} = (0.498 \pm 0.155) \times 10^{-4}$
$s = 0.770 \pm 0.027$	$s = 0.777 \pm 0.025$

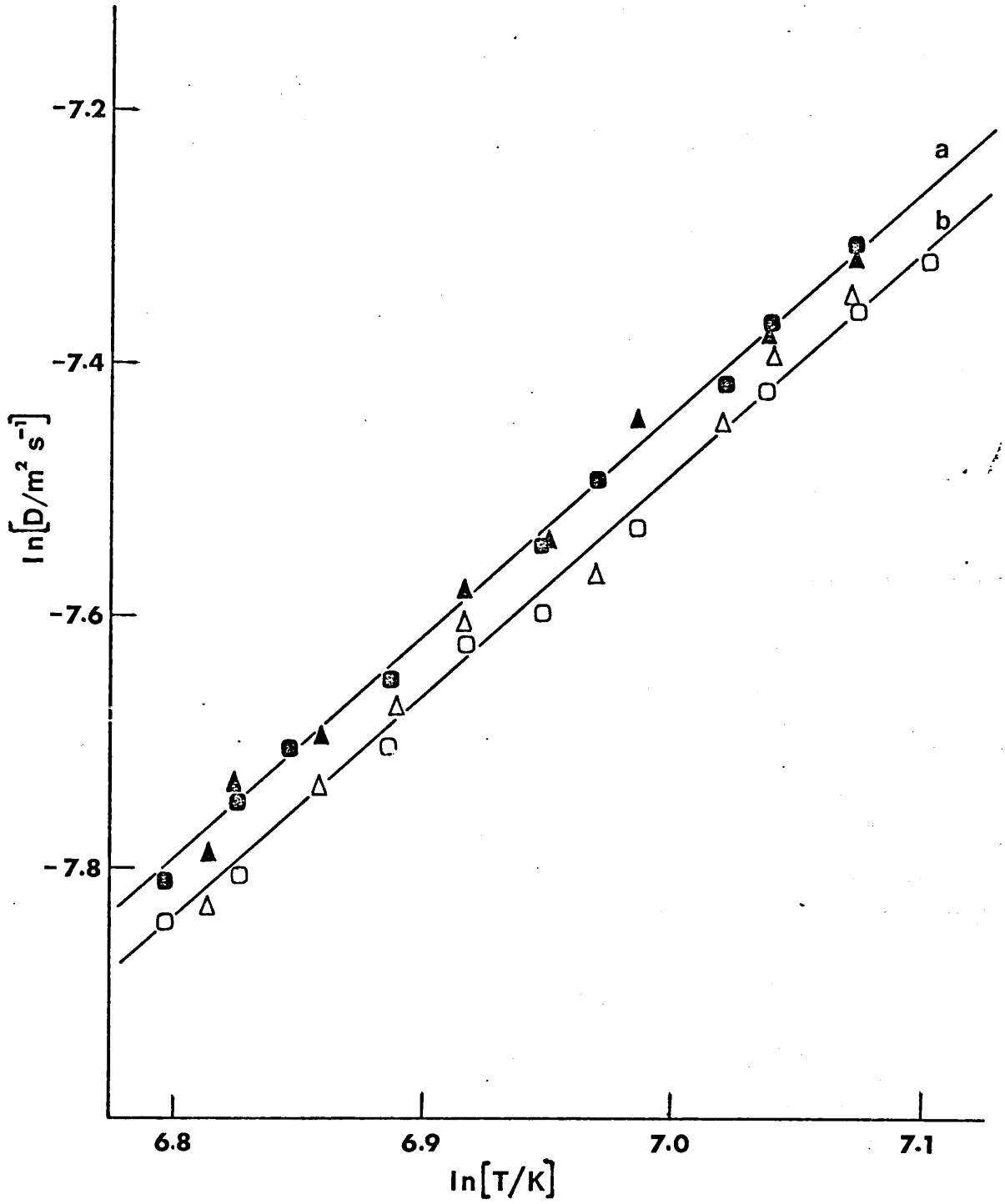

FIG. 3.10 Variation of D_{HBr,H_2} with temperature: Diffusion coefficients dependent on concentration.
a 'Least squares' fit ■ , ε = 0.0591; ▲ , ε = 0.0354.
b 'Graham's Law' fit □ , ε = 0.0591; △ , ε = 0.0354.

3.5.4 Discussion

The dominant transport reactions over our experimental temperature range are:

$$In(l) + HCl(g) \leftrightarrows InCl(g) + \tfrac{1}{2} H_2(g) \qquad (3.3)$$

$$In(l) + HBr(g) \leftrightarrows InBr(g) + \tfrac{1}{2} H_2(g) \qquad (3.4)$$

Equilibrium constants were estimated using literature data.[7,8,9,10] There is some uncertainty as to the correct value of ΔH_f^o (InBr(g)); however, using any of the reported values a large equilibrium constant is obtained ($> 10^{10}$) over the temperature range 800 - 1200 K. Similarly large equilibrium constants were found for reaction (3.3). The equilibria are thus well to the right and the partial pressures of the hydrogen halides over the indium in the capsule is nearly zero. Hence both the reactions are suitable for the investigation of gaseous interdiffusion as the rate of weight loss is entirely dependent on the rate of diffusion of hydrogen halide down the channel and not on the equilibrium constant for the transporting reaction.

The empirical approach described in sections 3.5.2 and 3.5.3 yields values for a_{HX} and b_{HX} which are in adequate agreement with estimated values. Small arbitrary changes in a_{HX} and b_{HX} make little difference to the least squares deviations in slope and intercept because of the scatter of experimental points. Final values from the 'least squares fit' are given in table 3.14.

Table 3.14

Empirical values of a_{HX}, b_{HX}, D^{o}_{HX,H_2} and s from the 'least squares fit'.

Indium-hydrogen chloride	Indium-hydrogen bromide
$a_{HCl} = 10.1 \pm 1.0$, $b_{HCl} = 8.4 \pm 1.0$	$a_{HBr} = 10.8 \pm 1.0$, $b_{HBr} = 4.9 \pm 1.0$
$D^{o}_{HCl,H_2} = (0.462 \pm 0.372) \times 10^{-4}$	$D^{o}_{HBr,H_2} = (0.498 \pm 0.155) \times 10^{-4}$
$s = 0.964 \pm 0.064$	$s = 0.777 \pm 0.025$

Owing to the considerable error in the results obtained from the transport of indium in hydrogen chloride experiment, no definite conclusions may be drawn from these results. However, the indium-hydrogen bromide results (table 3.12) do show that s is independent of ε, the fractional concentration of hydrogen bromide in the gas stream, within experimental error.

Using Graham's Law,[6] the expected ratio of the diffusivities of hydrogen chloride and hydrogen bromide in hydrogen is 1.49. This value lies within the error limits of the ratio of the experimental diffusion coefficients:

$$\frac{D^{o}_{HCl,H_2}}{D^{o}_{HBr,H_2}} = 0.928 \pm 0.931$$

The temperature dependence of D_{HCl,H_2} has been estimated from viscosity measurements by Weissman,[11] in the temperature range 294 - 523 K. These data yield $D^{o}_{HCl,H_2} = (0.57 \pm 0.04) \times 10^{-4} m^2 s^{-1}$.

3.6 References

1. D. Battat, M.M. Faktor, I. Garrett, R.H. Moss, J. Chem. Soc. Faraday Trans. I, 70, 2293 (1974).

2. S.W. Yardley, unpublished work.

3. D. Battat, M.M. Faktor, I. Garrett, R.H. Moss, J. Chem. Soc. Faraday Trans. I, 70, 2302 (1974).

4. J.A.N.A.F., Thermochemical Tables 2nd edition, U.S. Department of Commerce, National Bureau of Standards (1971).

5. A. Levy, J. Phys. Chem., 62, 570 (1958).

6. T. Graham, Phil. Trans. Roy. Soc., 136, 573 (1846).

7. 'Selected Values of Thermodynamic Properties', U.S. National Bureau of Standards, Tech. Note 270-3 (1968).

8. A.V. Sandulova, E.G. Zaidovskii, V.A. Prokhorov, Russ. J. Phys. Chem., 47(3), 429 (1973).

9. F.J. Smith, R.F. Barrow, Trans. Faraday Soc., 51, 1478 (1955).

10. R.F. Barrow, A.C.P. Pugh, F.J. Smith, Trans. Faraday Soc., 51, 1657 (1955).

11. S. Weissman, J. Chem. Phys., 40(11), 3397 (1964).

Chapter 4

Indium arsenide-hydrogen chloride and indium arsenide-hydrogen bromide systems

Chapter 4

4.1 Introduction

Chemical vapour transport reactions between Group $III_A - V_A$ compounds and the hydrogen halides find extensive use in the electronics industry for the deposition of thin films of these semiconductors. The reaction of gallium arsenide with hydrogen chloride has been the subject of various thermodynamic[1] and mass spectrometric[2] studies, usually in parallel with crystal growth experiments. The reactions of gallium arsenide with both hydrogen chloride and hydrogen bromide gases have been studied using the modified entrainment method.[3,4] The transport of indium arsenide by hydrogen halides, however, has not been so thoroughly investigated.

In this chapter, the transport of indium arsenide by hydrogen chloride and by hydrogen bromide is described in detail. A thermodynamic analysis of the transport reactions is carried out, starting with estimates from existing data (some of which is rather inaccurate). Computer fitting of the experimental curves permits the thermodynamic parameters of the transport reactions to be estimated with more confidence.

4.2 Experimental

The apparatus has been described in detail in section 2.2.

The indium arsenide sample was polycrystalline undoped material (MCP Electronics Ltd., see Appendix 6). It was washed in a 5% (by volume) bromine in methanol solution (previously saturated with nitrogen) then left to dry under anhydrous conditions.

Pieces off the InAs slab were then pulverised in an agate mortar and the powder introduced into the silica bottle via a fine glass funnel. After the bottle had been weighed it was kept in a desiccator prior to suspension from loop A of the electrobalance (see fig. 2.1). Rates of weight loss, $\dot{w}$, were recorded as a function of temperature and hydrogen halide concentration.

4.3 Results for the InAs/HCl system

Five experiments (4.3.1 - 4.3.5) were carried out under different conditions (see Table 4.1). All the experimental results are tabulated in Appendix 3 (Tables 1 - 5) and presented graphically as $\ln\dot{w}$ vs. inverse temperature in figures 4.1 - 4.3.

Table 4.1

InAs/HCl system - summary of experiments (4.3.1 - 4.3.5). The diameter of the channel of the silica bottle is given in mm (See Appendix 1).

Experiment	Sample	Figure	$\epsilon(= p_{HCl}/P)$	Channel d.	Comment
4.3.1	InAs(1)	4.1	0.0506	2 mm	Sample melted during experiment.
4.3.2	InAs(2)	4.1	0.0506	2 mm	Sample kept below melting point (1213 K)
4.3.3	InAs(3)	4.2	0.0506 0.0871	2 mm	Some results at end of experiment above m.pt. (ϵ = 0.0506).
4.3.4	InAs(4)	4.2	0.0506	1 mm	Last few results with melted sample.
4.3.5	In-InAs (5)	4.3	0.0506	2 mm	Sample consisted of 0.22 g InAs + 0.05g In. Last few results with melted sample.

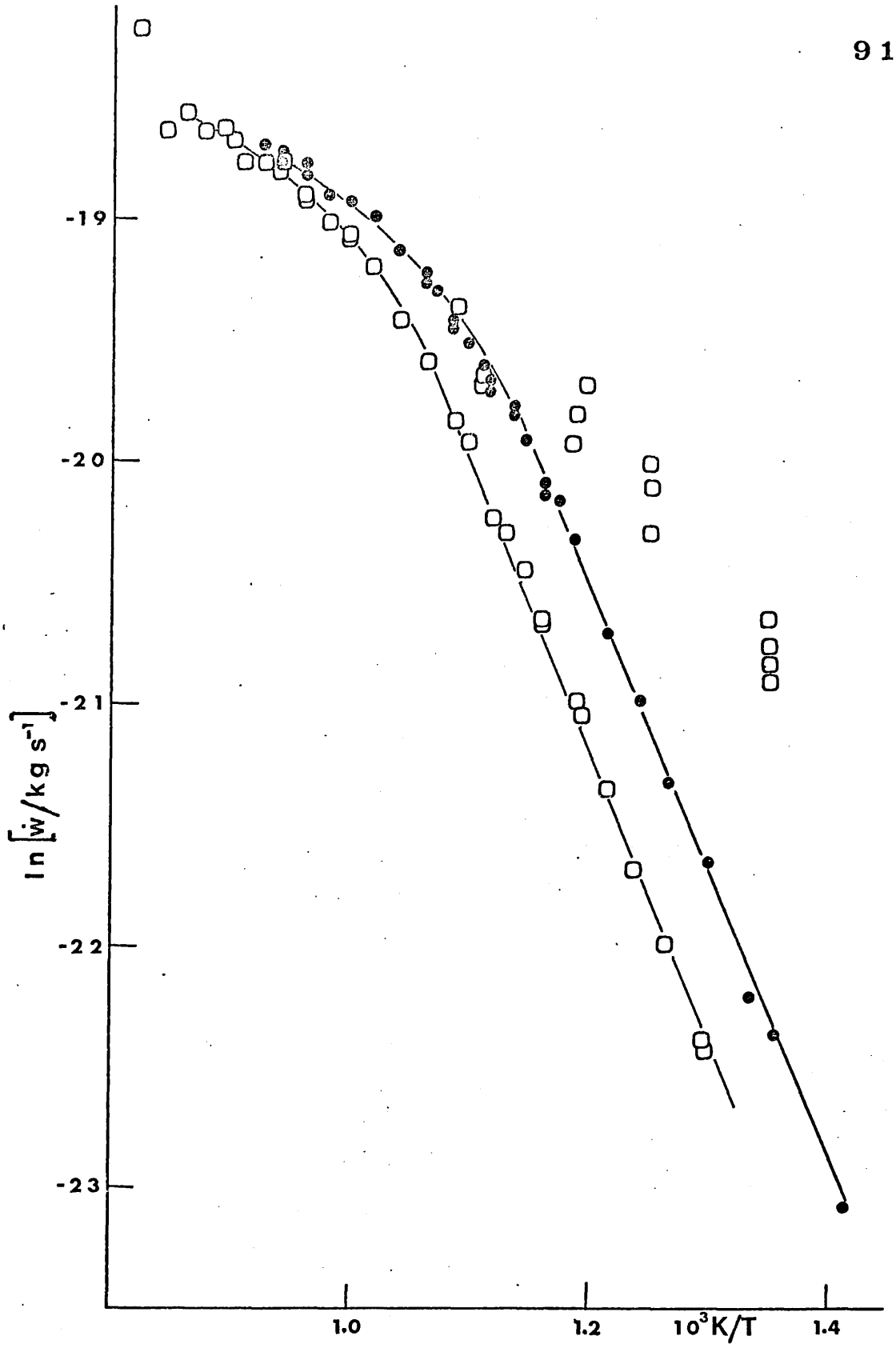

FIG. 4.1 Transport of InAs by HCl (ε = 0.0506)

□ Sample melted during experiment(4.3.1.).

• Sample kept below melting point for experiment(4.3.2).

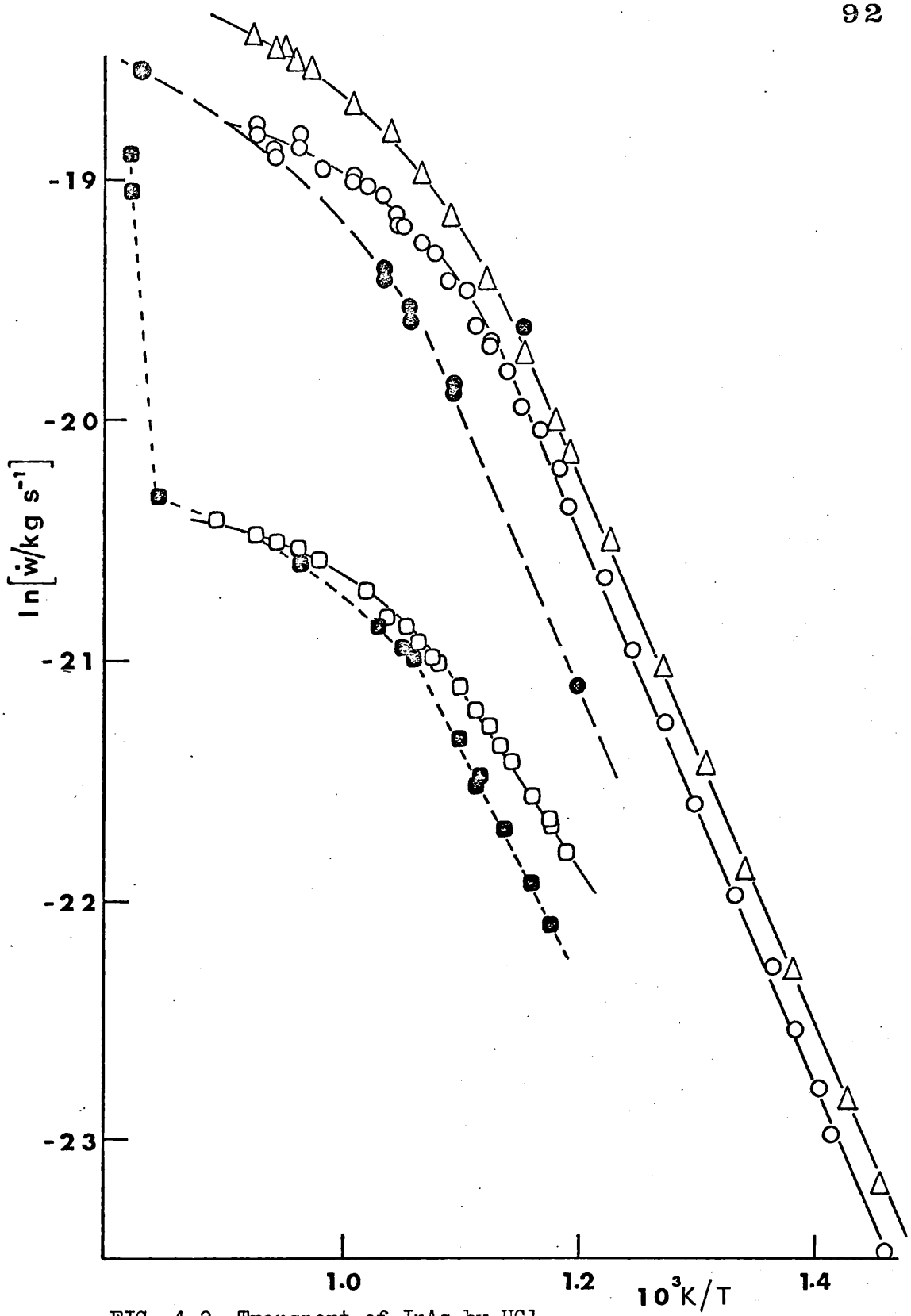

FIG. 4.2 Transport of InAs by HCl.

○ Experiment (4.3.3) $\varepsilon = 0.0506$ (2 mm diameter channel).

● As above with melted sample.

△ Experiment (4.3.3) $\varepsilon = 0.0871$ (2 mm diameter channel).

□ Experiment (4.3.4) $\varepsilon = 0.0506$ (1 mm diameter channel).

■ As above with melted sample.

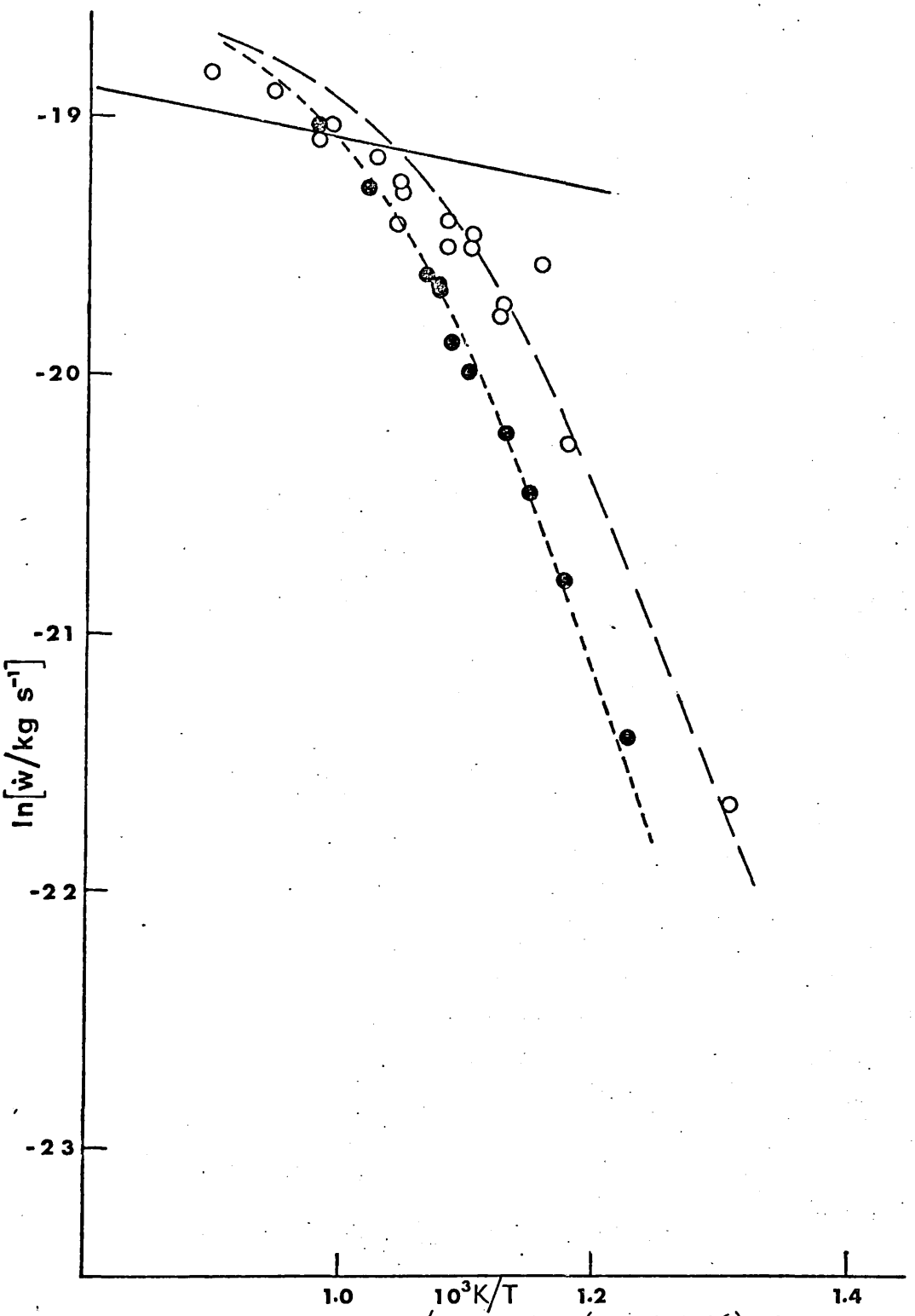

FIG. 4.3 Summary of InAs/HCl system ($\epsilon = 0.0506$), 2 mm diameter channel. Bold line In/HCl. Broken line InAs/HCl. Specked line InAs/HCl with sample melted.

○ In-InAs/HCl experiment (4.3.5).

● As above with sample melted.

4.4 Discussion

After the first few runs of experiment (4.3.1) the indium arsenide sample was melted and the consequent decrease in surface area of the sample was probably sufficient to cause the depression of rate of weight loss from its equilibrium value. The scattered points at much higher weight losses are more difficult to interpret. There are several possible explanations: a) the temperature of the sample had not equilibrated, b) some indium trichloride was formed at lower temperatures during equilibration and it was subsequently lost at a higher rate of weight loss, c) particular crystal faces or whiskers[5] were formed during lower temperature equilibration and these reacted preferentially at higher temperatures.

The results from the second experiment reproduce the pre-melting results of the first experiment (see fig. 4.1). The third experiment (fig. 4.2) not only confirms the line from the second experiment but also validates the post-melting line obtained in the first experiment.

Using a bottle with a narrower channel, a similar effect after melting was observed (fig. 4.2) to that in figure 4.1. However, the depression of weight loss after melting the sample was not so great, nor was it observed until lower temperatures.

The melting phenomenon can be explained in the following manner:- consider figure 4.4 where l is the length of the channel of the sample bottle and c its cross-sectional area, A is the surface area of the sample, $\dot{w}^{o}$ is the equilibrium $\dot{w}$ and $\dot{w}^{*}$ is the observed rate of weight loss (see section 1.4).

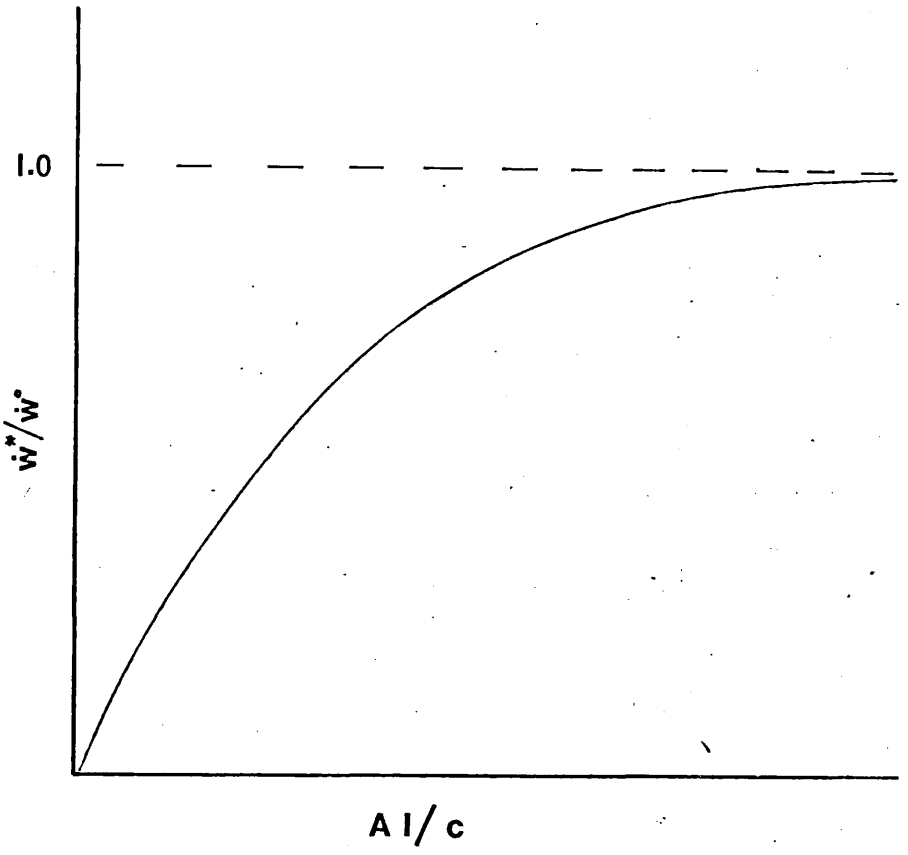

FIG. 4.4 Graph demonstrating the departure from equilibrium conditions in the bottle resulting from a decrease in channel resistance or surface area of the sample.

At high channel resistances (1/c large) equilibrium conditions are maintained in the bottle and a large decrease in A will only produce a small depression in $\dot{w}^*$ (the observed rate of weight loss). However, when using a larger diameter channel 1/c is small and the same decrease in surface area will result in a larger decrease in rate of weight loss. So for the wider channel bottle there is a greater departure from equilibrium conditions extending to higher temperatures than for the narrower channel bottle.

Each of the curves for experiments (4.3.1 - 4.3.4) exhibits two regions, a linear section and then a curved region at higher temperatures. It is likely that only one endothermic transport reaction is taking place in this system (with the $As_4 \leftrightharpoons 2As_2$ equilibrium also taking part):

$$InAs(c) + HCl(g) \leftrightharpoons InCl(g) + 1/4As_4(g) + \tfrac{1}{2}H_2(g) \qquad (4.1)$$

and it is dominant over the temperature range investigated. The curving off at higher temperatures is a result of the equilibrium constant for this dominant reaction becoming large (>10), see section 1.4 .

An x-ray diffraction analysis of three samples of InAs : a) stock, b) unmelted residue and c) post-melting residue, showed that the lattice parameters of all three samples were the same to within one part in 10^3. Hence, the lower curve produced after melting a sample is not due to the formation of a non-stoichiometric phase. In addition, the diffraction results indicated that free indium (a few per cent) was present in the melted residue. This excess of indium results from incongruent evaporation of InAs at high temperatures.

The In-InAs/HCl experiment (4.3.5) was designed to investigate the possibility of the presence of a second phase. The results of this experiment are compared with those from other systems, using the same value of ε , in figure 4.3. The high temperature points lie between the InAs curve and the In line for the same value of ε . At lower temperatures the results of the In-InAs/HCl experiment lie well below the In/HCl line but only very slightly above the InAs/HCl curve.

The presence of a small amount of indium in the InAs at high temperatures has the effect of reducing the rate of weight loss from the sample. However, at lower temperatures the presence of the excess indium slightly increases the rate of weight loss from the sample.

During the last few results for the In-InAs sample, the effect of melting was investigated. A few points were recorded above the melting point of indium arsenide and further points below. The latter results lay on the curve for the melted sample of InAs.

The results of experiment (4.3.5) illustrate the improbability of the presence of a second phase. However, they confirm that decreasing the surface area of a sample by melting causes a depression of the rate of weight loss.

4.5 Results for the InAs/HBr system

The results from these two experiments are tabulated in Appendix 3 (tables 6 - 7).

4.5.1 InAs/HBr (1)

The silica bottle with the 2 mm diameter channel was used for this experiment and $\varepsilon = 0.0354$. Results are presented graphically in figure 4.5, the last few points being recorded after the sample had been melted.

4.5.2 InAs/HBr (2)

A new sample was used for this experiment in the same 2 mm diameter channel bottle. A few initial points were taken to check the reproducibility of the results in (1), then a higher value of ε (0.0591) was investigated.

4.6 Discussion

Both curves (fig. 4.5) have two regions; the straight section at lower temperatures which probably represents the effect of the endothermic transport reaction:

$$InAs(c) + HBr(g) \leftrightharpoons InBr(g) + 1/4As_4(g) + \tfrac{1}{2}H_2(g) \qquad (4.2)$$

(in conjunction with the $As_4 \leftrightharpoons 2As_2$ equilibrium) and the curving off at higher temperatures due to the limitation of the reaction rate by the rate of diffusion of HBr down the channel (see section 1.4).

The effect of melting the sample was the same as in the InAs/HCl system; a depression of the rate of weight loss was observed. At lower temperatures some scatter of results was noted, this could be due to the presence of free bromine or to the formation of $InBr_3$. (During some of the low temperature GaAs/HBr results (chapter 5) a weight gain was recorded and the white sublimate in the furnace tube subsequently observed indicated that a tribromide had been formed).

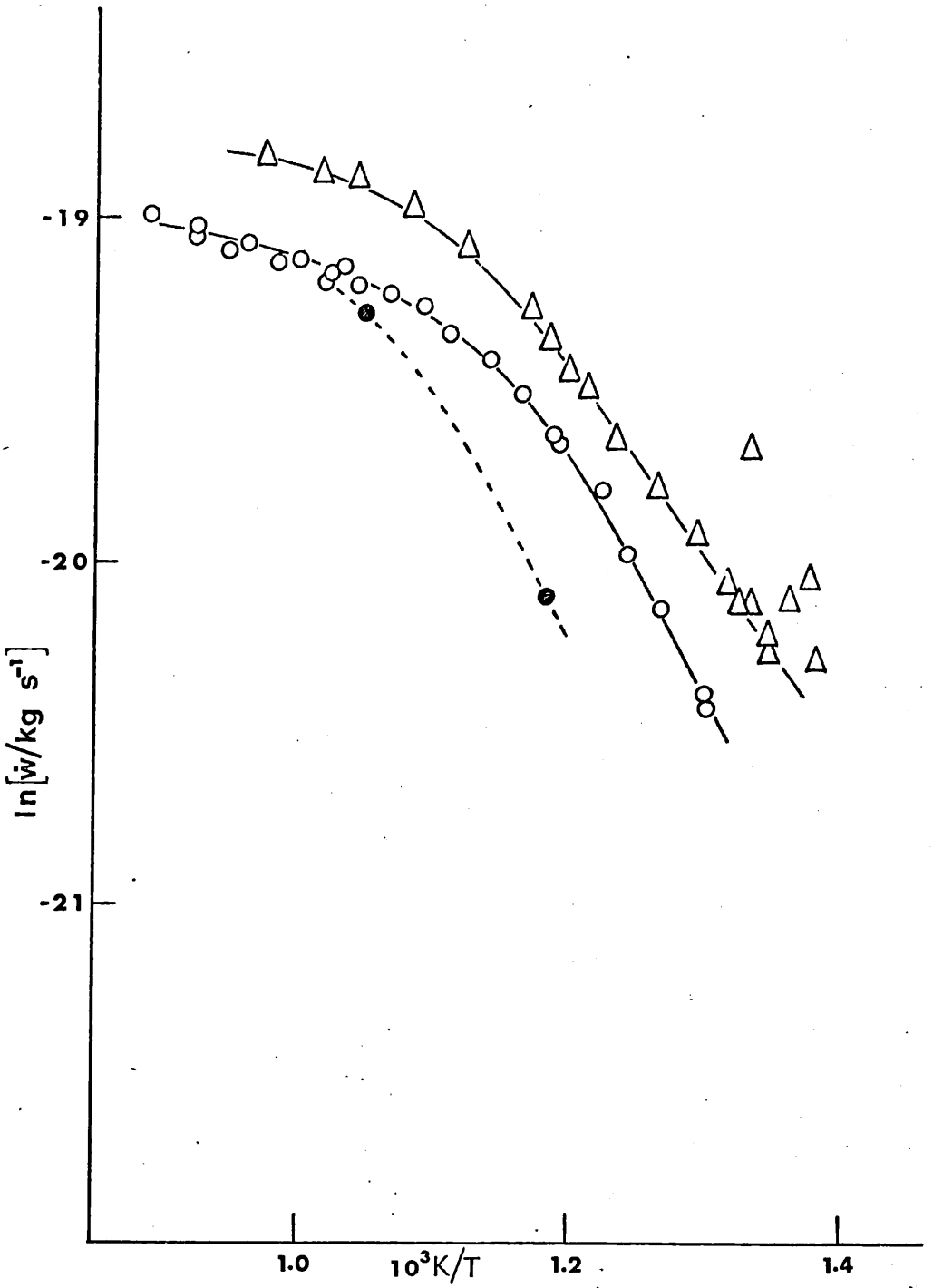

FIG. 4.5 Transport of InAs by HBr (2 mm diameter channel).

o Experiment (4.5.1), $\varepsilon = 0.0354$.

● As above with sample melted.

△ Experiment (4.5.2), $\varepsilon = 0.0591$.

4.7 Measurement of the heat capacity of indium arsenide using a Differential Scanning Calorimeter.

4.7.1 Introduction

The measurement of the heat capacity of a sample by means of a differential scanning calorimeter is an extension of the basic function of the calorimeter, which is to measure the power input to a sample required to maintain it at the same temperature as an inert reference material in the same environment.

The power to the individual heaters, located in the sample and reference holders, is varied continuously in response to sample thermal effects (this prevents the development of a differential temperature between the sample and the reference). The differential power provided is recorded as ordinate versus programmed temperature as abscissa.

4.7.2 Experimental

A Perkin-Elmer differential scanning calorimeter (Model DSC 2) was used with gold,volatile sample pans and a sapphire calibrant (Union Carbide Electronics). Temperature scans (usually of 100 K) were made at a scan speed of 10 K min^{-1} and a range setting corresponding to a full scale deflection of 8.4×10^{-3} J s^{-1}. For each scan, equilibrium isothermal base lines were recorded for the sapphire calibrant, the empty sample pans and for the powdered, polycrystalline InAs (MCP Electronics Ltd., see Appendix 6). Heat capacities were calculated at 10 K intervals in the temperature range 340 - 700 K.

The sample and reference system was slowly flushed with argon throughout this experiment.

Temperature calibration was carried out using the melting points of pure lead and indium as fixed points.

4.7.3 Results

The results are presented in Table 4.2 as heat capacities,

Table 4.2

Experimental Heat capacities of indium arsenide, C_p, at temperatures T

T/K	$C_p/JK^{-1}\ mol^{-1}$	T/K	$C_p/JK^{-1}\ mol^{-1}$
341.93	48.656	509.42	50.971
351.78	48.815	519.27	51.006
361.64	49.117		
371.49	49.109	519.27	51.157
		529.13	51.141
341.93	48.490	538.98	51.173
351.78	48.895	548.83	51.237
361.64	48.982	558.68	51.387
371.49	49.252	568.53	51.459
381.34	49.268	578.39	51.530
391.19	49.482	588.24	51.522
401.05	49.482	598.09	51.570
410.90	49.625		
420.75	49.696	607.94	51.467
430.60	49.720	617.80	51.606
		627.65	51.443
430.60	49.831	637.50	51.364
440.45	49.895	647.35	51.570
450.31	49.966	657.20	52.015
460.16	50.093	667.06	51.713
470.01	50.220	676.91	51.737
479.86	50.339	686.76	52.030
489.72	50.641	696.61	52.062
499.57	50.863		

C_p, at temperatures T, they were calculated using equation (4.3) and literature values[6] for C_p(sapphire).

$$C_p(\text{sample}) = C_p(\text{sapphire}) \left(\frac{\text{Amplitude sample}}{\text{Amplitude sapphire}}\right)\left(\frac{\text{Weight sapphire}}{\text{Weight sample}}\right) \quad (4.3)$$

The weights of InAs and sapphire used were 0.09505g and 0.03527g respectively (0.02542g sapphire for last range of temperature). Least squares analysis of the results yielded the following equation for the specific heat of InAs, C_p, at temperatures T:

$$C_p/JK^{-1}mol^{-1} = (9.6157 \pm 0.3635)\,10^{-3}(T/K) + (45.6746 \pm 0.1868) \quad (4.4)$$

A similar experiment was carried out on the DSC 2 using a programmable calculator (Tektronix Model 31) and aluminium,volatile sample pans. Results, computed at 2 K intervals, in the temperature range 364 - 452 K, yielded the following equation:

$$C_p/JK^{-1}mol^{-1} = (8.7023 \pm 1.0362)\,10^{-3}(T/K) + (46.0287 \pm 0.4208) \quad (4.5)$$

which confirms equation (4.4) within experimental error.

In figure 4.6 these results are compared with literature values.[7,8,9]

4.7.4 Discussion

The accuracy of the heat capacities obtained by the scanning calorimeter depends on the uncertainty in the heat capacity of sapphire ($\pm$ 0.08 JK^{-1} mol^{-1} at 300 K to $\pm$ 0.13 JK^{-1} mol^{-1} at 1000 K) and on the random error in measuring pen displacement ($\pm$ 1%). Including the error due to the noncoincidence of the isothermal base lines, an overall accuracy of $\pm$ 0.8 JK^{-1} mol^{-1} is estimated (probably better at lower temperatures due to superior base line stability).

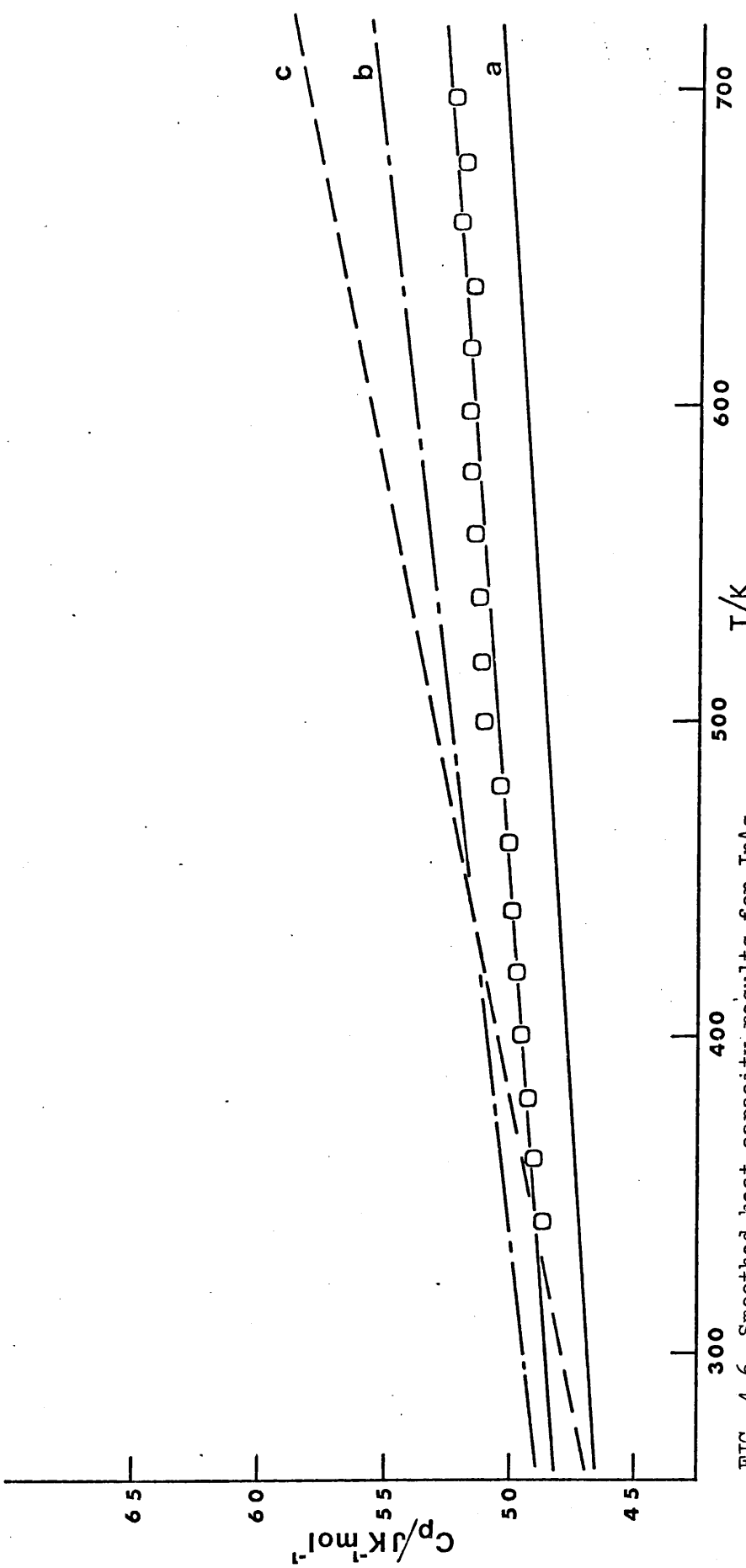

FIG. 4.6 Smoothed heat capacity results for InAs.
□ this work, equation (4.4), (a) Cox and Pool, (b) Lichter and Sommelet, (c) Kudman and Steigmeier.

These results, equation (4.4), are systematically higher than those of Cox and Pool (given by $C_p = 44.35 + 8.37 \times 10^{-3} T\ JK^{-1}\ mol^{-1}$) and lower than those of Lichter and Sommelet, see fig. 4.6. In ref. 7 the equation ($C_p = 40.04 + 0.0258T\ JK^{-1}\ mol^{-1}$) is derived using extrapolated C_p values for low temperatures.

4.8 Thermodynamic data for the reactions occurring in the InAs/HCl and InAs/HBr systems

The following reactions have been considered:-

$$InAs(c) + HCl(g) \leftrightarrows InCl(g) + 1/4As_4(g) + \tfrac{1}{2} H_2(g) \quad (4.6)$$

$$InAs(c) + 2HCl(g) \leftrightarrows InCl_2(g) + 1/4As_4(g) + H_2(g) \quad (4.7)$$

$$InAs(c) + 2HCl(g) \leftrightarrows \tfrac{1}{2}In_2Cl_4(g) + 1/4As_4(g) + H_2(g) \quad (4.8)$$

$$InAs(c) + HBr(g) \leftrightarrows InBr(g) + 1/4As_4(g) + \tfrac{1}{2}H_2(g) \quad (4.9)$$

$$InAs(c) + 2HBr(g) \leftrightarrows InBr_2(g) + 1/4As_4(g) + H_2(g) \quad (4.10)$$

In the temperature range investigated, the dissociation of As_4 must also be included:

$$As_4(g) \leftrightarrows 2As_2(g) \quad (4.11)$$

Thermodynamic data from various sources is presented in Table 4.3.

Table 4.3

Thermodynamic data at 298.15 K unless otherwise stated

	ΔH_f°/kJ mol^{-1}	S°/JK^{-1} mol^{-1}	C_p°/JK^{-1} mol^{-1}
InAs(c)	-58.58,[18] -64.02[11]	75.73[18]	47.78,[18] 48.54 (this work)
In(c)	0[18]	57.82[18]	26.74[18]
In(l)	3.26[17]	65.27[17]	
In(g)	243.30[18]	173.68[18]	20.84[18]
As_4(g)	143.93,[18] 156.23[13]±.84	313.8[18]	
As_4(c)			98.58[18]
As_2(g)	222.17,[18] 190.54[13]±2.09	239.33,[18] 425.14[14] (1000 K)	
InCl(g)	-75.3,[18] -74.06[12]	245.60[19](p.219)	37.656[19](p.204)
$InCl_2$(g)	-96.23,[12] -184(est)	338.9[19](p.219)	
$InCl_3$(g)	-374.05[18]	451.9[10](1044 K)	
In_2Cl_4(g)	-807.5[10] (1044 K)	702.9[10](1044 K)	
HCl(g)	-92.31[18]	186.799[18]	29.12[18]
Cl(g)	121.68[18]	165.09[18]	21.84[18]
Cl_2(g)	0[18]	222.96[18]	33.91[18]
HBr(g)	-36.44[15], - 15.02[15] (1000 K)	198.57,[15] 234.9[15] (1000 K)	29.12,[15] 32.30[15] (1000 K)
Br(g)	111.88[18]	174.91[18]	20.79[18]
Br_2(g)	30.91[18]	245.38[18]	36.07[18]
InBr(g)	-56.90,[18] -12.55[16]	259.37,[18] 277.8[16]	36.65[18]

The seccnd value given for $\Delta H^{o}_{f}(InCl_2(g))$ is estimated from bond energies. Data for the indium bromides is very scarce. Three values are considered here: $\Delta H^{o}_{f}(InBr(g), 1000K) = 12.6, -33.5$ and -75.3 kJ mol^{-1}. The first is a bond energy estimate, the second is derived from a paper by Sandulova[16] who measured the temperature dependence of a chemical vapour deposition equilibrium and the last is calculated using the calorimetric results described in references 20 and 21. S^{o} (InBr(g), 1000 K) is also uncertain; references 19 and 22 are used with Sandulova's[16] results to estimate a value. The As_4 dissociation has been studied by Murray, Tupp and Pottie[23] and a value for the equilibrium constant of reaction (4.11) is calculated from their work:

$$K_2 = \exp((-26270/T) + 17.106)$$

The entropy and enthalpy changes calculated for reactions (4.6) to (4.9) are given in table (4.4).

Table 4.4

Enthalpy and entropy changes for the transport reactions considered

Reaction	Gaseous indium halide	ΔH_{1000}/kJ mol^{-1}	ΔS_{1000}/$JK^{-1}mol^{-1}$
4.6	InCl	114.44	120.60
4.7	$InCl_2$	103.98 or 191.8	91.94
4.8	In_2Cl_4	-115.68	41.73
4.9	InBr	116.2 ± 37.7	122.1 ± 7.5

Insufficient data are available to calculate the parameters for equation (4.10).

The value of ΔH_{1000} for reaction (4.8) is surprising and throws some doubt on $\Delta H_f^o(In_2Cl_4)$, see table (4.3).

4.9 Computer analysis of the InAs/HCl and InAs/HBr systems

4.9.1 Introduction

In Appendix 4 the master equations (B.17) and (C.5) are derived for the InAs/HBr and InAs/HCl systems respectively. These relate the rate of weight loss, $\dot{w}$, to the equilibrium constants K_1 and K_2 for the reactions considered. K_2(the equilibrium constant for the As_4/As_2 equilibrium) is known, γ (the second order correction for multicomponent diffusion) may be calculated and ξ is a function of $\dot{w}$, T and the diffusion coefficient of the hydrogen halide in hydrogen. The master equations may be solved for any chosen combination of ΔH_1 and ΔS_1 (the enthalpy and entropy changes for reaction 1) and the rate of weight loss expected calculated as a function of temperature. Programmes were developed (Appendix 4D) to find the set of values of the thermodynamic parameters which gave the best fit to the experimental results. To save computer time, the search was restricted to values close to those estimated from the literature. These computer programmes were written in Fortran and run on the University of London CDC 6600.

4.9.2 Results of the computer analysis of the InAs/HCl system

Experimental results from melted samples are ignored in this analysis; the data presented in figure 4.2 is used. All the experimental curves obtained for this system indicate that only one

endothermic transport reaction is significant. The curving off of the ln $\dot{w}$ vs. inverse temperature plots at high temperatures is due to the equilibrium constant for the transport reaction becoming so large that the rate of weight loss is diffusion limited and depends only on D_{HCl/H_2}. The thermodynamic effect of the dissociation of As_4 to $2As_2$ is included over the temperature range investigated.

The results of the InAs/HCl experiment (4.3.4) (using the silica bottle with the 1 mm diameter channel) were analysed first.

Thermodynamic data from table 4.4 indicates that the participation of $InCl_3(g)$ can be excluded since the transport reaction taking place is endothermic. Two computer analyses were carried out on the InAs/HCl system, one including both $InCl(g)$ and $InCl_2(g)$ and the other omitting $InCl_2(g)$. It was found that $InCl_2(g)$ was not present to a significant extent.

The "best fit" theoretical curve is presented graphically in figure 4.7 and the cross-sections giving the shape of the minimum for 36 points (SIG_2^2 (see Appendix 4D) as a function of ΔH and ΔS for the transport reaction) are shown in figure 4.8.1. The value of $D_{HCl/H_2}{}^{24}$ was taken as $0.54 \times 10^{-4} \left(\frac{T}{273.15}\right)^{1.8}$ $m^2 s^{-1}$ which lies within the error limits of the value calculated in section 3.5.2.

A similar procedure was followed with the results from the 2 mm diameter channel bottle experiment. Theoretical curves are plotted in figure 4.7 and cross-sections in figures 4.8.2 and 4.8.3.

4.9.3 Results of the computer analysis of the InAs/HBr system

The experiments on this system (section 4.5) were carried out using a silica bottle with a 2 mm diameter channel. The curves,

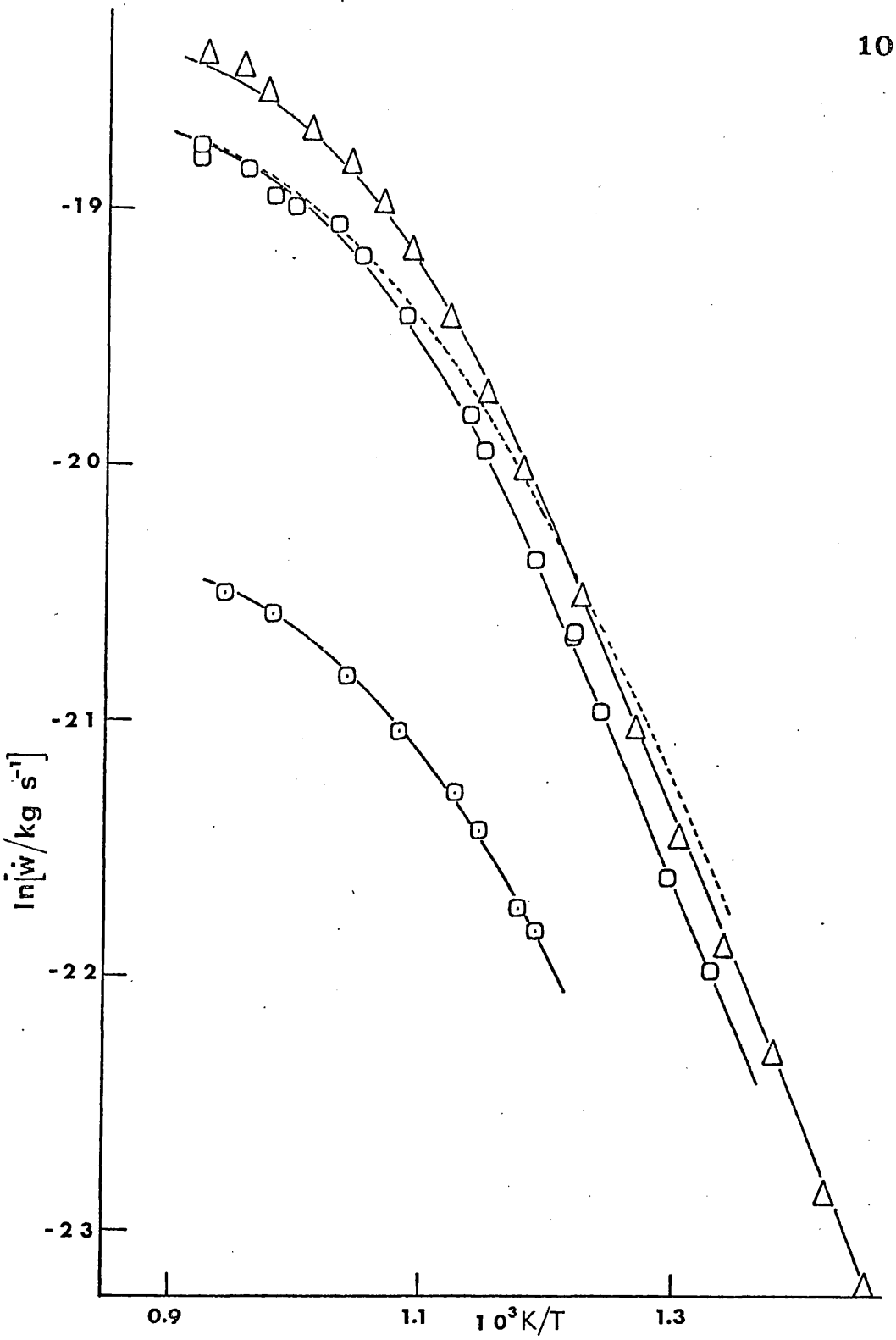

FIG. 4.7 Theoretical 'best fit' curves for the InAs/HCl system.

⊡ 1 mm diameter channel, $\varepsilon = 0.0506$, $H = 113$ kJ mol^{-1}, $S = 118$ JK^{-1}mol^{-1}

□ 2 mm " " , $\varepsilon = 0.0506$, $H = 123$ " , $S = 127$ "

△ 2 mm " " , $\varepsilon = 0.0871$, $H = 123$ " , $S = 126$ "

'scaled' 2 mm " " , $\varepsilon = 0.0506$, $H = 113$ " , $S = 118$ "

shown by a specked line.

Bold line, H constant

Dashed line, S constant.

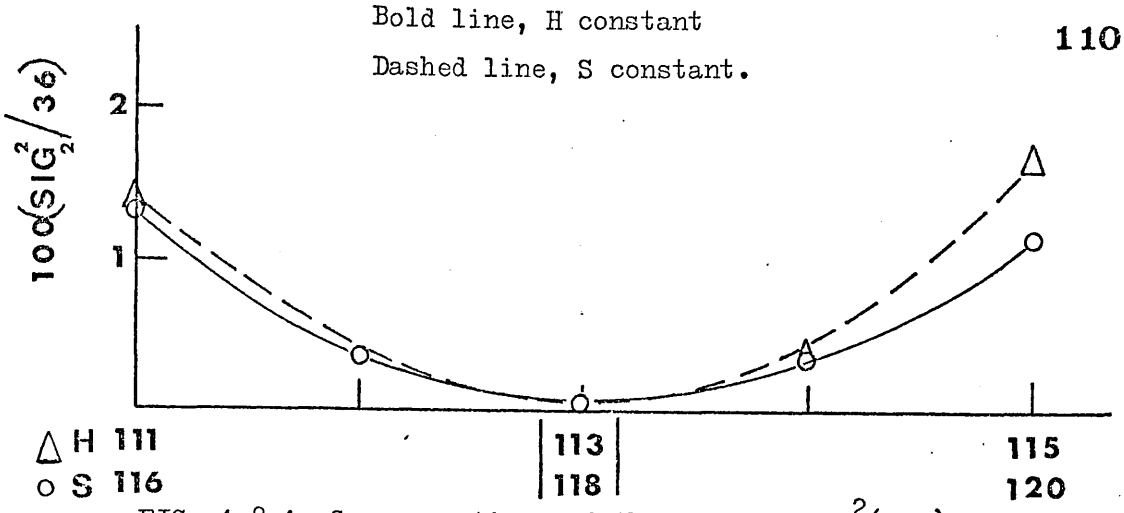

FIG. 4.8.1 Cross-sections of the minimum $SIG_2^2(H,S)$ for 36 points. InAs/HCl system (1 mm channel), $\varepsilon^2 = 0.0506$, $\Delta H = 113$ kJ mol^{-1} $\Delta S = 118$ J mol^{-1}K^{-1}.

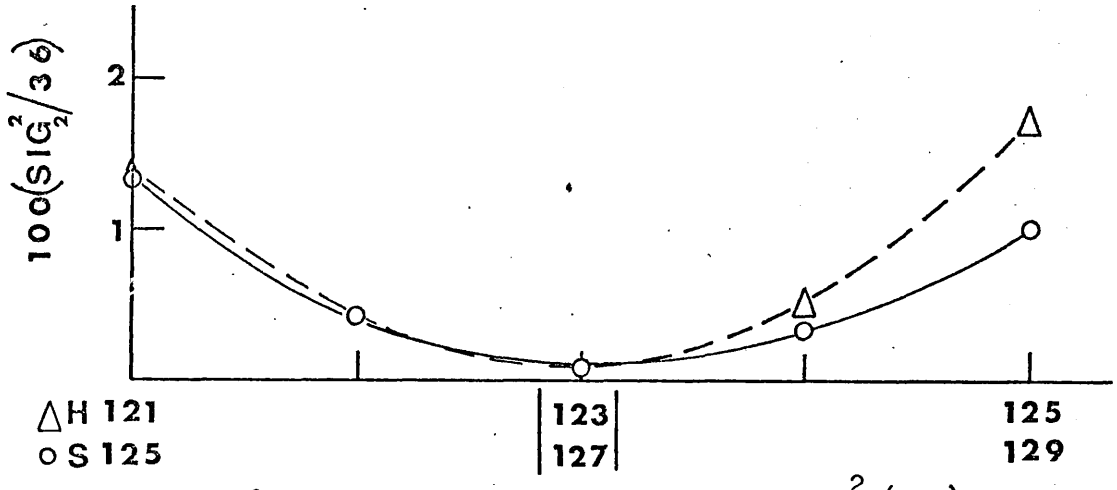

FIG. 4.8.2 Cross-sections of the minimum SIG_2^2 (H,S) for 36 points. InAs/HCl system (2 mm channel), $\varepsilon^2 = 0.0506$, $\Delta H = 123$ kJ mol^{-1} $\Delta S = 127$ J mol^{-1}K^{-1}.

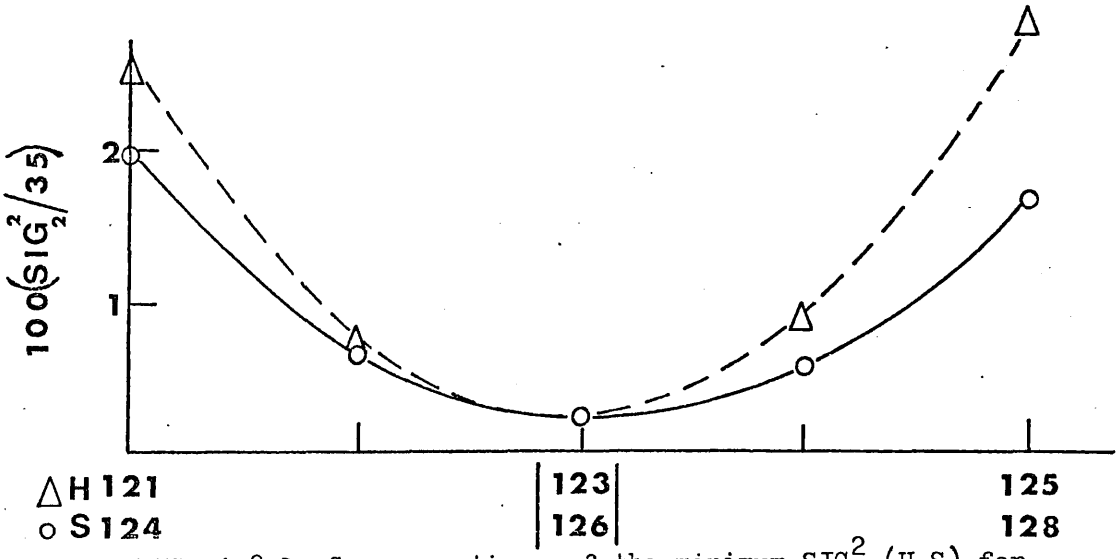

FIG. 4.8.3 Cross-sections of the minimum SIG_2^2 (H,S) for 35 points. InAs/HCl system (2 mm channel), $\varepsilon^2 = 0.0871$, $\Delta H = 123$ kJ mol^{-1} $\Delta S = 126$ J mol^{-1}K^{-1}.

presented in fig. 4.5, show that, in addition to the dissociation of As_4 to As_2, only one endothermic transport reaction is taking place. At high temperatures the equilibrium constant for the transport reaction becomes large and the rate of weight loss is diffusion limited (depends on D_{HBr/H_2}).

The value of D_{HBr/H_2} is taken from section 3.5.3 and the thermodynamic data from Table 4.4.

The "best fit" theoretical curves are presented graphically in figure 4.9 and the cross-sections, for each ε , giving the shape of the minimum (SIG_2^2, see Appendix 4D, as a function of ΔH and ΔS) are shown in figures 4.10.1 and 4.10.2.

4.9.4 Discussion of the computer analysis results

The results are summarised in table 4.5.

Table 4.5

Computed enthalpies and entropies for the transport reactions:

$InAs(c) + HX(g) \leftrightarrows InX(g) + 1/4As_4(g) + \frac{1}{2}H_2(g)$ (X = Cl, Br)

System	ΔH/kJ mol^{-1}	ΔS/$JK^{-1}mol^{-1}$
InAs/HCl (1 mm channel) ε = 0.0506	113.0 $\pm$ 1.0	118.0 $\pm$ 1.0
InAs/HCl (2 mm channel) ε = 0.0506	123.0 $\pm$ 1.0	127.0 $\pm$ 1.0
InAs/HCl (2 mm channel) ε = 0.0871	123.0 $\pm$ 1.0	126.0 $\pm$ 1.0
InAs/HBr (2 mm channel) ε = 0.0354	102.0 $\pm$ 2.0	118.0 $\pm$ 2.0
InAs/HBr (2 mm channel) ε = 0.059	100.0 $\pm$ 3.0	115.0 $\pm$ 3.0

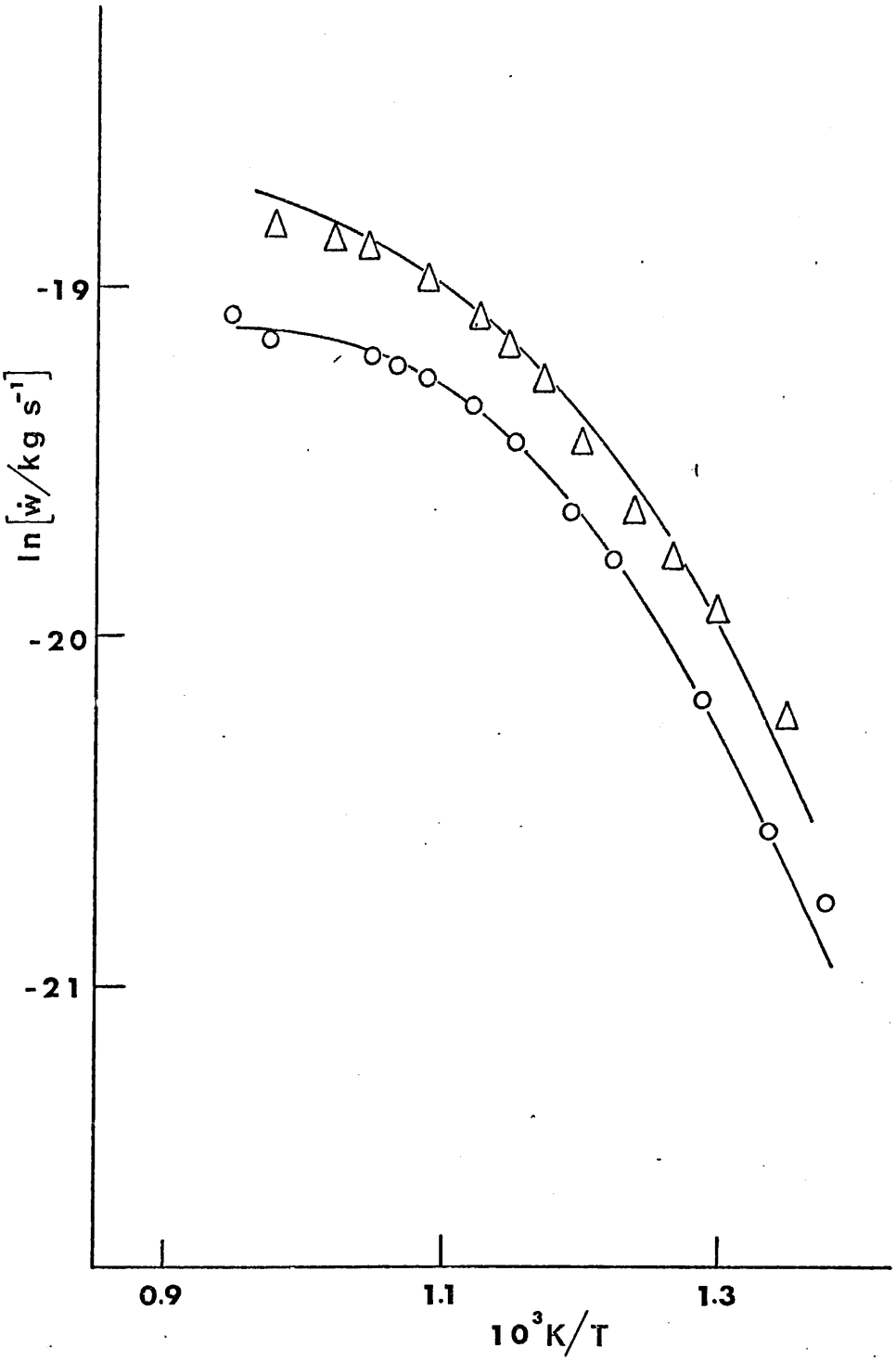

FIG. 4.9 Theoretical 'best fit' curves for InAs/HBr system.

o $\varepsilon = 0.0354$, $\Delta H = 102$ kJ mol^{-1}, $\Delta S = 118$ JK^{-1} mol^{-1}.

Δ $\varepsilon = 0.059$, $\Delta H = 100$ kJ mol^{-1}, $\Delta S = 115$ JK^{-1} mol^{-1}.

Bold line, H constant.
Dashed line, S constant.

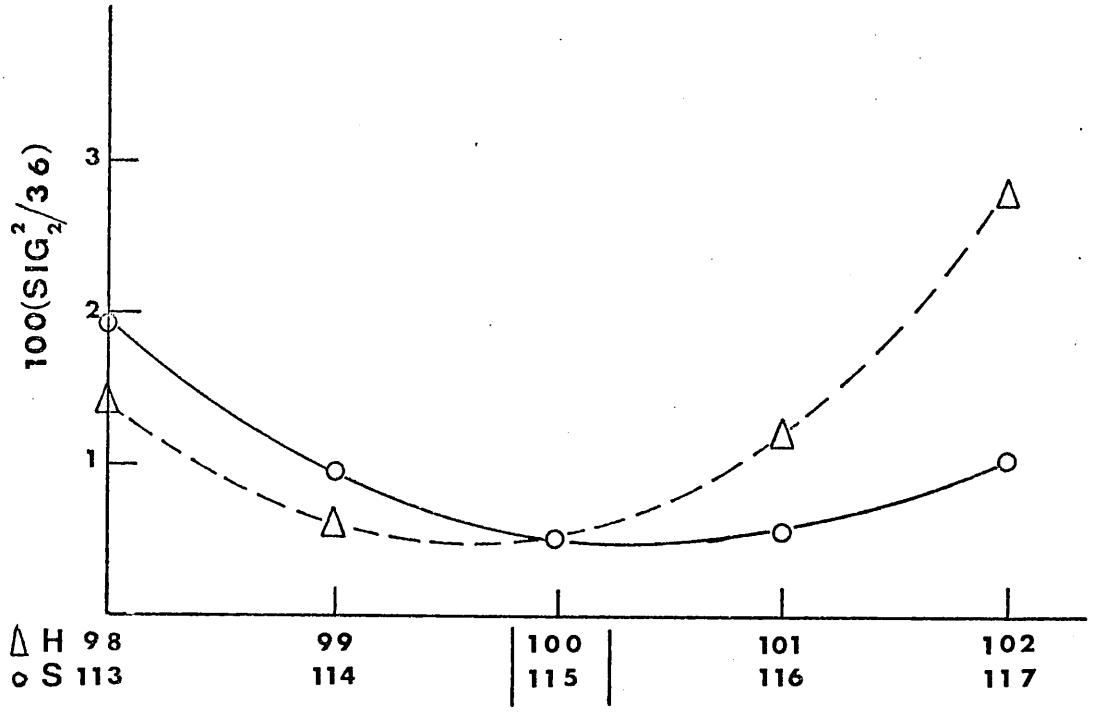

FIG. 4.10.1 Cross-sections of the minimum SIG_2^2 (H,S) for 36 points. InAs/HBr system, $\varepsilon = 0.059$, $\Delta H = 100$ kJ mol^{-1}, $\Delta S = 115$ JK^{-1}mol^{-1}.

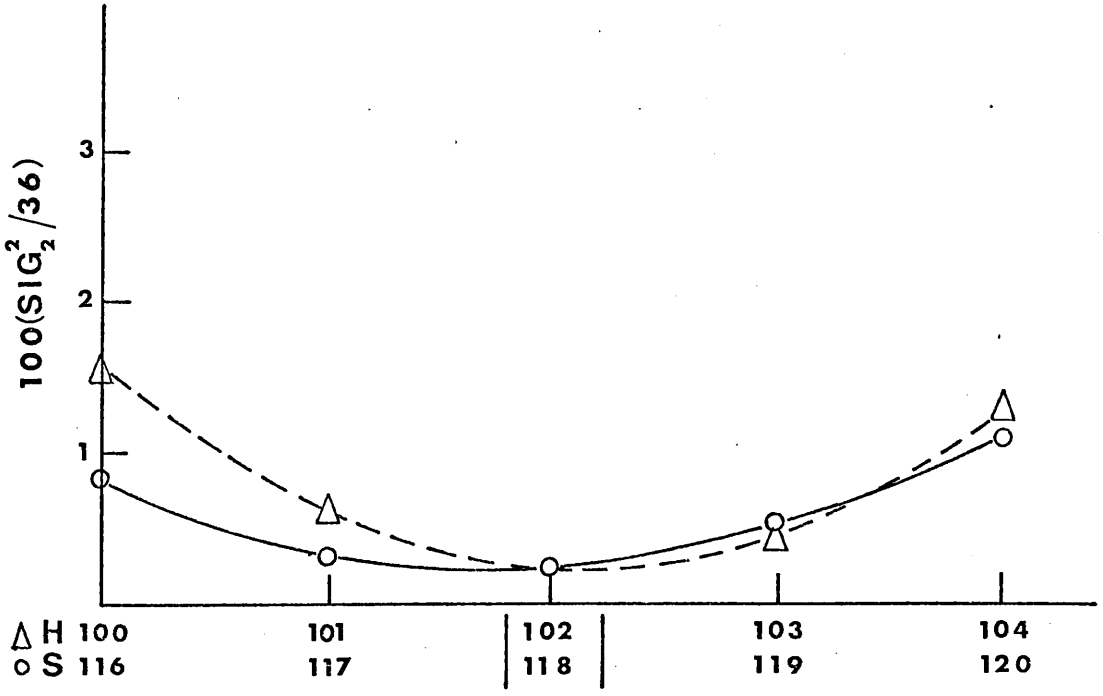

FIG. 4.10.2 Cross-sections of the minimum SIG_2^2 (H,S) for 36 points. InAs/HBr system, $\varepsilon = 0.0354$. $\Delta H = 102$ kJ mol^{-1}, $\Delta S = 118$ JK^{-1}mol^{-1}.

The "best fit" results obtained for the InAs/HCl system (reaction 4.6) using the 1 mm diameter channel bottle compare favourably with those calculated from the literature (table 4.4). However, the enthalpies and entropies computed for the same reaction from the results obtained using the 2 mm diameter channel bottle are both significantly higher than the calculated values. A possible explanation for this is that equilibrium conditions do not obtain when the diffusive resistance is low (2 mm diameter channel bottle). It has been assumed so far that equilibrium inside the bottle is closely approached because either the channel is sufficiently resistive to partial pressure flows or the surface area of the sample is large enough to compensate quickly for weight loss. Departure from equilibrium is explored, using the GaAs/HBr system, in chapter 5.

The InAs/HBr curves proved more difficult to fit. The initial calculated enthalpies and entropies for the transport reaction (4.9) are more uncertain. The "best fit" value for ΔH indicates that $\Delta H_f^o(InBr(g), 1000\ K)$ should be approximately -53 kJ mol^{-1}. If this system is also tending towards non-equilibrium conditions then ΔH could become low enough to confirm Smith and Barrow's result[20,21]:

$\Delta H_f^o(InBr(g),\ 1000\ K) = -75.3\ kJ\ mol^{-1}$.

Although the results for these two systems cannot be analysed confidently because of the possibility of a departure from equilibrium, they still provide valuable information to Crystal growers. The ln $\dot{w}$ vs. inverse temperature plots give a direct quantitative measure of the maximum thermodynamic efficiency of the vapour transport systems.

4.10 References

1. A. Boucher, L. Hollan, J. Electrochem. Soc., 117, 932 (1970).
2. V.S. Ban, J. Electrochem. Soc., 119, 761 (1972).
3. D. Battat, M.M. Faktor, I. Garrett, R.H. Moss, J. Chem. Soc. Faraday Trans. 1, 70, 2302 (1974).
4. M.M. Faktor, I. Garrett, M.H. Lyons, R.H. Moss, J. Chem. Soc. Faraday Trans. 1, 73, 1446 (1977).
5. "Compound Semiconductors", 1 (1962) Reinhold Publ. Co., editors R. Willardson, H. Goering.
6. D.C. Ginnings, G.T. Furukawa, J. Amer. Chem. Soc., 75, 522 (1953).
7. I. Kudman, E. Steigmeier, Phys. Rev., 133A, 1665 (1964).
8. R.H. Cox, M.J. Pool, J. Chem. Eng. Data, 12, 247 (1967).
9. B.D. Lichter, P. Sommelet, Trans. Met. Soc. AIME, 245, 1021 (1969).
10. Y. Kuniya, M. Hosaka, J. Crystal Growth, 28, 385 (1975).
11. C. Pupp, J. Murray, R. Pottie, J. Chem. Thermodynamics, 6, 123 (1974).
12. O.G. Polyachenok, O.N. Komshilova, High Temp. USSR, 10(1), 195 (1972).
13. H. Rau, J. Chem. Thermodynamics, 7, 27 (1975).
14. R.J. Capwell, G.M. Rosenblatt, J. Mol. Spectroscopy, 33, 525 (1970).
15. J.A.N.A.F., Thermochemical Tables 2nd edition, U.S. Department of Commerce, National Bureau of Standards (1971).
16. A.V. Sandulova et al, Russian J. Phys. Chem., 47(3), 429 (1973).
17. D.R. Stull, G.C. Sinke, "Thermodynamic Properties of the Elements", American Chemical Society (1956).

18. 'Selected Values of Chemical Thermodynamic Properties', U.S. National Bureau of Standards, Tech. Note 270-3 (1968).

19. O. Kubaschewski, E.L. Evans, C.B. Alcock, 'Metallurgical Thermochemistry', Pergamon Press (1967).

20. F. Smith, R.F. Barrow, Trans. Faraday Soc., 51, 1478 (1955).

21. R.F. Barrow, A.C.P. Pugh, F. J. Smith, Trans. Faraday Soc., 51, 1657 (1955).

22. V.O. Voronin et al., Inorg. Materials, 8, 1151 (1972).

23. J.J. Murray, C. Pupp, R.F. Pottie, J. Chem. Phys., 58, 2569 (1973).

24. D. Battat, M.M. Faktor, I. Garrett, R.H. Moss, J. Chem. Soc., Faraday Trans. 1, 70, 2293 (1974).

Chapter 5

The gallium arsenide-hydrogen bromide system

Chapter 5

5.1 Introduction

The modified entrainment method[1-4] has been described in previous chapters in connection with measurements of vapour pressures and diffusion coefficients and the investigation of the thermodynamics of various transport reactions. It has been assumed so far that the pressure inside the sample bottle differs from the equilibrium value by an insignificant amount. For this assumption to be valid, either the channel of the bottle must be sufficiently resistive, or the sample surface area be large enough to compensate quickly for the weight loss from the sample. If these constraints are relaxed then the rate of weight loss, which is a function of the partial pressures, now measures pressures which are determined by surface kinetics. A brief outline of the mathematical formalism[5] which relates the modified entrainment results to surface kinetics is given in section 1.4 .

This chapter describes the study of the transport of gallium arsenide by hydrogen bromide gas[6] using three sample bottles having different capillary dimensions and hence differing diffusive resistances. By decreasing the resistance of the capillary and decreasing the surface area of the sample it is shown that the rate of weight loss of the sample is not only controlled by vapour transport but also by the rates of surface reactions. A computer analysis is carried out on the experimental results to obtain thermodynamic data for the transport reactions. The influence of surface kinetics on these results is discussed.

5.2 Experimental

The apparatus has been described in detail in section 2.2.

The polycrystalline gallium arsenide sample (MCP Electronics Ltd., see Appendix 6) was ground, using a glass pestle and mortar, under anhydrous conditions. Three different silica sample bottles were used having 1 mm, 2 mm or 3 mm diameter channels (see Appendix 1). The bottle, containing the sample, was suspended from loop A of the electrobalance by means of a long silica fibre (see fig. 2.1). Rates of weight loss, $\dot{w}$, were recorded as a function of temperature and hydrogen bromide concentration, the hydrogen bromide being generated in situ (see chapter 3).

5.3 Results

Five experiments were completed (5.3.1 - 5.3.5) under various conditions (see table 5.1). All the experimental results are tabulated in Appendix 5 (tables 1 - 5) and presented graphically as ln $\dot{w}$ vs. inverse temperature in figures 5.1 - 5.3.

5.4 Discussion

The initial experiment with the 3 mm diameter channel bottle (5.3.2) used a fairly coarse sample since fine grinding was not required to introduce the sample into the bottle.

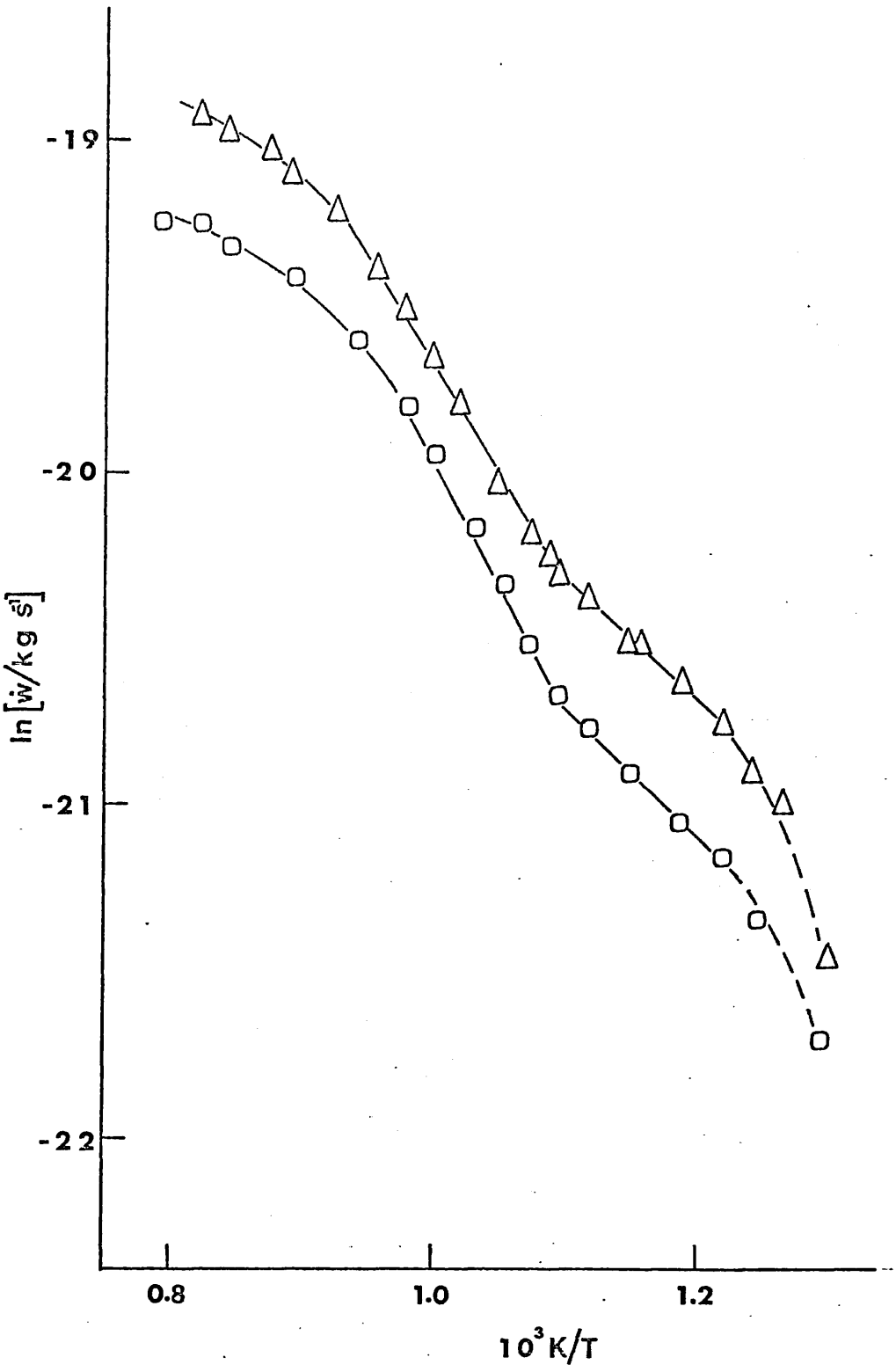

FIG. 5.1 GaAs/HBr system, 2 mm diameter channel

□ $\varepsilon = 0.0354$

△ $\varepsilon = 0.0591$

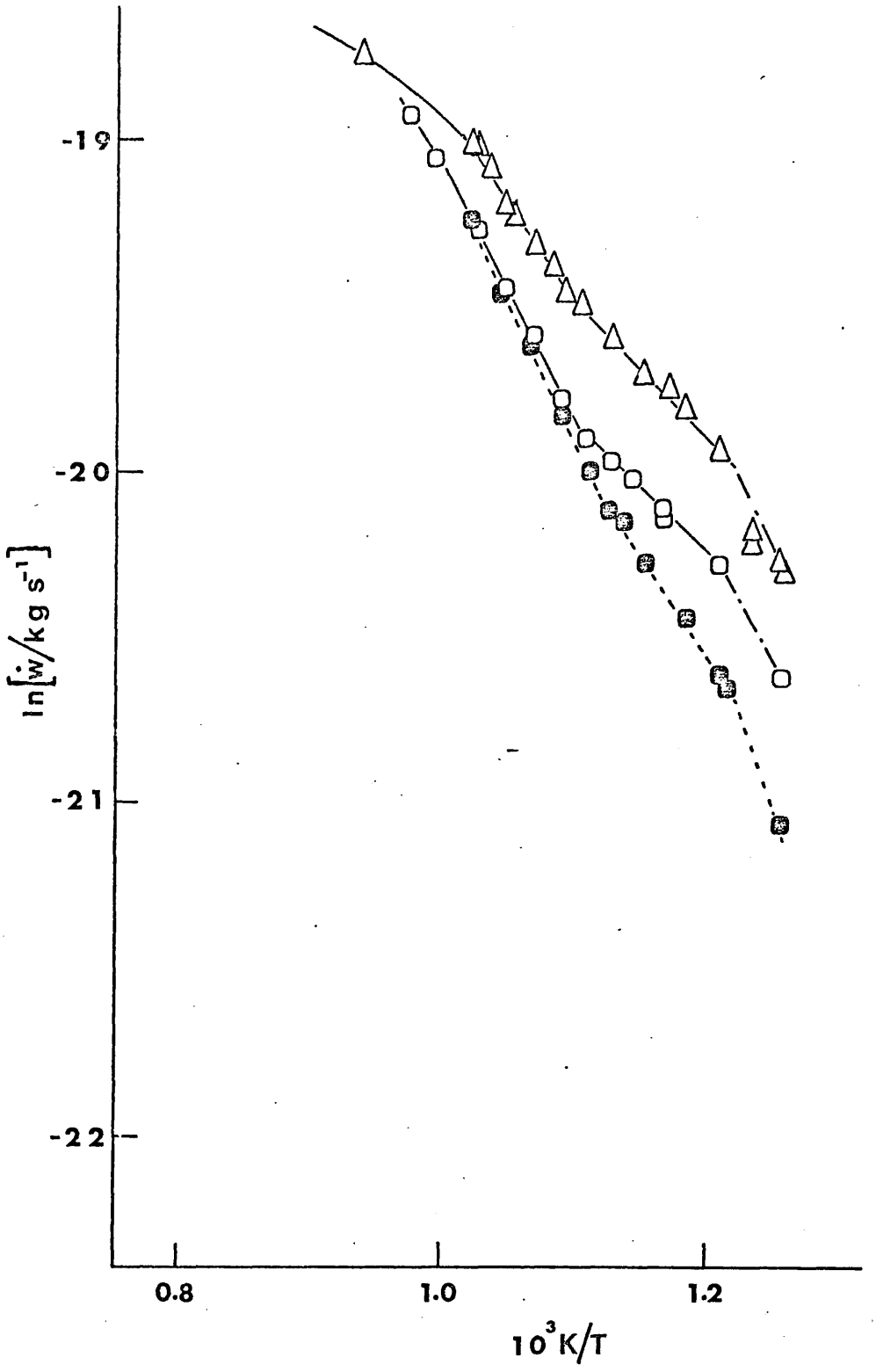

FIG. 5.2 GaAs/HBr system, 3 mm diameter channel.

△ $\varepsilon = 0.0591$

□ $\varepsilon = 0.0354$

■ $\varepsilon = 0.0354$, coarse sample.

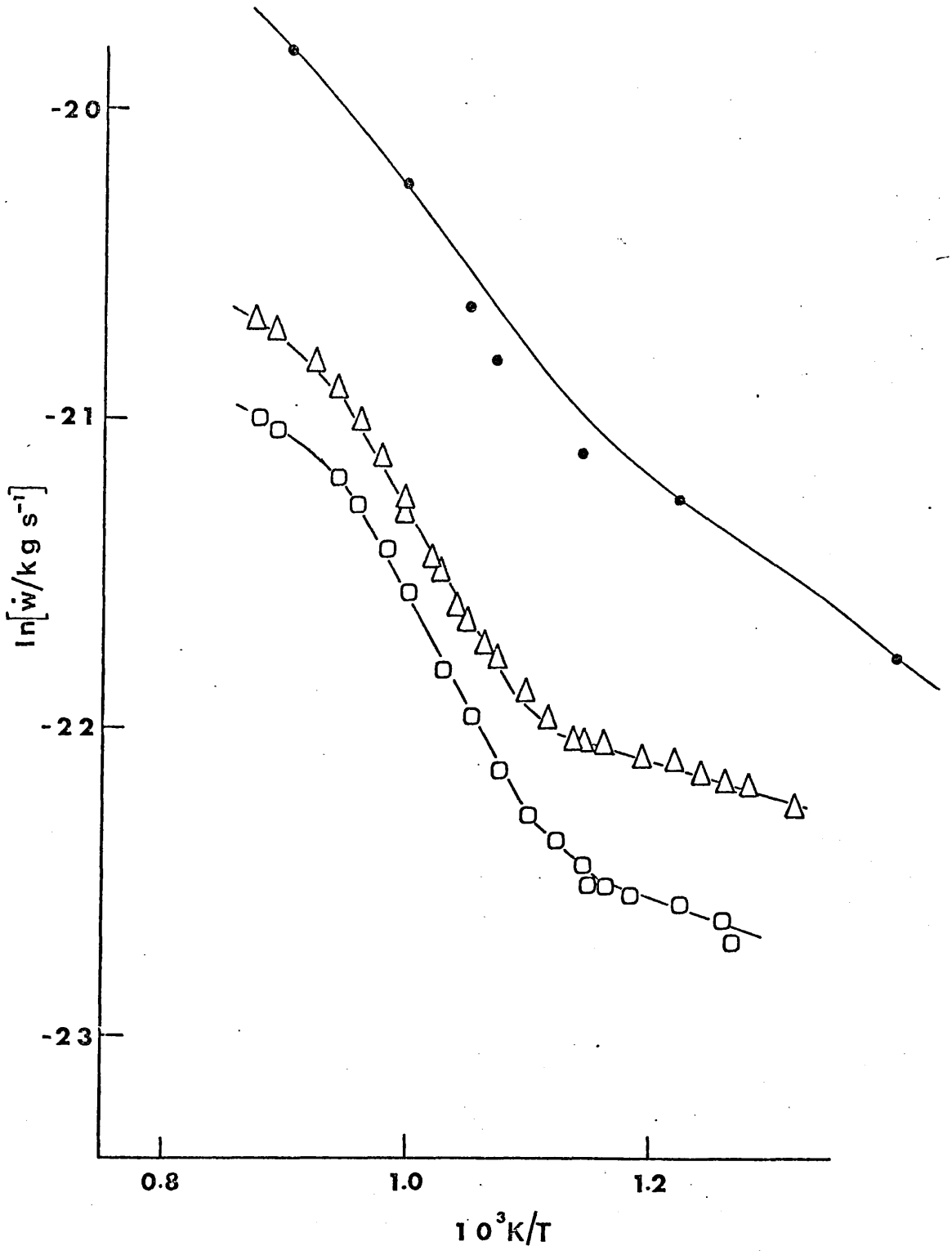

FIG. 5.3 GaAs/HBr system.

□ $\varepsilon = 0.0354$ (1 mm diameter channel).

Δ $\varepsilon = 0.0591$ (1 mm diameter channel).

• $\varepsilon = 0.0551$ (1.2 mm diameter, 20 mm long channel) ref. 6.

'Best fit' theoretical curve.

Table 5.1

Summary of experiments on GaAs/HBr system using silica bottles having different channel dimensions

Experiment	Sample	ε ($=p_{HBr}/P$)	Figure	Channel dimensions		Comment
				diameter	length	
5.3.1	GaAs/HBr(1)	0.0354 0.0591	5.1	2 mm	16 mm	
5.3.2	GaAs/HBr(2)	0.0354	5.2	3 mm	15 mm	Coarse sample
5.3.3	GaAs/HBr(3)	0.0354 0.0591	5.2	3 mm	15 mm	Finely divided sample
5.3.4	GaAs/HBr(4)	0.0354 0.0591	5.3	1 mm	17 mm	
5.3.5	GaAs/HBr(5)	0.0354 0.0591	5.3	1 mm	17 mm	Mostly low temperature results

The results from experiment 5.3.5 agreed with the low temperature results from experiment 5.3.4.

The general shape of the curves for these five experiments is the same (see figs. 5.1 - 5.3). There are two main linear sections due to two different endothermic transport reactions taking place in conjunction with the As_4 dissociation. One of the transport reactions is dominant at high temperatures and one at low temperatures. At very high temperatures, the equilibrium constant of the dominant reaction is large (see section 1.4) and so the rate of weight loss is proportional to the value of the diffusion coefficient of HBr in H_2

at the given temperature. At very low temperatures, there is a significant decrease in $\dot{w}$, except in the case of the 1 mm diameter channel experiments (fig. 5.3). This effect is probably due to the limitation of the low-temperature reaction by surface processes. In figure 5.2 two sets of results are shown, corresponding to two different samples, one of which was more finely-ground than the other. The sample with the smaller surface area gave consistently lower results and at lower temperatures the effect became more pronounced. It is clear that equilibrium is not attained in the bottle with the 3 mm diameter channel. Furthermore, in the case of the sample with a smaller surface area the effect of the surface kinetics becomes greater.

The results obtained using the 1 mm diameter channel bottle do not exhibit the low-temperature depression of weight loss. This behaviour indicates that equilibrium conditions probably exist in the bottle with the 1 mm diameter channel.

5.5 Thermodynamic data for the reactions occurring in the GaAs/HBr system

The following reactions have been considered[6]:-

$$GaAs(c) + HBr(g) \leftrightarrows GaBr(g) + 1/4As_4(g) + \tfrac{1}{2}H_2(g) \qquad (5.1)$$

$$GaAs(c) + 2HBr(g) \leftrightarrows GaBr_2(g) + 1/4As_4(g) + H_2(g) \qquad (5.2)$$

In the temperature range studied, the dissociation of As_4 must also be included:-

$$As_4(g) \leftrightarrows 2As_2(g) \qquad (5.3)$$

Thermodynamic data for these reactions is presented in table 5.2 and in section 4.8.

Table 5.2

Thermodynamic data at 298.15 K unless stated otherwise

	ΔH_f°/kJ mol^{-1}	S°/Jmol^{-1}K^{-1}	C_p°/J mol^{-1}K^{-1}
GaAs(c)	(-71.13,[7] -81.59[9]) -90.79 ± 2.93[8]	64.18[7]	46.233[7]
Ga(g)	276.98[7]	168.95[7]	25.355[7]
GaBr(g)	-49.79,[7] -64.02[12]	251.88[7]	36.401[7]
$GaBr_3$(g)	-292.88[7]	361.08[10]	78.659[10]
HBr(g)	-36.44,[11] -54.02[11] (1000 K)	198.57,[11] 234.93[11] (1000 K)	
Br(g)	111.71[7]	174.89[7]	20.795[7]
$GaBr_2$(g)	(-125.52) estimated	(351.5) estimated	

Data for the gallium dibromide species are estimated from bond energy calculations using relevant literature values.[12] The heat of formation of gallium monobromide is also uncertain. Enthalpy and entropy changes (calculated from data in table 5.2) for reactions (5.1) and (5.2) are given in table 5.3 together with confidence limits. (The formation of $GaBr_3$ would result in an exothermic transport reaction).

Table 5.3

Enthalpy and entropy changes at 1000 K for the transport reactions (5.1) and (5.2)

Reaction	Gaseous gallium halide	$\Delta H_{1000}/kJmol^{-1}$	$\Delta S_{1000}/Jmol^{-1}K^{-1}$
5.1	GaBr	120 ± 10	120 ± 10
5.2	$GaBr_2$	108 ± 40	100 ± 20

5.6 Computer analysis of the GaAs/HBr system

5.6.1 Introduction

In Appendix 4 a master equation is derived (A.37), for the GaAs/HBr system, which relates the rate of weight loss, $\dot{w}$, to the equilibrium constants K_1, K_2 and K_3 for the reactions (5.1), (5.2) and (5.3). K_3, the equilibrium constant for reaction (5.3) is known,[13] γ may be calculated and ξ is a function of $\dot{w}$, T and the diffusion coefficient of hydrogen bromide in hydrogen. The master equation may be solved for any combination of ΔH_1, ΔH_2, ΔS_1 and ΔS_2 (the enthalpy and entropy changes for reactions (5.1) and (5.2)) the solution yielding the rate of weight loss calculated as a function of temperature.

The programmes previously developed to find the set of values of the thermodynamic parameters which give the best fit to the experimental results are presented in Appendix 4.

5.6.2 Results of the computer analysis of the GaAs/HBr system

The curves obtained from each of the experiments show that two endothermic transport reactions are taking place (in addition to the dissociation of $As_4(g)$). At high temperatures the rate of weight loss is limited by the rate of diffusion of HBr down the channel of the bottle. At very low temperatures (below 820 K) there is a decrease in the rate of weight loss due to kinetic limitations (see section 5.4), this portion of the curves (shown as a broken line in figs. 5.1 and 5.2) was ignored in the computer analysis. Also, results of experiment (5.3.2), using the coarse sample, were not included in the analysis.

The 'best fit' theoretical curves are presented in figures 5.4 and 5.5 and the cross sections for each value of ε, giving the shape of the minimum (SIG_2^2, see Appendix 4D, as a function of ΔH_1, ΔH_2, ΔS_1 and ΔS_2) are given in figures 5.6 and 5.7. Table 5.4 summarises these results.

Table 5.4

Values of ΔH and ΔS from the computer analysis of the transport reactions

Channel d	ε	ΔH_1/kJ mol^{-1}	ΔH_2/kJ mol^{-1}	ΔS_1/JK^{-1}mol^{-1}	ΔS_2/JK^{-1}mol^{-1}
1 mm	0.059	128 ± 2	21 ± 2	117 ± 1	37 ± 1
1 mm	0.0354	128 ± 2	19 ± 2	118 ± 1	36 ± 1
2 mm	0.059	135 ± 5	62 ± 5	121 ± 5	79 ± 5
2 mm	0.0354	137 ± 5	61 ± 5	122 ± 5	82 ± 5
3 mm	0.059	137 ± 3	62 ± 3	122 ± 2	80 ± 2
3 mm	0.0354	135 ± 3	61 ± 3	122 ± 2	82 ± 2

5.6.3 Discussion

On departure from equilibrium conditions in the bottle, the rate of weight loss is controlled by surface processes. Figure 5.8 illustrates the depression of the rate of weight loss from the sample at

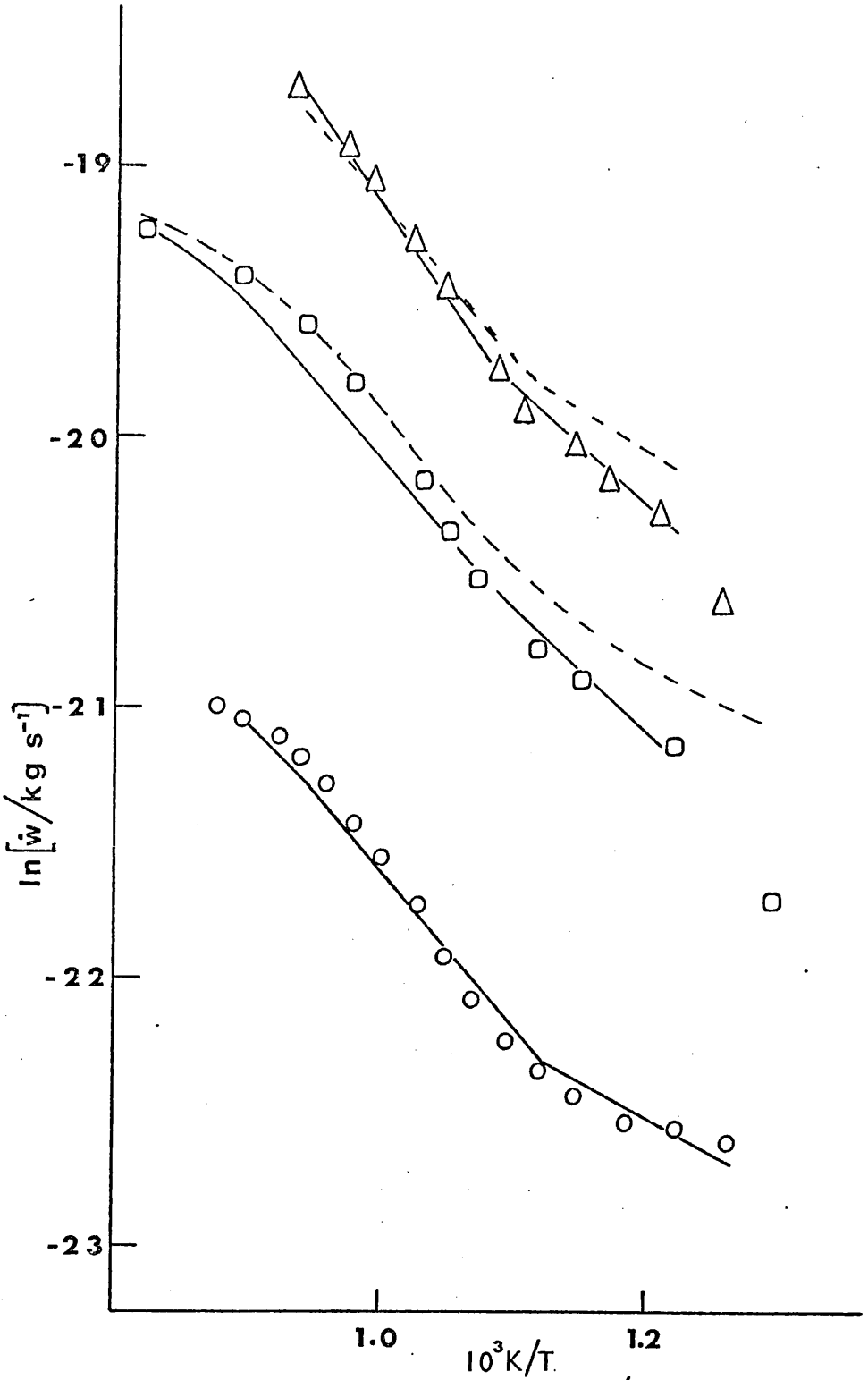

FIG. 5.4 Theoretical 'best fit' curves, GaAs/HBr system, $\varepsilon = 0.0354$.

○ 1 mm d. channel, ΔH_1=128 kJmol^{-1}, ΔH_2=19 kJmol^{-1}, ΔS_1=118 JK^{-1}mol^{-1} ΔS_2= 36 JK^{-1}mol^{-1}.

□ 2 mm d. channel, ΔH_1=137 kJmol^{-1}, ΔH_2=61 kJmol^{-1}, ΔS_1=122 JK^{-1}mol^{-1} ΔS_2= 82 JK^{-1}mol^{-1}.

△ 3 mm d. channel, ΔH_1=135 kJmol^{-1}, ΔH_2=61 kJmol^{-1}, ΔS_1=122 JK^{-1}mol^{-1} ΔS_2=82 JK^{-1}mol^{-1}.

Specked lines are 'thermodynamically scaled' 2 mm and 3 mm channel results using 1 mm channel 'best fit' H_1, H_2, S_1 and S_2.

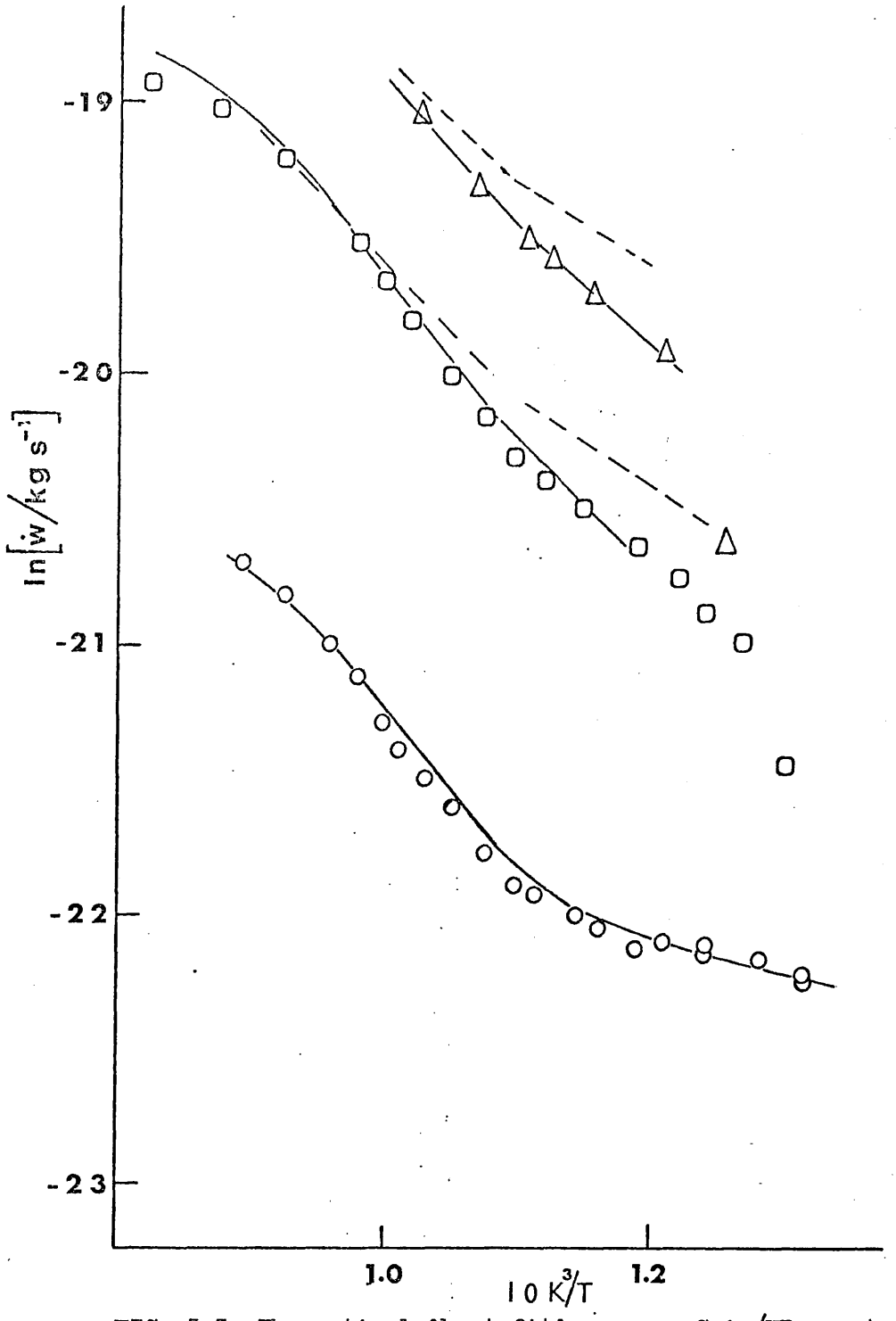

FIG. 5.5 Theoretical 'best fit' curves, GaAs/HBr system, $\varepsilon = 0.059$.

o 1 mm d.channel, ΔH_1=128 kJmol^{-1}, ΔH_2=21 kJmol^{-1}, ΔS_1=117 JK^{-1}mol^{-1} ΔS_2 = 37 JK^{-1}mol^{-1}.

□ 2 mm d.channel, ΔH_1=135 kJmol^{-1}, ΔH_2=62kJ mol^{-1}, ΔS_1= 121 JK^{-1}mol^{-1} ΔS_2=79 JK^{-1}mol^{-1}.

△ 3 mm d.channel, ΔH_1=137 kJmol^{-1}, ΔH_2=62 kJmol^{-1}, ΔS_1= 122 JK^{-1}mol^{-1} ΔS_2= 80 JK^{-1}mol^{-1}.

Specked lines are 'thermodynamically scaled' 2 mm and 3 mm channel results using 1 mm channel 'best fit', H_1, H_2, S_1 and S_2.

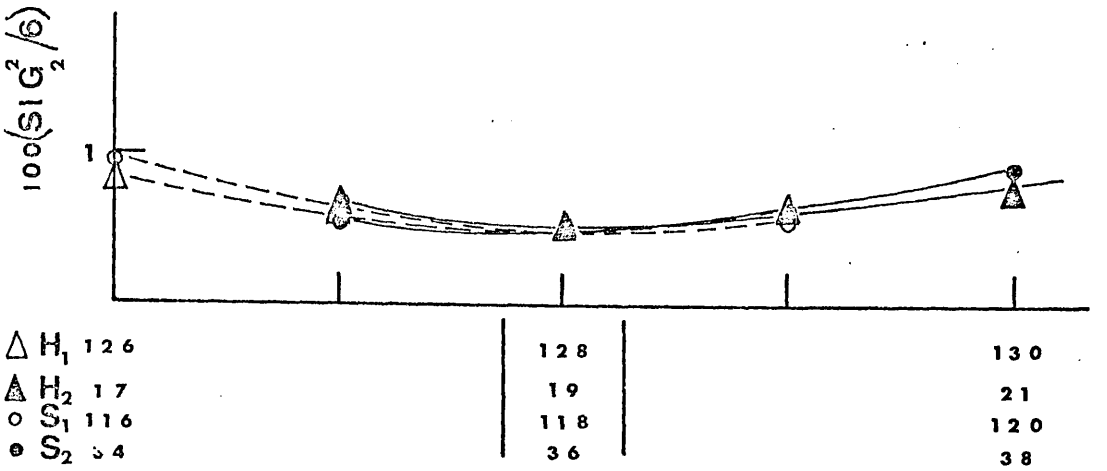

FIG. 5.6.1 Cross sections of the min. $SIG_2^2(H_1,H_2,S_1,S_2)$, 6 points, GaAs/HBr (1mm channel) $\varepsilon = 0.0354$. $\Delta H_1 = 128$ kJ mol^{-1}, $\Delta H_2 = 19$ kJ mol^{-1} $\Delta S_1 = 118$ JK^{-1}mol^{-1}, $\Delta S_2 = 36$ JK^{-1}mol^{-1}.

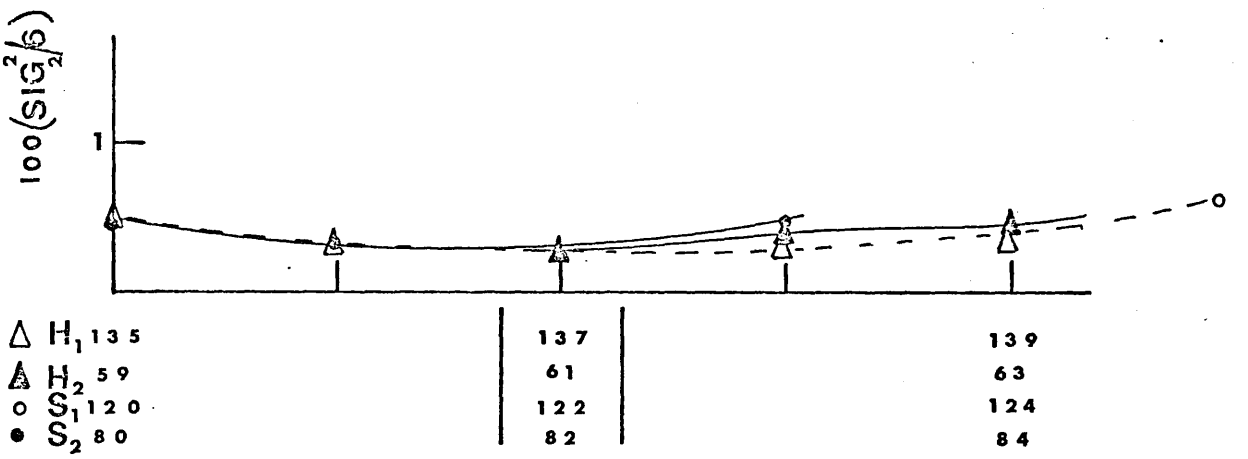

FIG. 5.6.2 Cross sections of the min. $SIG_2^2(H_1,H_2,S_1,S_2)$, 6 points, GaAs/HBr (2 mm channel) $\varepsilon = 0.0354$. $\Delta H_1 = 137$ kJ mol^{-1}, $\Delta H_2 = 61$ kJ mol^{-1}, $\Delta S_1 = 122$ JK^{-1}mol^{-1}, $\Delta S_2 = 82$ JK^{-1}mol^{-1}.

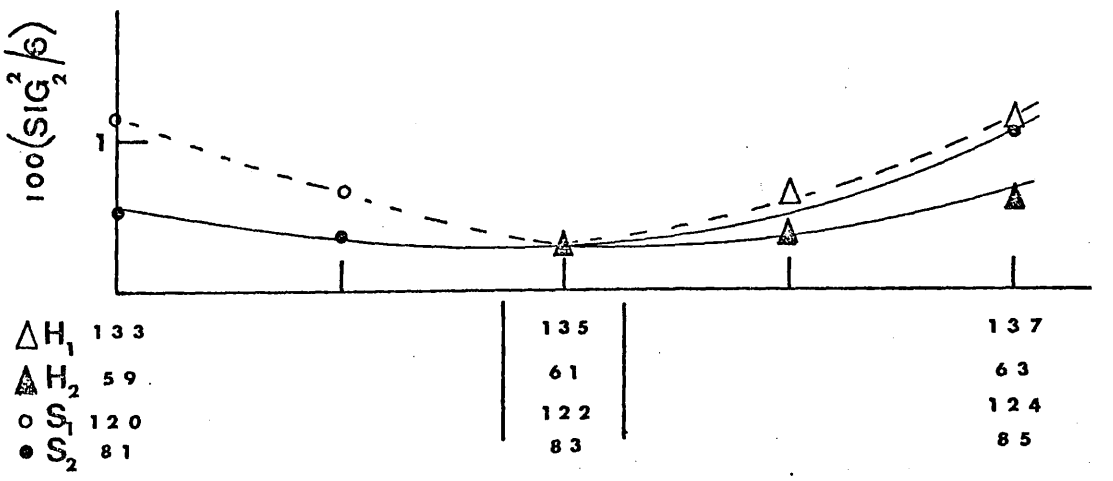

FIG. 5.6.3 Cross sections of the min. $SIG_2^2(H_1,H_2,S_1,S_2)$ 6 points, GaAs/HBr (3 mm channel) $\varepsilon = 0.0354$. $\Delta H = 135$ kJ mol^{-1}, $\Delta H = 61$ kJ mol^{-1} $\Delta S = 122$ JK^{-1}mol^{-1}, $\Delta S = 83$ JK^{-1}mol^{-1}.

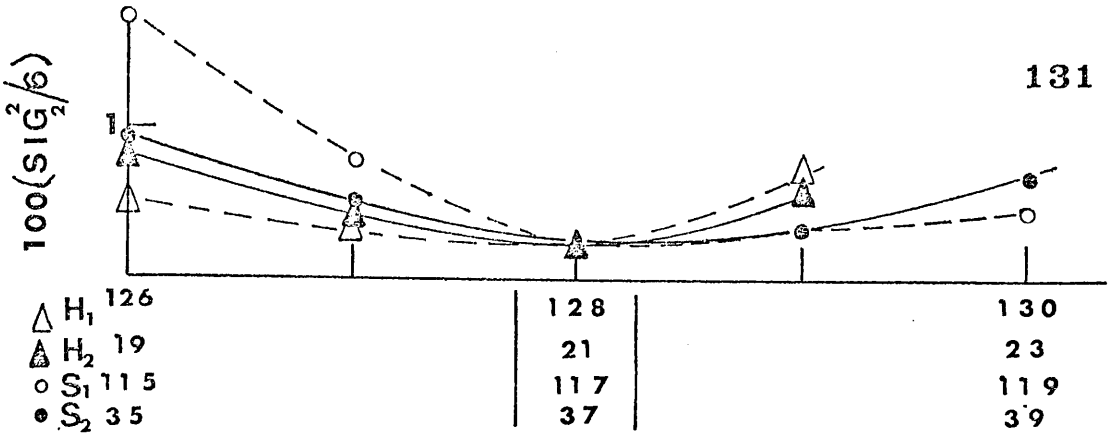

FIG. 5.7.1 Cross sections of the minimum $SIG_2^2(H_1,H_2,S_1,S_2)$ 6 points GaAs/HBr (1 mm channel), $\varepsilon = 0.059$, $\Delta H_1 = 128$ kJ mol^{-1}, $\Delta H_2 = 21$ kJ mol^{-1}, $\Delta S_1 = 117$ JK^{-1}mol^{-1}, $\Delta S_2 = 37$ JK^{-1}mol^{-1}.

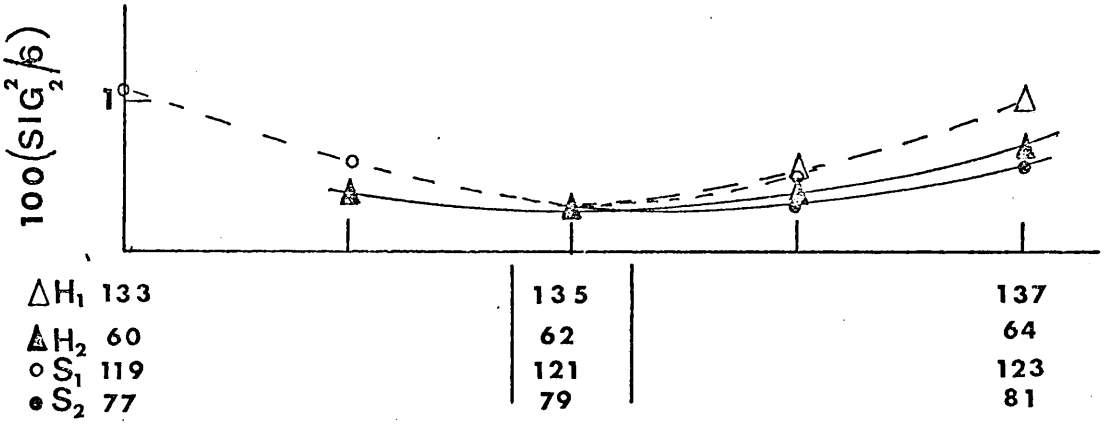

FIG. 5.7.2 Cross sections of the minimum $SIG_2^2(H_1,H_2,S_1,S_2)$ 6 points GaAs/HBr (2 mm channel), $\varepsilon = 0.059$, $\Delta H_1 = 135$ kJ mol^{-1}, $\Delta H_2 = 62$ kJ mol^{-1}, $\Delta S_1 = 121$ JK^{-1} mol^{-1}, $\Delta S_2 = 79$ JK^{-1}mol^{-1}.

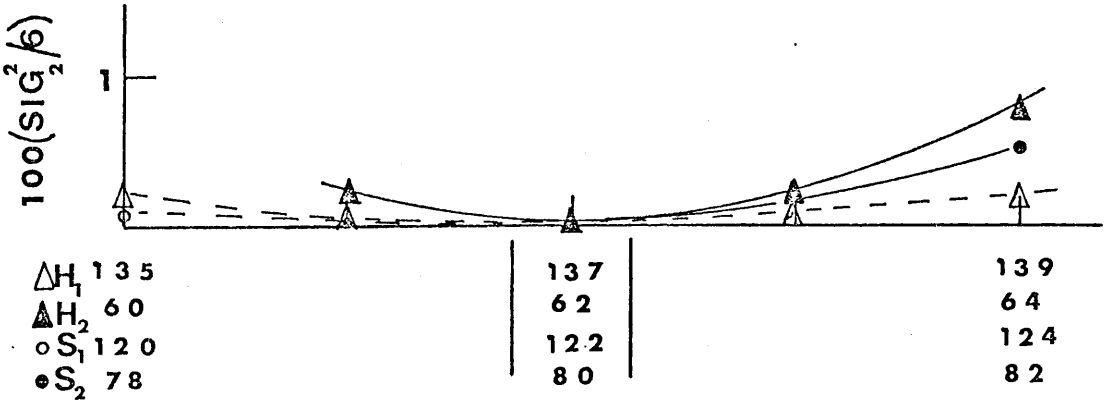

FIG. 5.7.3 Cross sections of the minimum $SIG_2^2(H_1,H_2,S_1,S_2)$ 6 points, GaAs/HBr (3 mm channel) $\varepsilon = 0.059$, $\Delta H_1 = 137$ kJ mol^{-1}, $\Delta H_2 = 62$ kJ mol^{-1}, $\Delta S_1 = 122$ JK^{-1} mol^{-1}, $\Delta S_2 = 80$ JK^{-1}mol^{-1}.

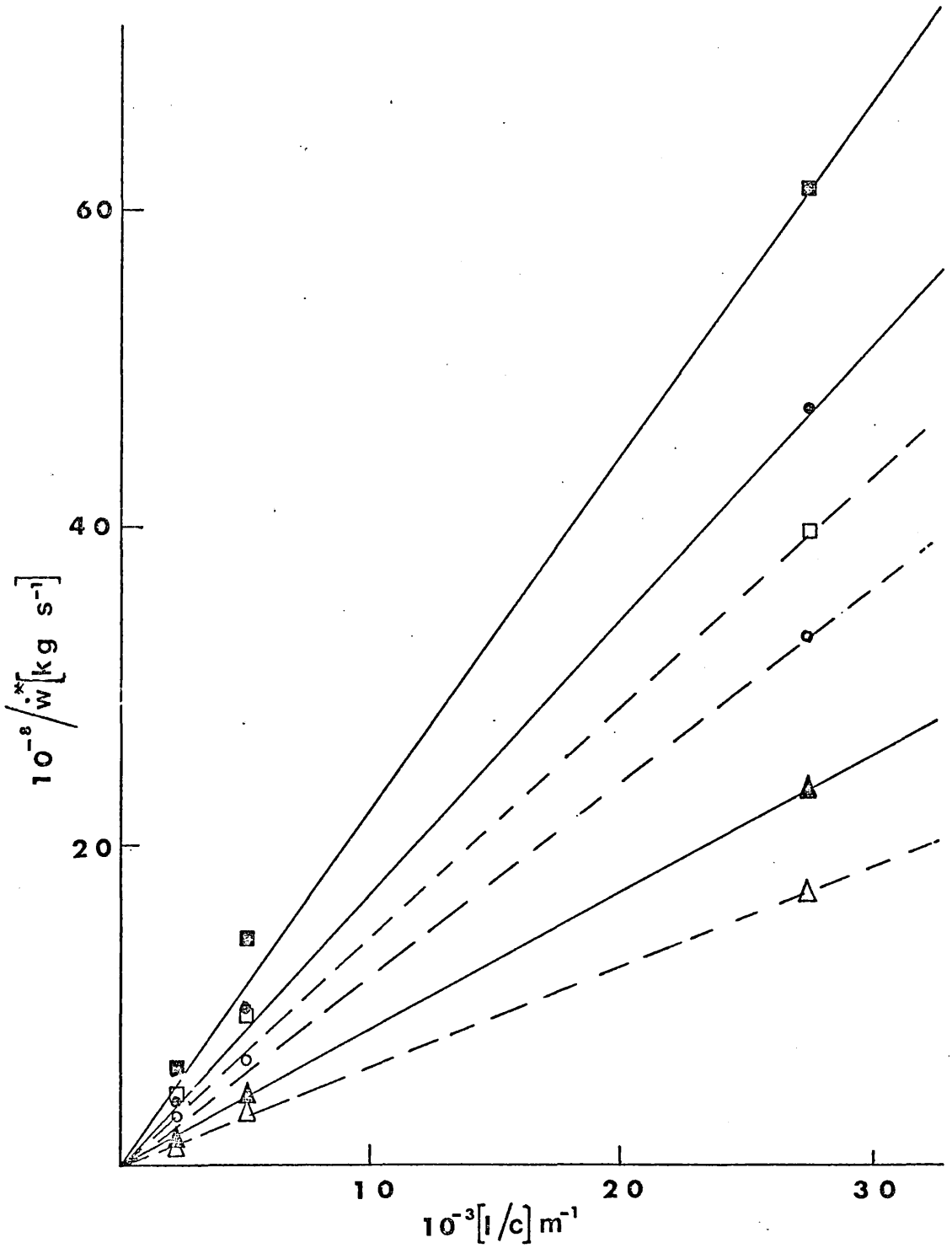

FIG. 5.8 Illustrating the depression of rate of weight loss obtained on decreasing channel resistance.

Closed symbols, bold lines represent $\varepsilon = 0.0354$.

Open symbols, specked lines represent $\varepsilon = 0.059$.

△	1000 K	▲	1000 K
○	909 K	●	909 K
□	833 K	■	833 K

low temperatures when the resistance of the channel of the bottle is decreased. (l is the length of the channel and c its cross-sectional area, $\dot{w}^*$ is the observed rate of weight loss).

The results from the 1 mm diameter channel bottle are not kinetically limited and may be taken to represent equilibrium conditions for this system. They may be 'thermodynamically scaled' to give equilibrium 2 mm and 3 mm channel results by computing $\dot{w}_{CALC}$ using the 1 mm channel 'best fit' values of ΔH_1, ΔH_2, ΔS_1, and ΔS_2 (see figures 5.4 and 5.5). The 'scaled results' demonstrate the effect of the departure from equilibrium conditions inside the bottle. In the non-equilibrium situation, both ΔH and ΔS become larger, see table 5.4.

The results from the 1 mm diameter channel bottle may be used to calculate the enthalpies and entropies of formation of GaBr(g) and $GaBr_2$(g). In table 5.5 the values calculated from experimental results are compared with literature and estimated data.

Table 5.5

Calculated thermodynamic data for GaBr(g) and $GaBr_2$(g) at 1000 K, literature[7,12] and estimated data[9] is given in parentheses.

	ΔH_f^o/kJ mol^{-1}	S^o/JK^{-1}mol^{-1}
GaBr(g)	-52.2 (-60.7)	288.5 (290.8)
$GaBr_2$(g)	-214.2 (-125.5)	359.5 (422.6)

These results compare favourably with literature data for GaBr(g) but disagree markedly with estimated $GaBr_2$(g) values.

Experimental results from transport experiments may be used to calculate 'unknown' thermodynamic data.

5.7 Conclusion

This study of the GaAs/HBr system shows that for bottles with channels larger than 1 mm in diameter there is a significant departure from equilibrium conditions above the sample. Computed values of ΔH and ΔS for the transport reactions become larger as the channel diameter increases (this was also demonstrated in Chapter 4 with the InAs/HCl system) and decreasing the surface area of the sample has a similar effect.

A previous investigation[6] of this system produced significantly different results for ΔH and ΔS for the two transport reactions (see table 5.6).

Table 5.6

Thermodynamic data for the transport reactions:

$$GaAs(c) + HBr(g) \rightleftharpoons GaBr(g) + 1/4As_4(g) + \tfrac{1}{2}H_2(g) \qquad (5.1)$$

$$GaAs(c) + 2HBr(g) \rightleftharpoons GaBr_2(g) + 1/4As_4(g) + H_2(g) \qquad (5.2)$$

	ΔH_1/kJ mol^{-1}	ΔS_1/J mol^{-1}K^{-1}	ΔH_2/kJ mol^{-1}	ΔS_2/J mol^{-1}K^{-1}
This work	128	118	19	36
Ref. 6	183	162	126	140

Some experimental results from reference 6 are plotted in figure 5.3. with their theoretical 'best fit' curve. It is clear that the low temperature portion was not correctly interpreted and that the strong influence of surface kinetics was ignored in this analysis.

Crystal growers require a high rate of transport i.e. a large variation of equilibrium constant with temperature. This can be achieved by enlarging the channel of the capsule or by decreasing the sample surface area. However, if either of these methods is taken too

far then non-equilibrium conditions will develop in the capsule. The extent of the departure from equilibrium may be measured by the ratio $\dot{w}^*/\dot{w}^o$ where $\dot{w}^*$ is the measured rate of weight loss and $\dot{w}^o$ is the equilibrium rate of weight loss. By studying different systems with a selection of channel sizes equilibrium conditions may be found (as illustrated in fig. 5.8). The crystal grower can then determine the optimum conditions for growth.

5.8 References

1. D. Battat, M.M. Faktor, I. Garrett, R.H. Moss, J. Chem. Soc. Faraday Trans. 1, 70, 2267 (1974).

2. D. Battat, M.M. Faktor, I. Garrett, R.H. Moss, J. Chem. Soc. Faraday Trans. 1, 70, 2280 (1974).

3. D. Battat, M.M. Faktor, I. Garrett, R.H. Moss, J. Chem. Soc. Faraday Trans. 1, 70, 2293 (1974).

4. D. Battat, M.M. Faktor, I. Garrett, R.H. Moss, J. Chem. Soc. Faraday Trans. 1, 70, 2302 (1974).

5. M.M. Faktor, I. Garrett, M.H. Lyons, unpublished work.

6. M.M. Faktor, I. Garrett, M.H. Lyons, R.H. Moss, J. Chem. Soc. Faraday Trans. 1, 73, 1446 (1977).

7. 'Selected Values of Chemical Thermodynamic Properties', U.S. National Bureau of Standards, Tech. Note 270-3 (1968).

8. C. Pupp, J. Murray, R. Pottie, J. Chem. Thermodynamics, 6, 123 (1974).

9. S. Martosudirdjo, J.N. Pratt, 10 (1), 23 (1974).

10. M.G. Drake, G.M. Rosenblatt, J. Chem. Phys., 65, 4067 (1976).

11. J.A.N.A.F., Thermochemical Tables 2nd edition, U.S. Department of Commerce, National Bureau of Standards (1971).

12. O. Kubaschewski, E.L. Evans, C.B. Alcock, 'Metallurgical Thermochemistry', Pergamon Press (1967).

13. J.J. Murray, C. Pupp, R.F. Pottie, J. Chem. Phys., 58, 2569 (1973).

Chapter 6

The indium antimonide–hydrogen chloride system

Chapter 6

6.1 Introduction

A rapid evaluation of a potential crystal growth system may be undertaken using the modified entrainment method, as is illustrated in previous chapters. Thermodynamic data for the relevant transport reactions can usually be obtained from the results, although no direct information is provided on the nature of gas-phase species present.

In this chapter an investigation of the indium antimonide/hydrogen chloride system is described. It is clear from the results that this system is probably unsuitable for crystal growth from the vapour.

6.2 Experimental

The apparatus has been described in detail in section 2.2.

The polycrystalline indium antimonide sample (MCP Electronics Ltd., see Appendix 6) was crushed inside a polythene bag and loaded into the silica bottle with the 2 mm diameter channel (see Appendix 1). The bottle containing the sample was suspended from loop A of the electrobalance and rates of weight loss, $\dot{w}$, recorded at temperatures T. The temperature range 665 - 820 K was studied using the hydrogen chloride concentration $\varepsilon = 0.0506$.

6.3 Results

Experimental results are given in table 6.1 and a representative sample is presented graphically, as ln $\dot{w}$ vs. inverse temperature, in figure 6.1.

Table 6.1

Transport of indium antimonide in hydrogen chloride gas ($\xi = 0.0506$). Rates of weight loss, $\dot{w}$, at temperatures T (listed chronologically).

Run	T/K	$10^{10}\dot{w}$/kg $\bar{s}^{-1}$	Run	T/K	$10^{10}\dot{w}$/kg $\bar{s}^{-1}$
1	689.35	4.621	25	690.95	5.833
2	705.15	5.976	26	692.35	6.113
3	726.85	8.417	27	707.55	8.200
4	726.85	8.417	28	706.65	8.011
5	664.65	1.946	29	709.65	19.240
6	706.95	18.288	30	709.65	8.991
7	706.95	19.906	31	707.75	8.741
8	706.95	18.629	32	747.65	15.624
9	706.95	18.158	33	747.65	16.539
10	726.85	36.000	34	718.95	10.960
11	726.85	35.607	35	718.95	11.040
12	689.95	10.158	36	670.15	2.367
13	689.95	10.221	37	693.15	10.074
14	747.65	57.294	38	718.85	26.514
15(a,b)	747.65	56.95, 14.74	39	718.85	25.556
16	747.65	14.286	40	718.85	11.269
17	691.15	5.292	41	725.75	31.500
18	691.15	5.392	42	716.25	10.714
19	707.35	14.815	43	774.15	18.577
20	699.85	6.667	44	770.25	17.886
21	696.15	6.297	45	805.95	23.070
22	728.45	11.880	46	805.15	23.103
23	730.25	11.120	47	740.65	8.940
24	730.25	10.891	48	742.55	9.700

Table 6.1 (continued)

Run	T/K	$10^{10}\dot{w}$/kg s^{-1}	Run	T/K	$10^{10}\dot{w}$/kg s^{-1}
49	690.35	5.952	78	728.55	8.183
50	690.35	6.188	79	728.55	8.755
51	712.45	8.267	80	728.55	9.083
52	709.65	7.888	81	733.35	10.281
53	709.15	8.360	82	731.85	10.458
54	770.85	17.207	83	731.85	11.381
55	769.85	17.190	84	752.65	14.508
56	717.35	6.117	85	720.85	10.627
57	717.35	6.732	86	720.85	10.989
58	694.15	5.575	87	720.85	11.247
59	693.25	6.327	88	707.65	9.590
60	806.05	21.933	89	709.75	9.370
61	806.05	21.886	90	709.75	9.760
62	707.55	5.072	91	694.55	8.557
63	707.55	5.553	92	694.55	8.818
64	707.55	5.897	93	694.55	8.640
65	707.55	6.271	94	752.15	15.290
66	708.15	6.786	95	752.15	15.172
67	707.65	6.993	96	711.25	10.611
68	707.65	6.957	97	710.35	10.467
69	707.65	7.282	98	710.35	10.144
70	707.65	7.600	99	694.15	8.809
71	708.45	7.864	100	695.15	8.600
72	708.45	8.287	101	695.15	8.818
73	820.15	23.429	102	742.15	13.458
74	820.15	23.140	103	742.15	13.284
75	820.15	22.884	104	731.15	12.040
76	727.65	7.021	105	731.15	12.453
77	727.65	7.496			

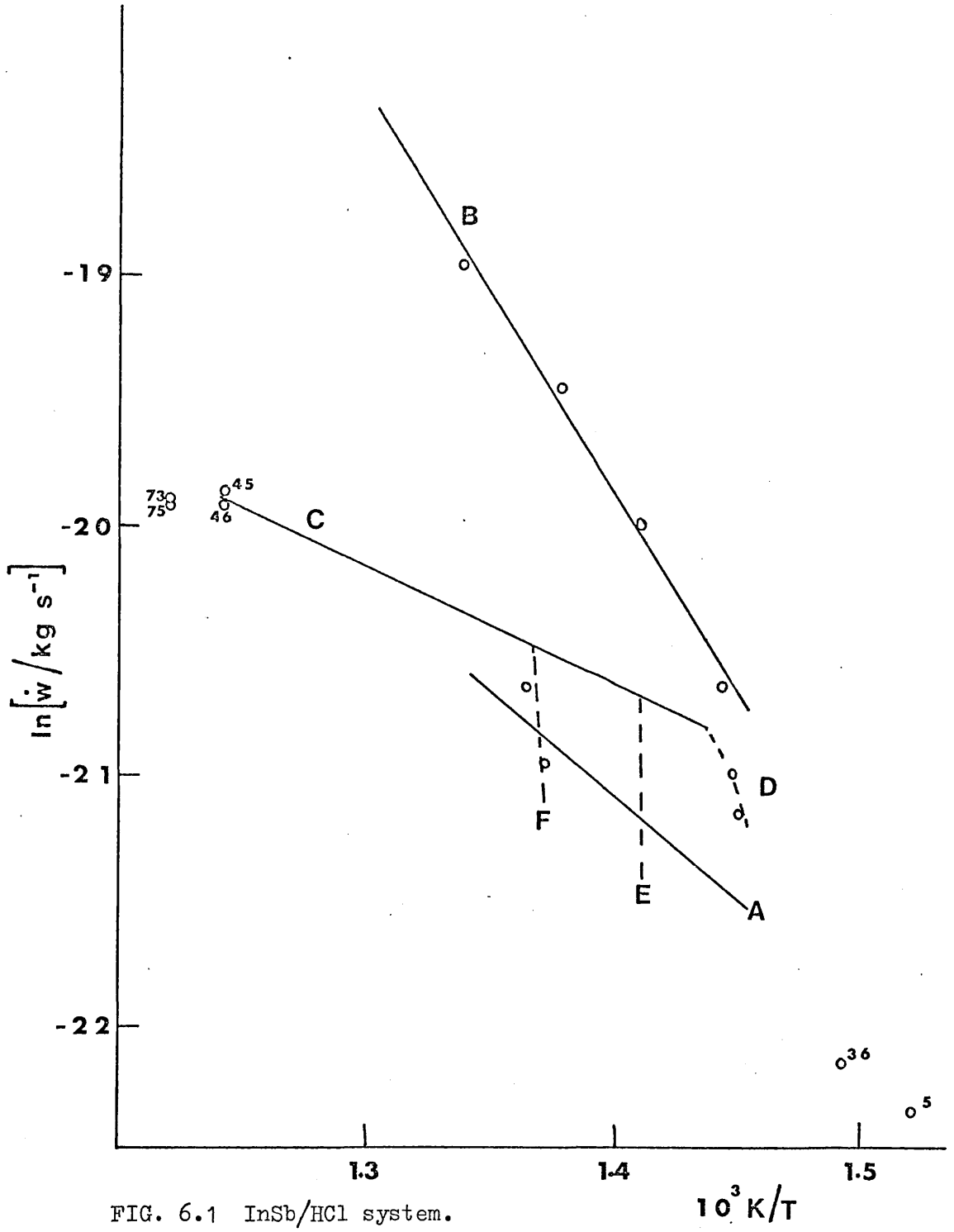

FIG. 6.1 InSb/HCl system.

o 2 mm diameter channel, ε = 0.0506.

6.4 Discussion

Three lines, having different slopes, can be drawn through the points in figure 6.1 : (A), (B) and (C). Points 1-4 lie on line (A) and are possibly due to:

$$InSb(c) + HCl(g) \leftrightarrows InCl(g) + \tfrac{1}{2}H_2(g) + 1/4Sb(g) \qquad (6.1)$$

Point 5 is at a much lower temperature and lies below extrapolated line (A). At this temperature $InCl_3$ may be formed in the bottle and only partially transported away:

$$InSb(c) + 3HCl(g) \leftrightarrows InCl_3(c) + 1/4Sb_4(c) + 3/2H_2(g) \qquad (6.2)$$

During the InAs/HBr transport experiments a weight gain was observed when the sample was held at low temperatures and after subsequent runs at higher temperatures a white sublimate ($InBr_3$) appeared in the furnace tube below the capsule.

Points 6-15 fell on line (B) ($\Delta H_B \simeq 142$ kJ mol^{-1}, $\Delta S_B \simeq 270$ JK^{-1}mol^{-1}). It is postulated that this line results from the sublimation of $InCl_3$ from the surface of the sample (for $InCl_3$ sublimation[1] $\Delta H \simeq 158$ kJ mol^{-1}, $\Delta S \simeq 301$ JK^{-1}mol^{-1}). When most of the $InCl_3$ has sublimed off, the rate of weight loss falls rapidly to line (c) (points 16-20).

Points 21-35, line (D), are at low temperatures but not low enough for the formation of $InCl_3$. The 'tailing off' of low temperature CVT curves is often due to surface kinetic inhibition.

Point 36 is similar to point 5, points 37-41 reproduce line (B) and points 42-44 fall to line (C) as before.

The sample was melted (bulk melting point InSb is 796 K) during runs 45-46. The scatter of points 47-60 between lines (A) and (C) suggests that melting the sample resulted in a departure from equilibrium conditions in the bottle.

After melting the sample again (points 60-61) a series of points were obtained at 708 K (line (E)), the rate of weight loss increased with time possibly due to surface changes. Points 73-75 were above the melting point of InSb and points 76-83, line (F), were again time dependent. The last 22 points fell on or near line (C), ΔH_C = 40 kJ mol^{-1} and ΔS_C = 123 $JK^{-1}mol^{-1}$. These values compare unfavourably with estimated values for likely transport reactions, given in table 6.2 (the estimates ignore any contribution from $Sb_4 \leftrightarrows 2Sb_2$ equilibrium).

Table 6.2

Estimated values of the enthalpies and entropies for the transport reactions (1), (2) and (3), ignoring the presence of the $Sb_4 \leftrightarrows 2Sb_2$ equilibrium.

$InSb(c) + HCl\ (g) \leftrightarrows InCl(g) + 1/4Sb_4(g) + \frac{1}{2}H_2(g)$ (1)

$InSb(c) + 2HCl(g) \leftrightarrows InCl_2(g) + 1/4Sb_4(g) + H_2(g)$ (2)

$InSb(c) + 3HCl(g) \leftrightarrows InCl_3(g) + 1/4Sb_4(g) + 3/2H_2(g)$ (3)

Reaction	ΔH/kJ mol^{-1}	$\Delta S/JK^{-1}$ mol^{-1}
(1)	99	192
(2)	171	229
(3)	-15	286

A study of the behaviour of InSb surfaces during heat treatment[2] has shown that the nature of InSb surfaces changes at 673 K due to thermal decomposition and evaporation processes. Excess indium is left on the surface in the form of droplets after preferential evaporation of antimony. This phenomenon could have influenced the results from the transport experiment described in this chapter.

6.5 Conclusion

Investigation of the InSb/HCl system has provided little information about the transport reactions or vapour species present. However, it has shown the crystal grower that it is probably an unsuitable system for crystal growth from the vapour.

6.6 References

1. O. Kubaschewski, E.L. Evans, C.B. Alcock, 'Metallurgical Thermochemistry', Pergamon Press (1967).

2. D. Haneman in 'Compound Semiconductors', 1 (1962) Reinhold Publ. Co., editors R. Willardson, H. Goering.

APPENDIX 1

Channel Dimensions

Several different bottles were used for the experiments described in this thesis. Their channel (or stopper) dimensions were measured accurately with a travelling microscope ($\pm$ 2 x 10^{-7}m). Six to ten separate readings were taken for each measurement and a standard deviation, $\sigma = \sqrt{\frac{\Sigma (x-\bar{x})^2}{n-1}}$ (where $\bar{x}$ is mean and n is the number of points), calculated.

End corrections β and β' were established to allow for the opening out of the channel at its lower end.

Correction for transport in a non-parallel-sided tube[1]

On elimination of the Stefan velocity U from the flow equations (see section 1.4) and substitution of UP = JRTs (where s is the sum of the stoichiometric coefficients in the transport equation) the following expression results:

$$\left[\frac{p_i^o - P/s}{p_i^1 - P/s}\right] = \exp\left[-\frac{RTs}{DP}\int_1^o J\,dx\right] \qquad (1)$$

This is in terms of boundary conditions x = 0 and x = 1 (see fig. 1.1).

$Jr^2 = A$ = constant, due to conservation of mass.

If r(x) is known (r is radius of capillary) then equation (1) can be integrated.

a) Uniform taper

$r = ax + b$, $b = r(o)$, $a = \frac{r(1) - r(o)}{1}$

Then $\int_o^1 \frac{dx}{r^2} = \frac{1}{r(1)\ r(o)}$

b) Mixed tube (see fig. 1)

Region I : $r = ax + b$

Region II: $r = r(l)$ = constant.

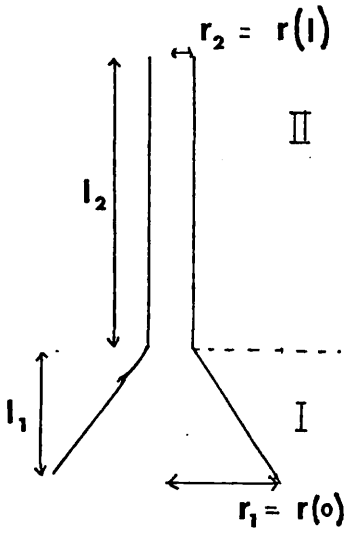

FIG. 1

In region I : $$\left[\frac{p(o) - P/s}{p(l_1) - P/s}\right] = \exp\left[\frac{-RTAl_1 s}{PDr_2 r_1}\right]$$

In region II: $$\left[\frac{p(l_1) - P/s}{p(l_2) - P/s}\right] = \exp\left[\frac{-RTAl_2 s}{PDr_2^2}\right]$$

Multiplying gives:

$$\left[\frac{p(o) - P/s}{p(l) - P/s}\right] = \exp\left[\frac{-RTsA}{PD}\left(\frac{l_1 r_2 + l_2 r_1}{r_1 r_2^2}\right)\right]$$

the measured rate of weight loss is $J(l)\ \pi\ r_2^2\ M = \dot{w}$

so $\dot{w} = \pi AM$ or $A = \dot{w}/\ \pi M$

To a first order approximation:

$$p(o) = (p(l) - P/s)\left[1 - \frac{\dot{w}RTs}{\pi MPD}\left(\frac{l_1 r_2 + l_2 r_1}{r_1 r_2^2}\right)\right] + P/s$$

$$\therefore \quad \xi' = \frac{\dot{w}RT(l_2 + l_1)}{DMPc}\left(\frac{l_1 r_2 + l_2 r_1}{r_1(l_1 + l_2)}\right)$$

$$\text{or } \xi' = \frac{\dot{w}RTl_2}{DMPc}\left(1 + \frac{r_2 l_1}{r_1 l_2}\right)$$

$$\text{let} \qquad 1 + \frac{r_2 l_1}{r_1 l_2} = \beta$$

A similar correction term may be derived for the channel shown in fig. 2.

$$\text{Here} \qquad \xi' = \frac{\dot{w}RTl_2}{DMPc}\left(1 + \frac{r_2^2 l_1}{r_1^2 l_2}\right)$$

$$\text{and} \qquad \beta' = 1 + \frac{r_2^2 l_1}{r_1^2 l_2}$$

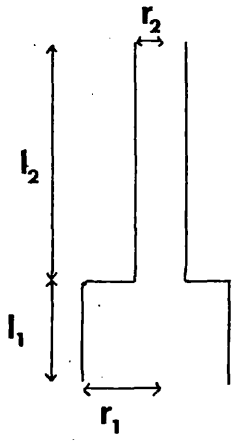

FIG. 2

Channel dimensions (d = diameter of channel)

Pyrex stoppered bottle - Evaporation of water experiments

$l_1 = (0.61323 \pm 0.00173)\ 10^{-2}$m

$l_2 = (1.68665 \pm 0.00297)\ 10^{-2}$m

$d_1 = (0.24593 \pm 0.00257)\ 10^{-2}$m

$d_2 = (0.10223 \pm 0.00052)\ 10^{-2}$m

$\beta^1 = 1.0629$

Silica bottle, 2 mm diameter channel - Zn/He, Zn/Ar experiments

$l_1 = (0.1300 \pm 0.0433)\ 10^{-2}$m

$l_2 = (2.0226 \pm 0.0577)\ 10^{-2}$m

$d_1 = (0.68918 \pm 0.1137)\ 10^{-2}$m

$d_2 = (0.1993 \pm 0.0021)\ 10^{-2}$m

$\beta = 1.01859$

Silica bottle, 2 mm diameter channel - In/HCl, In/HBr, InAs/HCl(1)-(3), In-InAs/HCl, InAs/HBr(1)-(2), GaAs/HBr(1), InSb/HCl.

$l_1 = (0.09088 \pm 0.00976)\ 10^{-2}$m

$l_2 = (1.5592 \pm 0.0196)\ 10^{-2}$m

$d_1 = (0.28478 \pm 0.01293)\ 10^{-2}$m

$d_2 = (0.20370 \pm 0.00057)\ 10^{-2}$m

$\beta = 1.0417$

Silica bottle, 1 mm diameter channel - InAs/HCl(4), GaAs/HBr(4)-(5)

$l_1 = (0.08048 \pm 0.11150)\ 10^{-2}$m

$l_2 = (1.7288 \pm 0.01154)\ 10^{-2}$m

$d_1 = (0.17574 \pm 0.00987)\ 10^{-2}$m

$d_2 = (0.09098 \pm 0.00565)\ 10^{-2}$m

$\beta = 1.0241$

Silica bottle, 3 mm diameter channel - GaAs/HBr (2)-(3)

$l_1 = (0.19434 \pm 0.04203)\ 10^{-2}$m

$l_2 = (1.45005 \pm 0.01909)\ 10^{-2}$m

$d_1 = (0.54155 \pm 0.01277)\ 10^{-2}$m

$d_2 = (0.29723 \pm 0.01129)\ 10^{-2}$m

$\beta = 1.0736$

Reference

1. I. Garrett, unpublished work.

APPENDIX 2

Furnace Profiles

Furnace Specifications

Modular furnace, type 2A (Severn Science Ltd.).

Size: A tubular furnace with a tube 12" (300 mm) long, of internal diameter 1½" (38 mm). External diameter of furnace case is 6" (150 mm).

Materials of Construction: The sillimanite tube is gradient wound with "Kanthal A1" wire. A thermocouple tube is fitted between the windings and the furnace tube. The outer casing is of aluminium with "Sindanyo" end plates.

Power rating: 825 watts at 100 volts.

Maximum operating temperature: 1100°C.

The above furnace was employed for the experiments described in this thesis. Furnace profiles (temperature, t°C vs. distance from furnace base, inches) are presented in figures 1-8.

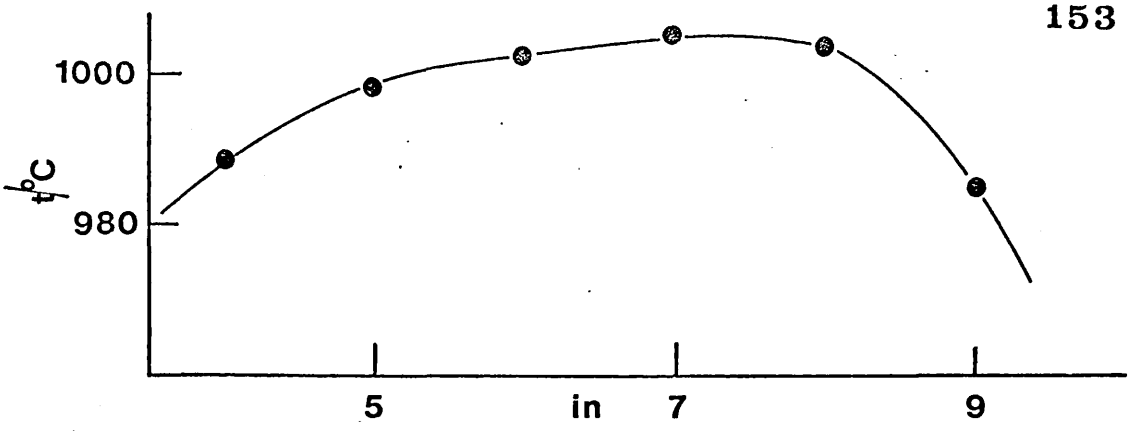

FIG. 1. Centre controller 1007°C, upper controller 1000°C.

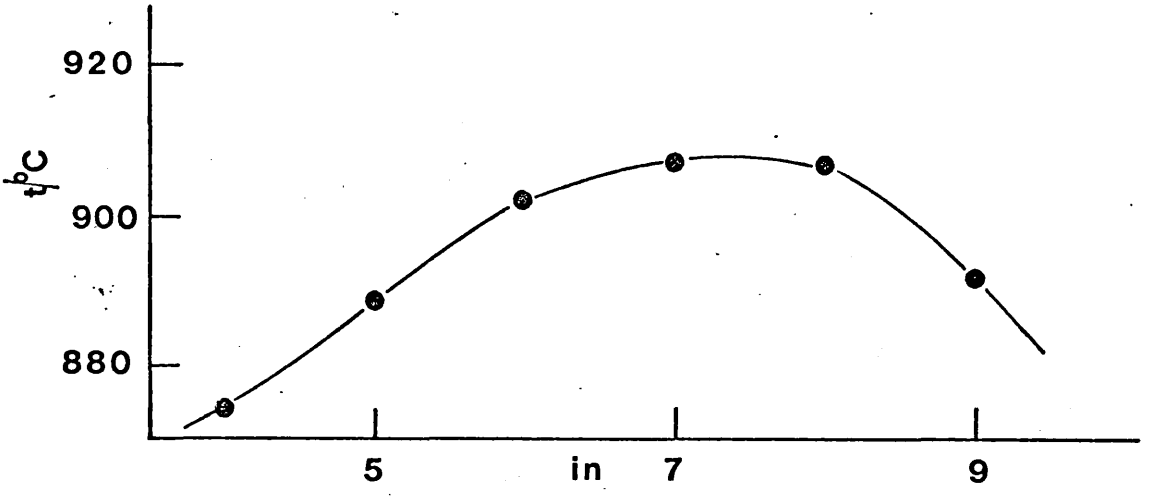

FIG. 2. Centre controller 906°C, upper controller 900°C.

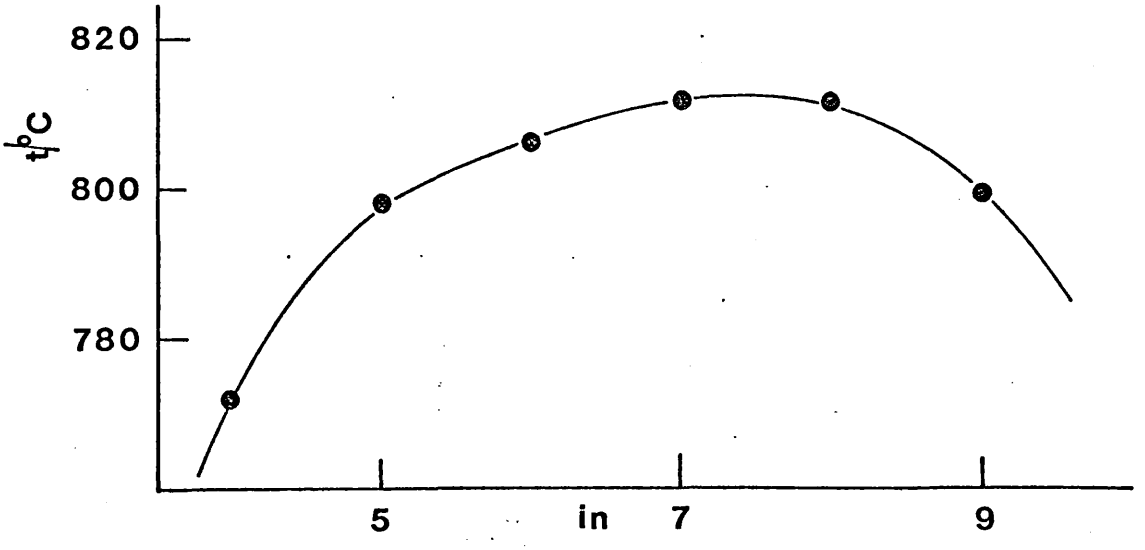

FIG. 3. Centre controller 810°C, upper controller 800°C.

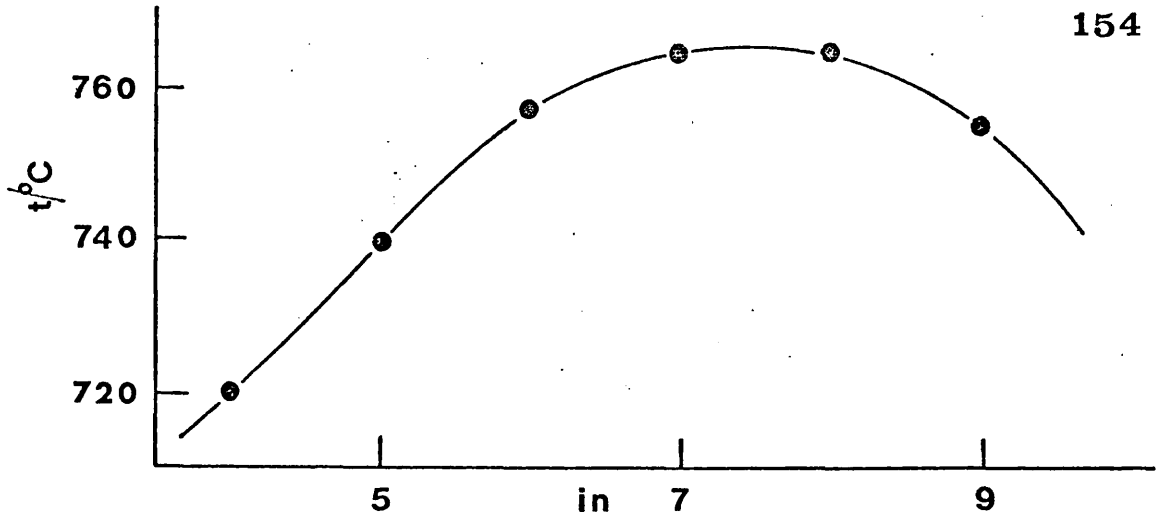

FIG. 4. Centre controller 765°C, upper controller 750°C.

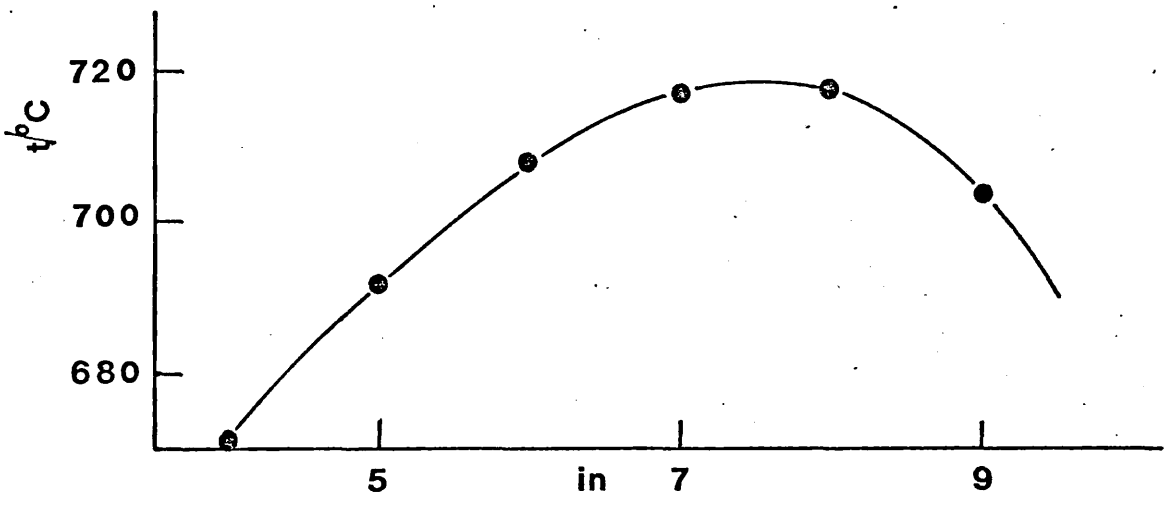

FIG. 5. Centre controller 716°C, upper controller 700°C.

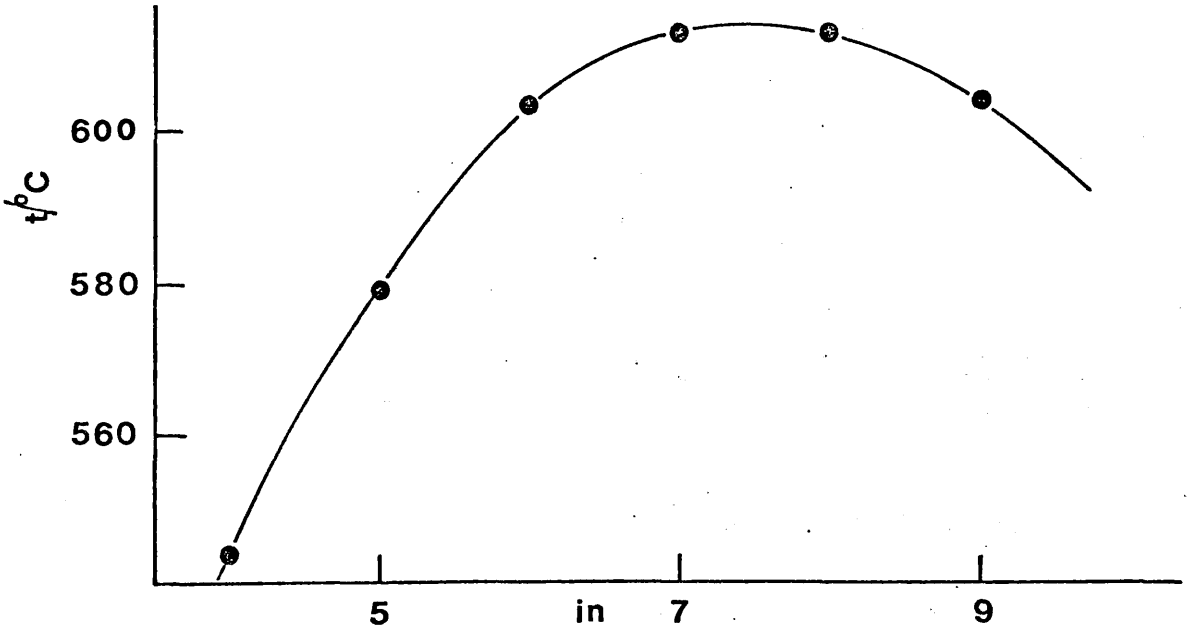

FIG. 6. Centre controller 617°C, upper controller 600°C.

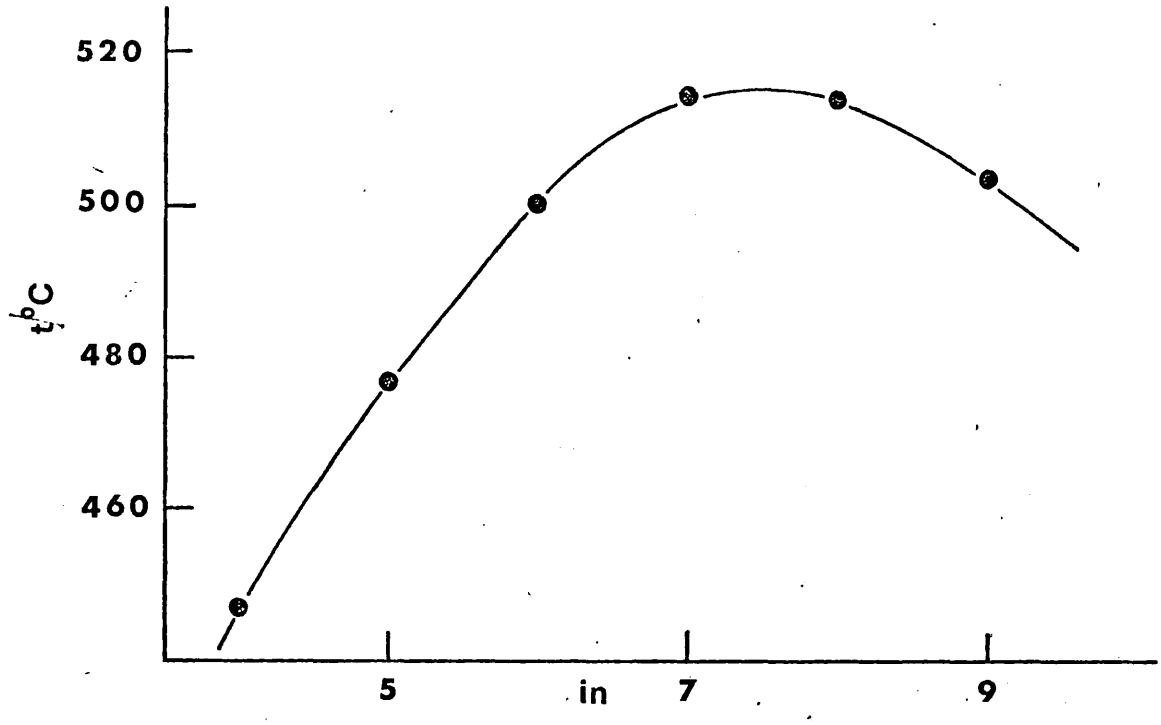

FIG. 7. Centre controller 520°C, upper controller 500°C.

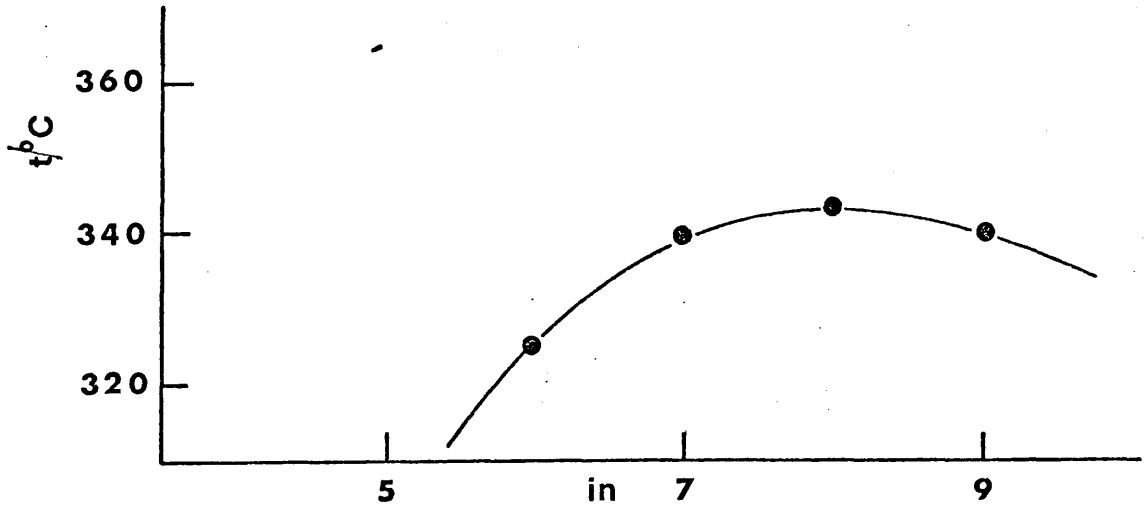

FIG. 8. Centre controller 360°C, upper controller 340°C.

APPENDIX 3

Experimental Results

Table 1 : InAs/HCl, ε = 0.0506 (2 mm diameter channel)

Table 2 : InAs/HCl, ε = 0.0506 (2 mm diameter channel)

Table 3 : InAs/HCl, ε = 0.0506 and ε = 0.0871 (2 mm diameter channel)

Table 4 : InAs/HCl, ε = 0.0506 (1 mm diameter channel)

Table 5 : In-InAs/HCl, ε = 0.0506 (2 mm diameter channel)

Table 6 : InAs/HBr, ε = 0.0354 (2 mm diameter channel)

Table 7 : InAs/HBr, ε = 0.0354 and ε = 0.0591 (2 mm diameter channel)

Table 1

Transport of indium arsenide in hydrogen chloride gas ($\varepsilon = 0.0506$). Rates of weight loss, $\dot{w}$, at temperatures T (listed chronologically).

T/K	$10^{10}\dot{w}$/kg s^{-1}	T/K	$10^{10}\dot{w}$/kg s^{-1}
919.75	39.120	1021.15	56.471
919.75	39.120	1021.15	54.444
1062.65	72.059	1143.65	80.726
1062.65	71.739	1143.65	79.426
1062.25	74.697	1111.35	76.875
1121.05	79.839	892.15	16.164
1121.05	83.051	892.15	16.383
1121.05	82.373	841.55	25.032
1163.15	85.982	841.55	22.353
1162.95	86.875	942.15	31.206
1162.75	87.018	921.40	24.550
1182.65	80.917	862.15	10.816
1182.65	80.738	862.65	10.539
1182.55	80.242	821.45	5.372
1217.45	121.625	1065.15	65.931
1217.45	121.342	1064.65	66.690
1082.65	72.132	982.65	46.476
1082.65	70.071	911.85	22.446
1083.15	68.944	911.85	22.541
1042.05	61.548	841.55	7.643
1042.05	59.515	791.45	2.811
1002.25	52.649	771.65	1.873
1001.95	50.769	771.60	1.806
962.15	37.308	884.15	15.568
962.15	36.453	883.85	15.341
1101.85	71.143	806.65	3.820
1101.85	70.423	805.95	3.792

Table 1 (continued)

(ε = 0.0506)

T/K	$10^{10}\dot{w}$/kg s^{-1}	T/K	$10^{10}\dot{w}$/kg s^{-1}
872.55	13.090	836.75	7.298
872.15	13.253	799.55	15.567
740.65	9.055	799.55	18.571
740.65	8.230	799.55	20.711
740.65	9.590	836.15	29.046
740.65	8.125	836.15	28.462
740.65	9.130	836.15	29.200
740.65	10.844	900.15	27.914
836.75	7.193	899.75	29.540
		898.85	27.941

Table 2

Transport of indium arsenide in hydrogen chloride gas ($\epsilon = 0.0506$). Rates of weight loss, $\dot{w}$, at temperatures T (listed chronologically).

T/K	$10^{10}\dot{w}$/kg s^{-1}	T/K	$10^{10}\dot{w}$/kg s^{-1}
1064.15	71.304	895.15	28.059
1063.05	68.592	769.15	3.956
1063.05	67.603	1064.55	74.478
1020.05	62.645	1064.55	74.478
1020.05	62.968	910.85	33.966
851.25	17.777	910.85	34.104
851.25	17.689	789.15	5.554
1081.05	75.606	789.15	5.482
1081.05	75.615	880.85	26.041
997.25	61.000	880.85	25.707
997.25	61.250	803.75	7.816
1039.15	70.929	804.25	7.760
1039.15	70.286	871.15	23.012
921.40	36.037	871.15	22.824
921.40	36.667	1041.85	67.466
841.55	15.154	1041.85	70.571
841.55	15.031	901.15	31.168
981.55	57.455	901.15	30.816
981.55	57.294	933.15	41.575
940.85	43.244	933.15	41.660
940.85	45.349	738.15	1.927
820.35	10.368	849.55	16.131
820.85	10.242	849.55	16.082
961.25	49.000	706.45	0.931
961.25	49.700	859.95	18.109
895.15	29.274	859.95	18.914
		747.55	2.274

Table 3

Transport of indium arsenide in hydrogen chloride gas ($\varepsilon = 0.0506$). Rates of weight loss, $\dot{w}$, at temperatures T (listed chronologically).

T/K	$10^{10}\dot{w}$/kg s^{-1}	T/K	$10^{10}\dot{w}$/kg s^{-1}
1062.75	65.000	881.45	25.658
1062.75	61.500	770.75	4.129
1020.55	58.667	970.85	53.189
1020.55	58.424	970.85	52.000
871.15	22.089	940.85	43.864
871.15	21.756	941.15	42.913
1040.15	65.200	751.65	2.870
1040.15	65.241	952.35	46.571
1000.15	55.771	952.35	47.048
1000.15	55.278	1042.25	68.643
900.15	30.464	1042.25	67.724
900.15	30.976	819.65	10.844
1077.05	69.236	819.65	10.573
1077.05	67.123	931.35	42.174
1083.85	67.397	931.05	41.125
1083.85	71.214	708.55	1.042
841.15	14.533	1053.05	70.143
841.15	14.255	1053.05	68.786
805.15	7.967	1018.45	63.355
981.35	53.833	1018.45	62.774
981.35	55.429	906.35	35.746
961.45	48.800	906.35	35.393
961.45	47.143	734.15	2.097
921.15	36.593	847.05	17.182
921.15	36.885	847.05	17.078
991.95	55.353	724.35	1.618
991.95	56.824	857.15	20.000
881.45	25.368	918.85	37.057

Table 3 (continued)

Rates of weight loss, $\dot{w}$, at temperatures T and HCl concentrations ε .

T/K	$10^{10}\dot{w}$/kg s^{-1}	ε	T/K	$10^{10}\dot{w}$/kg s^{-1}	ε
918.85	37.808	0.0506	787.15	7.404	0.0871
786.15	5.845	0.0506	746.35	3.168	0.0871
687.35	0.639	0.0506	1027.75	90.000	0.0871
892.85	28.314	0.0506	1027.75	89.818	0.0871
892.85	29.576	0.0506	947.75	62.279	0.0871
713.65	1.262	0.0506	947.75	64.026	0.0871
989.95	58.606	0.0506	1049.45	98.200	0.0871
989.95	57.235	0.0506	1049.45	99.082	0.0871
989.95	76.462	0.0871	1049.45	72.246	0.0506
917.55	48.350	0.0871	1059.85	80.902	0.0506
917.55	48.650	0.0871	1059.85	97.157	0.0871
724.85	2.063	0.0871	1079.75	79.758	0.0506
891.95	37.019	0.0871	1079.75	79.127	0.0506
892.15	37.808	0.0871	1079.25	103.750	0.0871
766.15	4.955	0.0871	1079.25	103.936	0.0871
766.15	4.850	0.0871	1215.15	89.091	0.0506
961.15	68.069	0.0871	1215.15	87.946	0.0506
961.15	68.483	0.0871	948.15	30.938	0.0506
848.15	20.822	0.0871	968.65	38.720	0.0506
848.15	20.519	0.0871	968.65	36.906	0.0506
688.45	0.831	0.0871	916.15	24.474	0.0506
938.15	57.697	0.0871	916.15	23.472	0.0506
938.15	57.059	0.0871	945.95	33.931	0.0506
868.35	27.578	0.0871	916.15	23.394	0.0506
868.35	27.417	0.0871	916.15	22.847	0.0506
816.35	12.619	0.0871	835.15	6.917	0.0506
816.35	12.323	0.0871	948.85	33.983	0.0506
703.95	1.204	0.0871	949.15	33.148	0.0506
1040.95	94.423	0.0871	949.15	32.696	0.0506
1040.95	91.482	0.0871	868.15	31.300	0.0506
838.75	17.924	0.0871	868.15	31.008	0.0506
838.75	18.177	0.0871			

Table 4

Transport of indium arsenide in hydrogen chloride gas ($\varepsilon = 0.0506$) using silica bottle with 1 mm diameter channel. Rates of weight loss, $\dot{w}$, at temperatures T (listed chronologically).

T/K	$10^{10}\dot{w}$/kg s^{-1}	T/K	$10^{10}\dot{w}$/kg s^{-1}
899.05	6.119	911.15	6.821
897.65	6.063	911.15	6.693
963.55	9.005	850.85	3.643
962.75	9.143	850.85	3.600
863.25	4.230	941.05	8.289
863.25	4.265	941.05	8.233
923.15	7.292	1021.05	11.447
922.15	7.508	1021.05	11.600
872.45	4.845	980.15	9.950
873.25	4.954	980.45	10.082
852.15	3.750	980.45	10.041
852.95	3.876	930.65	7.648
890.15	5.764	930.15	7.616
890.15	5.651	930.15	7.569
889.40	5.571	1061.45	12.487
909.65	6.704	1061.15	12.594
909.65	6.829	1038.95	11.216
909.15	6.843	939.55	8.100
850.00	3.777	939.55	8.131
850.00	3.731	909.15	6.538
880.15	5.341	909.95	6.579
880.15	5.328	909.95	6.614
861.15	4.196	909.95	6.593
861.15	4.187	1040.15	11.781
950.65	8.747	1040.15	11.817
950.65	8.786	1081.85	12.816
840.95	3.326	1081.95	12.579
840.95	3.390	1040.15	11.768
911.65	6.914	1040.15	11.643

Table 4 (continued)

(ε = 0.0506)

T/K	$10^{10}\dot{w}$/kg s^{-1}	T/K	$10^{10}\dot{w}$/kg s^{-1}
1023.15	11.577	949.15	7.942
1021.35	11.120	1040.05	11.685
1021.35	11.063	1039.15	11.721
1119.65	13.614	1212.45	54.722
1119.65	13.444	1038.85	11.441
1050.35	12.263	1038.85	11.500
1050.35	12.025	950.15	7.864
910.55	6.964	950.15	8.025
910.55	6.814	894.95	4.732
1180.65	14.561	895.65	4.662
1180.65	15.061	861.35	2.968
1050.65	12.397	861.35	3.012
1051.45	12.175	943.15	7.331
921.45	7.014	942.15	7.569
921.45	7.107	971.65	8.936
1215.35	62.387	970.85	8.844
1215.35	63.226	1213.85	53.571
981.75	9.320	970.15	8.855
981.75	9.747	970.15	8.848
921.15	5.879	910.45	5.406
921.15	5.982	910.45	5.345
871.35	3.368	894.85	4.464
871.35	3.358	894.85	4.441
895.05	4.710	880.75	3.731
895.05	4.760	880.75	3.835
949.15	7.752	850.75	2.508

Table 5

Transport of indium arsenide (with added indium) in hydrogen chloride gas ($\varepsilon = 0.0506$) using silica bottle with 2 mm diameter channel. Rates of weight loss, $\dot{w}$, at temperatures T (listed chronologically).

T/K	$10^{10}\dot{w}$/kg s^{-1}	T/K	$10^{10}\dot{w}$/kg s^{-1}
957.25	41.696	978.15	47.900
957.25	41.391	978.15	48.150
925.75	38.080	890.75	25.733
926.65	36.500	890.75	26.213
886.65	27.056	889.90	25.421
887.55	27.528	1008.15	54.471
908.85	34.607	1007.65	54.588
907.15	33.483	1059.75	61.813
907.15	35.482	1059.25	62.800
865.85	32.300	1058.95	61.438
866.75	31.839	1116.65	66.200
926.40	34.000	1116.15	65.310
925.55	33.148	1205.45	139.231
1015.40	49.263	1206.15	149.231
1014.55	51.474	1019.75	53.778
766.35	3.890	1018.95	53.667
767.15	3.804	1018.15	53.333
849.65	16.033	961.25	37.423
848.65	15.850	960.35	36.808
958.45	42.955	871.15	13.107
957.65	43.591	870.85	12.880
1018.15	55.333	870.85	12.800
1017.15	55.086	849.65	9.381
1058.65	61.677	849.65	9.476
1058.15	60.750	980.95	43.727
1057.85	61.000	979.75	42.565

Table 5 (continued)

(ε = 0.0506)

T/K	$10^{10}\dot{w}$/kg s^{-1}	T/K	$10^{10}\dot{w}$/kg s^{-1}
978.90	42.609	889.15	16.348
930.45	29.212	889.15	16.435
929.55	29.600	931.75	28.171
1221.75	248.857	929.95	27.943
909.55	21.178	849.55	9.512
909.55	20.779	849.55	9.154
940.45	30.129	849.55	9.079
939.65	29.424	815.95	5.068
939.15	29.656	817.15	5.126
919.45	23.707		
919.45	23.610		

Table 6

Transport of indium arsenide in hydrogen bromide gas ($\varepsilon = 0.0354$) using silica bottle with 2 mm diameter channel. Rates of weight loss, $\dot{w}$, at temperatures T (listed chronologically).

T/K	$10^{10}\dot{w}$/kg s^{-1}	T/K	$10^{10}\dot{w}$/kg s^{-1}
977.75	45.273	957.25	45.143
976.35	44.136	979.65	45.810
976.35	48.283	978.05	47.650
938.35	46.050	977.15	46.600
937.15	44.619	878.75	37.346
937.15	45.857	876.95	37.360
917.35	43.087	876.95	37.115
916.15	44.273	899.85	39.840
916.65	42.000	898.15	40.522
1058.15	51.474	898.15	39.800
1058.15	51.000	837.25	29.046
1057.35	50.611	836.35	28.892
1080.35	52.056	835.45	27.908
1078.35	52.222	1041.15	51.889
1077.55	51.105	1040.35	51.778
1019.15	49.474	1039.55	51.632
1017.85	49.632	908.65	41.739
1016.55	48.800	907.35	40.304
1015.75	49.790	906.15	41.478
959.85	45.667	949.40	45.571
957.75	46.191	947.65	45.182

Table 6 (continued)

(ε = 0.0354)

T/K	$10^{10}\dot{w}$/kg s^{-1}	T/K	$10^{10}\dot{w}$/kg s^{-1}
946.90	45.619	804.55	21.155
858.25	33.418	805.45	21.089
858.25	33.418	765.45	13.614
982.15	48.737	767.35	13.476
980.40	48.158	1083.05	55.000
978.75	48.100	1081.35	54.667
867.95	35.250	1124.15	56.412
867.05	35.214	1121.65	56.588
1001.45	49.158	1120.15	56.941
999.75	49.632	834.35	27.083
997.75	49.500	833.95	26.667
928.65	44.591	789.25	17.061
927.35	44.273	787.95	16.696
845.25	30.212	787.15	16.217
846.15	30.188	894.15	38.920
971.15	48.250	894.15	38.840
969.15	48.800	777.35	15.008
967.90	48.050	777.85	13.435
814.45	22.659	1228.85	385.000
815.35	22.675	952.75	42.864
815.85	22.729	950.65	42.591
		845.25	18.440

Table 7

Transport of indium arsenide in hydrogen bromide gas ($\varepsilon = 0.0354$) using silica bottle with 2 mm diameter channel. Rates of weight loss, $\dot{w}$, at temperatures T (listed chronologically).

T/K	$10^{10}\dot{w}$/kg s^{-1}	T/K	$10^{10}\dot{w}$/kg s^{-1}
979.55	48.350	818.15	25.771
978.35	47.850	818.15	25.447
1059.85	51.737	893.95	40.167
1058.95	51.474	892.15	39.583
1058.15	52.368	748.95	11.903
957.35	46.333	748.95	11.927
958.15	46.950	1019.65	50.211
958.15	46.850	1020.45	49.526
777.15	17.327	802.15	21.378
777.65	17.127	802.55	21.647
921.15	43.727	850.95	32.167
919.85	43.318	850.95	32.032
726.75	9.720	767.15	14.119
728.15	9.551	768.05	14.193
941.45	45.286	841.40	30.000
940.65	45.000	840.15	29.546
939.75	44.818	788.15	17.771
870.15	36.444	789.55	17.873
870.15	36.148		

Table 7 (continued)

(ε = 0.0591)

T/K	$10^{10}\dot{w}$/kg s^{-1}	T/K	$10^{10}\dot{w}$/kg s^{-1}
981.85	64.200	790.45	25.733
981.85	64.467	808.35	30.182
889.65	52.263	807.45	29.500
889.95	51.722	1024.35	67.357
771.55	22.546	1023.15	67.643
771.55	22.259	834.05	35.519
959.85	63.067	834.85	36.111
960.75	63.400	742.15	16.470
920.15	57.683	745.45	16.539
921.15	58.412	842.95	39.375
719.55	15.376	842.45	39.542
725.15	19.680	748.15	18.324
852.85	43.773	749.65	18.629
852.85	43.273	833.15	36.000
822.15	34.574	835.15	36.192
821.35	34.400	731.35	18.723
748.45	29.233	730.85	18.640
748.45	29.385	753.15	18.457
873.75	47.600	757.45	19.720
873.75	47.900	739.95	16.696
789.45	26.107	740.85	15.632

APPENDIX 4

Computer Programming

A GaAs/HBr system (in detail).

B InAs/HBr system.

C InAs/HCl system.

D Development of programmes.

Appendix 4

Computer analysis of the GaAs/HBr, InAs/HBr and InAs/HCl systems

A master equation[1] may be derived, for each system, which relates the rate of weight loss, $\dot{w}$, to the equilibrium constants of the transport reactions considered significant.

4A Derivation of the master equation for the GaAs/HBr system

The following equations can be used to describe the transport of gallium arsenide by hydrogen bromide gas (see Chapter 5):

$$GaAs(c) + HBr(g) \leftrightarrows GaBr(g) + 1/4As_4(g) + \tfrac{1}{2}H_2(g) \qquad (A.1)$$

$$GaAs(c) + 2HBr(g) \leftrightarrows GaBr_2(g) + 1/4As_4(g) + H_2(g) \qquad (A.2)$$

$$As_4(g) \leftrightarrows 2As_2(g) \qquad (A.3)$$

The equilibrium constants for reactions (A.1) and (A.2) are given by:

$$K_1 = \frac{p^o_{GaBr}(p^o_{As_4})^{1/4}(p^o_{H_2})^{\frac{1}{2}}}{p^o_{HBr}} \qquad (A.4)$$

and

$$K_2 = \frac{p^o_{GaBr_2}(p^o_{As_4})^{1/4}p^o_{H_2}}{(p^o_{HBr})^2} \qquad (A.5)$$

where p^o denotes the equilibrium partial pressure in the reaction bottle. The carrier gas, hydrogen, makes up the bulk of the transporting gas stream and the fractional concentration of HBr in the gas stream, ε, is small compared with unity ($\varepsilon = 0.05$). Partial pressures of the minority products at the open end of the bottle, p^1_i, are approximately zero due to the sweeping effect of the gas stream.[2]

The multicomponent diffusion of reactants, products and carrier gas in the channel of the reaction bottle may be described by a one-dimensional transport equation, (A.6), as hydrogen is present in excess ($p_{H_2} \simeq$ 720 torr).

$J_i = n_i U - D_{i/H_2} (dn_i/dx)$ (A.6), where J_i is the flux (mol $m^{-2}s^{-1}$) of species i, n_i is the molar concentration of species i, U is the mole-average Stefan velocity and D_{i/H_2} is the binary diffusion coefficient of species i in hydrogen.

Assuming ideal gas behaviour, then:

$$J_i = \frac{Up_i}{RT} - \frac{D_{i/H_2}}{RT} (dp_i/dx) \qquad (A.7)$$

For the carrier gas $J_i = 0$. Summing the fluxes results in the diffusion terms cancelling, (A.8), as there is no real pressure gradient along the channel

$$\Sigma_i J_i = J = \frac{UP}{RT} \qquad (A.8)$$

where $P = \Sigma_i p_i$. Substituting (A.8) into (A.6) gives:

$$\frac{dp_i}{dx} = \frac{RT}{D_{i/H_2}} \left[\frac{Jp_i}{P} - J_i \right]$$

Integrating:

$$\int_{p_0}^{p_1} \frac{dp_i}{\left[\frac{Jp_i}{P} - J_i\right]} = \int_0^1 \frac{RT}{D_{i/H_2}} dx$$

hence $$\frac{p_i^o}{P} = \frac{J_i}{J} + \left[\frac{p_i^1}{P} - \frac{J_i}{J}\right] e^{-\xi_i} \qquad (A.9)$$

where ξ_i the transport function is defined as:

$$\xi_i = \frac{JRTl}{PD_{i/H_2}} \qquad (1.4)$$

Since ξ_i is at most of the order of ε and hence small compared with unity, equation (A.9) may be simplified:

$$\frac{p_i^o}{P} = \frac{J_i}{J} + \left[\frac{p_i^1}{P} - \frac{J_i}{J}\right](1 - \xi_i)$$

$$\frac{p_i^o}{P} = \frac{J_i}{J}\,\xi_i + \frac{p_i^1}{P} \qquad (A.10)$$

The quantities p_i^1/P are known as boundary conditions. If there is a single reaction occuring, the J_i values are related by stoichiometric coefficients and may be related simply to the rate of weight loss. In this case three simultaneous reactions are being considered and the relationships between the J_i values become temperature-dependent.

The fluxes, J_i, of the species occuring in the transport reactions are related by stoichiometric conditions:

$$J_{HBr} + 2J_{H_2} = 0 \qquad (A.11)$$

$$J_{HBr} + J_{GaBr} + 2J_{GaBr_2} = 0 \qquad (A.12)$$

$$J_{GaBr} + J_{GaBr_2} = 4J_{As_4} + 2J_{As_2} = J_{GaAs} \qquad (A.13)$$

$$J_{HBr} + J_{H_2} + J_{As_4} + J_{As_2} + J_{GaBr} + J_{GaBr_2} = J \qquad (A.14)$$

If α and Θ are defined as:

$$\alpha = \frac{J_{As_2}}{J_{As_4}} \tag{A.15}$$

$$\Theta = J_{GaBr}/J_{GaBr_2} \tag{A.16}$$

Then from (A.12)

$$J_{HBr} + \Theta J_{GaBr_2} + 2J_{GaBr_2} = 0$$

and

$$J_{GaBr_2} = -J_{HBr}/(\Theta + 2) \tag{A.17}$$

from (A.13) $J_{GaBr_2}(\Theta + 1) = J_{As_4}(4 + 2\alpha)$

$$J_{As_4} = J_{GaBr_2}\frac{(1+\Theta)}{(4+\alpha)} = \frac{-J_{HBr}(1+\Theta)}{(\Theta+2)(4+2\alpha)} \tag{A.18}$$

Similarly

$$J_{As_2} = \frac{-\alpha(1+\Theta)\ J_{HBr}}{(2+\Theta)(4+2\alpha)} \tag{A.19}$$

$$J_{GaAs} = \frac{-(1+\Theta)}{(2+\Theta)}\ J_{HBr} \tag{A.20}$$

and from (A.14)

$$\frac{J_{HBr}}{J} = \frac{-2(2+\alpha)(2+\Theta)}{(\alpha+1)(1+2\Theta)+\Theta} \tag{A.21}$$

$$\frac{p^o_{GaBr}}{P} = \frac{J_{GaBr}}{J}\left[1 - \exp(-\xi_{GaBr})\right] \doteq \frac{J_{GaBr}}{J}\ \xi_{GaBr}$$

$$\frac{p^o_{GaBr_2}}{P} \doteq \frac{J_{GaBr_2}}{J}\ \xi_{GaBr_2}$$

$$\frac{p^{o}_{As_4}}{P} \simeq \frac{J_{As_4}}{J} \quad \xi_{As_4}$$

$$\frac{p^{o}_{As_2}}{P} \simeq \frac{J_{As_2}}{J} \quad \xi_{As_2}$$

$$\frac{p^{o}_{HBr}}{P} = \frac{J_{HBr}}{J} + \left[\frac{p^{l}_{HBr}}{P} - \frac{J_{HBr}}{J}\right](1 - \xi_{HBr})$$

but $\varepsilon = p^{l}_{HBr}/P$

so $$\frac{p^{o}_{HBr}}{P} \simeq \varepsilon + \frac{J_{HBr}}{J} \xi_{HBr}$$

but $$\xi_i = \frac{JRTl}{PD_{(i/H_2,T)}}$$

$$= \frac{J_{GaAs} RTl}{PD_{(i/H_2,T)}} \left[\frac{(\alpha+1)(1+2\Theta)+\Theta}{2(2+\alpha)(\Theta+1)}\right]$$

$$= \frac{\dot{w}_{GaAs} RTl}{cM_{GaAs} PD_{(i/H_2,T)}} \left[\frac{(\alpha+1)(1+2\Theta)+\Theta}{2(2+\alpha)(\Theta+1)}\right]$$

where c is the cross sectional area of the capillary of length l.

$$\xi_i = \bar{\xi}_i \left[\frac{(\alpha+1)(1+2\Theta)+\Theta}{2(2+\alpha)(\Theta+1)}\right] \qquad (A.22)$$

where $\bar{\xi}_i$ the reduced transport function is independent of the values of α and Θ.

Thus the partial pressures inside the reaction bottle are given by:

$$\frac{p^{o}_{GaBr}}{P} = \frac{\Theta}{\Theta+1} \quad \bar{\xi}_{GaBr} \tag{A.23}$$

$$\frac{p^{o}_{GaBr_2}}{P} = \frac{1}{\Theta+1} \quad \bar{\xi}_{GaBr_2} \tag{A.24}$$

$$\frac{p^{o}_{As_4}}{P} = \frac{1}{4+2\alpha} \quad \bar{\xi}_{As_4} \tag{A.25}$$

$$\frac{p^{o}_{As_2}}{P} = \frac{\alpha}{4+2\alpha} \quad \bar{\xi}_{As_2} \tag{A.26}$$

$$\frac{p^{o}_{HBr}}{P} = \varepsilon - \frac{2+\Theta}{1+\Theta} \quad \bar{\xi}_{HBr} \tag{A.27}$$

When more than one reaction is taking place, the relationship between J and $\dot{w}$ depends on quantities such as α and Θ .

For the arsenic equilibrium, reaction (A.3)

$$K_3 = \frac{(p^{o}_{As_2})^2}{p^{o}_{As_4}} = \frac{(\bar{\xi}_{As_2})^2}{(\bar{\xi}_{As_4})} \cdot \frac{\alpha^2}{(4+2\alpha)} \tag{A.28}$$

$$\text{Defining } A = \frac{D_{(As_4/H_2,T)}}{D_{(As_2/H_2,T)}} \cdot \frac{\bar{\xi}_{As_2}}{K_3} \tag{A.29}$$

$$\text{then} \quad \alpha = \frac{1 + \sqrt{1 + 4A}}{A} \tag{A.30}$$

Considering reactions (A.1) and (A.2):

$$\frac{K_1}{K_2} = \frac{p^o_{GaBr}\, p^o_{HBr}}{p^o_{GaBr_2}\sqrt{p^o_{H_2}}}$$

$$= \Theta\left[\varepsilon - \left(\frac{2+\Theta}{1+\Theta}\right)\bar{\xi}_{HBr}\right]\frac{D_{GaBr_2/H_2}}{D_{GaBr/H_2}}$$

$$\text{let}\quad \Theta' = \frac{K_1}{K_2}\cdot\frac{1}{\varepsilon}\,\frac{D_{GaBr/H_2}}{D_{GaBr_2/H_2}} \tag{A.31}$$

where Θ' is the value of Θ at the exit of the bottle and ξ' is a measure of the extent of the reaction (when K_1 is large $\xi' = 1$).

$$\xi' = \bar{\xi}_{HBr}/\varepsilon \tag{A.32}$$

$$\text{Then}\quad \Theta = -1 + \frac{(1+\Theta') + \left[(1-2\xi')^2 + \Theta'^2 + 2\Theta'\right]^{\frac{1}{2}}}{2(1-\xi')} \tag{A.33}$$

$$\text{Now}\quad K_1 = \frac{\dfrac{\Theta}{\Theta+1}\,\bar{\xi}_{GaBr}\left(\dfrac{\bar{\xi}_{As_4}}{4+2\alpha}\right)^{1/4}\sqrt{p_{H_2}}}{\varepsilon - \left[\dfrac{(2+\Theta)}{(1+\Theta)}\right]\bar{\xi}_{HBr}} \tag{A.34}$$

$$K_1^{\,o}{}_{\Theta\to\infty} = \frac{\bar{\xi}_{GaBr}\left(\dfrac{\bar{\xi}_{As_4}}{4+2\alpha}\right)^{1/4}}{\varepsilon - \bar{\xi}_{HBr}} \tag{A.35}$$

If K_2 becomes small, $\Theta \longrightarrow \infty$ and $K_1 \longrightarrow K_1^{\,o}$

$$\text{Similarly}\quad K_2^{\,o}{}_{\Theta\to 0} = \frac{\bar{\xi}_{GaBr_2}}{(\varepsilon - 2\bar{\xi}_{HBr})^2}\left[\frac{\bar{\xi}_{As_4}}{4+2\alpha}\right]^{1/4} \tag{A.36}$$

If K_1 becomes small, $\Theta \longrightarrow 0$ and $K_2 \longrightarrow K_2^{\,o}$.

Substituting for α and Θ in equations (A.23) to (A.27) and substituting the resulting equations into the expression for K_1, equation (A.4), a master equation is obtained:

$$\frac{K_2}{K_2^o} = \left[1 - \frac{K_1}{K_1^o}\right]\left[1 - \frac{\xi'}{1-\xi'}\,\frac{K_1}{K_1^o}\right] \qquad (A.37)$$

In the experimental temperature range, the second term on the right of equation (A.37) is nearly unity, hence:

$$\frac{K_2}{K_2^o} + \frac{K_1}{K_1^o} \simeq 1 \qquad (A.38)$$

A second-order approximation to multicomponent diffusion may be included in this analysis; this has the effect of multiplying each ξ_i by factors γ_i which are functions of the binary diffusion coefficients for all pairs of species in the system. Graham's Law (equation 1.20) is used to calculate the ratios of binary diffusion coefficients.

Nomenclature used in programme (see SUBROUTINE EQN51)

WOBS	weight loss recorded experimentally.
T	temperature.
K1	equilibrium constant reaction (A.1).
K3	equilibrium constant reaction (A.2).
KA	equilibrium constant reaction (A.3).
E	ε
B1	constant $(= \frac{RT1\beta}{cMP})$
D1	D_{GaBr/H_2}
D2	D_{As_2/H_2}
D3	D_{GaBr_2/H_2}
D4	D_{As_4/H_2}

AL	α
PH2	partial pressure of hydrogen
A1	a_1 (where 1 = GaBr, 2 = As_2, 3 = $GaBr_2$, 4 = As_4).
TH	Θ
AO	A (see equation (A.29)).
G1	γ_1 (where 1 = GaBr, 2 = As_2, 3 = $GaBr_2$, 4 = As_4).
X1	$\bar{\xi}_1$ (where 1 = GaBr, 2 = As_2, 3 = $GaBr_2$, 4 = As_4).

The subroutine presented in table 1 will solve the master equation (A.37) for any combination of the four thermodynamic quantities (ΔH_1, ΔS_1, ΔH_2, ΔS_2) for the two reactions and calculate the rate of weight-loss as a function of temperature (values of ΔH_3 and ΔS_3 are known constants). In an exact solution the value of F (the right-hand side minus the left-hand side of equation (A.37)) would be zero.

Calculation of parameters contained in subroutine EQN51 (Table 1) all in SI units

B1 $\quad B1 = \frac{Rl\beta}{MPc}$

where R is the gas constant, l the length of the capillary and β the capillary correction (see Appendix 1), M the molecular weight of GaAs, P the total pressure and c the cross-sectional area of the channel.

KA

Equilibrium constant for the dissociation of As_4 to $2As_2$ calculated from literature (see section 4.8).

Table 1.

SUBROUTINE EQN51,GaAs/HBr system (2mm channel).

```
      SUBROUTINE EQN51(WOBS,K1,K3,T,E,F)
      REAL K1,K3,KA
      B1=2.82727
      KA=EXP(17.106-26270./T)
      D5=0.498E-4*(T/273.15)**1.78
      D1=0.73538*D5
      D2=0.7349*D5
      D3=0.59374*D5
      D4=0.5196*D5
      PH2=1.-E
      A1=1.+5.3354*E
      W=WOBS
      TH=1.2386*K1/(K3*E)
      XID=B1*W*T
      A0=XID/(D2*KA*1.414)
      IF(1.+4.*A0)44,44,45
   44 RETURN
   45 CONTINUE
      AL=(1.+SQRT(1.+4.*A0))/A0
      Z1=2.*(2.+AL)*(TH+1.)
      Z2=(AL+1.)*(1.+2.*TH)+TH
      Z3=2.*(2.+AL)*(2.+TH)
      ZZ=XID*Z2/Z1
      A5=1.+(49.87412+26.96216*AL+22.8516*AL*TH+41.6530*TH)*E/Z3
      C5=-(36.81531+15.98399*AL+8.230424*AL*TH+21.30818*TH)/Z2
      G1=A1+(12.08528+4.63353*AL+0.4145985*AL*TH+3.64742*TH)*XID/(Z1*D1
      G2=A1+(12.073618+4.62784*AL+0.40922*AL*TH+3.636385*TH)*XID/(Z1*D2
      G3=A1+(8.96856+3.10339*AL-1.030985*AL*TH+0.6998025*TH)*XID/(Z1*D3
      G4=A1+(7.337785+2.30279*AL-1.78737*AL*TH-0.84253*TH)*XID/(Z1*D4)
      G5=A5-(C5+1.)*ZZ/(D5*2.)+E*Z2/Z3
      X1=G1*XID/D1
      X2=G2*XID/D2
      X3=G3*XID/D3
      X4=G4*XID/D4
      X5=G5*XID/D5
      Y=(X4/(4.+2.*AL))**.25
      Q=(E-2.*X5)**2*K3/(PH2*X3)
      R=K1/(X1*SQRT(PH2))
      S=(E-K1*(E-X5)/(SQRT(PH2)*X1*Y)*X5)
      F=Q+R*S-Y
      RETURN
      END
```

D1

$$D_{GaBr/H_2} = \frac{D_{GaBr/H_2}}{D_{HBr/H_2}} \; D_{HBr/H_2}$$

$$= \sqrt{\frac{80.917}{149.629}} \; D_{HBr/H_2}$$

$$D1 = 0.73538(D5)$$

All subsequent values for ratios of diffusion coefficients are calculated in this way (Graham's Law). The value for D_{HBr/H_2} is estimated in chapter 3.

A1

$$a_1 = a_2 = a_3 = a_4 = 1 + \left[\frac{D_{GaBr/H_2}}{D_{GaBr/HBr}} - 1\right] \varepsilon$$

$$a_1 = 1 + 5.3354\,\varepsilon$$

This is used in the calculation of γ.

A5

$$a_{HBr} = \left[1 - \left(\left[\frac{D_{HBr/H_2}}{D_{HBr/GaBr}} - 1\right]\frac{J_{GaBr}}{J_{HBr}} + \left[\frac{D_{HBr/H_2}}{D_{HBr/As_2}} - 1\right]\frac{J_{As_2}}{J_{HBr}}\right.\right.$$

$$\left.\left. + \left[\frac{D_{HBr/H_2}}{D_{HBr/GaBr_2}} - 1\right]\frac{J_{GaBr_2}}{J_{HBr}} + \left[\frac{D_{HBr/H_2}}{D_{HBr/As_4}} - 1\right]\frac{J_{As_4}}{J_{HBr}}\right)\varepsilon\right]$$

$$a_{HBr} = 1 + \frac{\varepsilon\left[49.87412 + 26.9622\alpha + 22.8516\alpha\Theta + 41.6530\Theta\right]}{(2 + \Theta)(4 + 2\alpha)}$$

AO

$$A = \frac{D_{As_4/H_2}}{D_{As_2/H_2}} \left[\frac{\bar{\xi}_{As_2}}{KA}\right]$$

$$= 0.7071 \frac{(B1)(W)(T)}{(D2)(KA)}$$

$$AO = 0.7071 \frac{(XID)}{(D2)(KA)}$$

G1 (G2, G3, G4)

$$\gamma_{GaBr} = a_{GaBr} - (1 + c_{GaBr}) \frac{\bar{\xi}_{GaBr}}{2}$$

Now

$$-C_{GaBr} = \left[\left[\frac{D_{GaBr/H_2}}{D_{GaBr/GaBr_2}} - 1\right]\left[\frac{D_{GaBr/H_2}}{D_{GaBr_2/H_2}} - 1\right]\frac{J_{GaBr_2}}{J}\right.$$

$$+\left[\frac{D_{GaBr/H_2}}{D_{GaBr/As_4}} - 1\right]\left[\frac{D_{GaBr/H_2}}{D_{As_4/H_2}} - 1\right]\frac{J_{As_4}}{J} + \left[\frac{D_{GaBr/H_2}}{D_{GaBr/As_2}} - 1\right]\left[\frac{D_{GaBr/H_2}}{D_{As_2/H_2}} - 1\right]\frac{J_{As_2}}{J}$$

$$\left.+\left[\frac{D_{GaBr/H_2}}{D_{GaBr/HBr}} - 1\right]\left[\frac{D_{GaBr/H_2}}{D_{HBr/H_2}} - 1\right]\frac{J_{HBr}}{J}\right]$$

$$-C_{GaBr} = \frac{25.1706 + 10.2671\alpha + 2.8292\alpha\theta + 10.2948\theta}{\theta + (\alpha + 1)(1 + 2\theta)}$$

$$\gamma_{GaBr} = a_{GaBr} + \bar{\xi}_{GaBr} \frac{(12.0853 + 4.6335\alpha + 0.4146\alpha\theta + 3.6474\theta)}{(1 + \theta)(4 + 2\alpha)}$$

Similarly for γ_{GaBr_2}, γ_{As_4} and γ_{As_2}.

G5

$$\gamma_{HBr} = a_{HBr} - (1 + C_{HBr}) \frac{\xi_{HBr}}{2} - \frac{\varepsilon J}{J_{HBr}}$$

$$= a_{HBr} - \frac{(1 + C_{HBr})}{2} \xi_{HBr} \left(\frac{Z2}{Z3}\right) + \varepsilon \left(\frac{Z2}{Z3}\right) \text{(see programme)}$$

$$= a_{HBr} - (1 + C_{HBr}) \frac{ZZ}{(D5)2} + \varepsilon \left(\frac{Z2}{Z3}\right)$$

where (Z2), (Z3) and (ZZ) are defined in the programme and C_{HBr} is calculated using:

$$-C_{HBr} = \left[\frac{D_{HBr/H_2}}{D_{HBr/GaBr}} - 1\right]\left[\frac{D_{HBr/H_2}}{D_{GaBr/H_2}} - 1\right]\frac{J_{GaBr}}{J} + \left[\frac{D_{HBr/H_2}}{D_{HBr/As_4}} - 1\right]\left[\frac{D_{HBr/H_2}}{D_{As_4/H_2}} - 1\right]\frac{J_{As_4}}{J}$$

$$+ \left[\frac{D_{HBr/H_2}}{D_{HBr/As_2}} - 1\right]\left[\frac{D_{HBr/H_2}}{D_{As_2/H_2}} - 1\right]\frac{J_{As_2}}{J} + \left[\frac{D_{HBr/H_2}}{D_{HBr/GaBr_2}} - 1\right]\left[\frac{D_{HBr/H_2}}{D_{GaBr_2/H_2}} - 1\right]\frac{J_{GaBr_2}}{J}$$

4B Derivation of the master equation for the InAs/HBr system

The following equations can be used to describe the transport of indium arsenide by hydrogen bromide gas in the temperature range 1110 - 730 K (see Chapter 4):

$$InAs(s) + HBr(g) \leftrightarrows InBr(g) + 1/4As_4(g) + \tfrac{1}{2}H_2(g) \qquad (B.1)$$

$$As_4(g) \leftrightarrows 2As_2(g) \qquad (B.2)$$

The equilibrium constants for reactions (B.1) and (B.2) are given by:

$$K_1 = \frac{p^\circ_{InBr}(p^\circ_{As_4})^{1/4}(p^\circ_{H_2})^{\frac{1}{2}}}{p^\circ_{HBr}} \tag{B.3}$$

$$K_2 = \frac{(p^\circ_{As_2})^2}{p^\circ_{As_4}} \tag{B.4}$$

(See section 4A for detailed derivations).

Considering the fluxes, J_i, of the species occuring in the transport equations:

$$J_{HBr} + 2J_{H_2} = 0 \tag{B.5}$$

$$J_{InBr} = 4J_{As_4} + 2J_{As_2} \equiv J_{InAs} \tag{B.6}$$

$$J_{HBr} + J_{H_2} + J_{As_4} + J_{As_2} + J_{InBr} = J \tag{B.7}$$

$$\text{Hence } J_{InBr} = J_{As_4}(4 + 2\alpha) = -J_{HBr} \tag{B.8}$$

$$\text{where } \alpha = \frac{J_{As_2}}{J_{As_4}}$$

$$J_{As_4} = \frac{-J_{HBr}}{(4+2\alpha)} \tag{B.9}$$

$$J_{As_2} = \frac{-J_{HBr}\,\alpha}{(4+2\alpha)} \tag{B.10}$$

$$\frac{J}{J_{HBr}} = \frac{-(3+2\alpha)}{(4+2\alpha)} \qquad (B.11)$$

$$\frac{J_{InAs}}{J} = \frac{(4+2\alpha)}{(3+2\alpha)} \qquad (B.12)$$

Following the same arguments as in 4A, the expressions obtained for the partial pressures inside the reaction bottle are:

$$\frac{p^{o}_{As_4}}{p} = \frac{\bar{\xi}_{As_4}}{(4+2\alpha)} \qquad (B.13)$$

$$\frac{p^{o}_{As_2}}{p} = \frac{\alpha\ \bar{\xi}_{As_2}}{(4+2\alpha)} \qquad (B.14)$$

$$\frac{p^{o}_{InBr}}{p} = \bar{\xi}_{InBr} \qquad (B.15)$$

and $$\frac{p^{o}_{HBr}}{p} = \varepsilon - \bar{\xi}_{HBr} \qquad (B.16)$$

Insertion of equations (B.13) to (B.16) into equation (B.3) and inclusion of the γ correction, yields equation (B.17):

$$K_1 = \frac{\gamma\bar{\xi}_{InBr}\left[\frac{\gamma\bar{\xi}_{As_4}}{4+2\alpha}\right]^{1/4}(p^{o}_{H_2})^{\frac{1}{2}}}{(\varepsilon - \gamma\bar{\xi}_{HBr})} \qquad (B.17)$$

The subroutine EQNS1 which can be set up using these equations (see 4A) is given in Table 2.

Here D1 = D_{InBr/H_2}

D2 = D_{As_2/H_2}

D4 = D_{As_4/H_2}

Similarly for G1 (γ_1), X1 ($\bar{\xi}_1$) and A1 (a_1).

Table 2.

SUBROUTINE EQN51,InAs/HBr system (2mm channel).

```
      FUNCTION EQN51(WOBS,K1,T,E,F)
      REAL K1,KA
      B1=2.066997*1.04169
      KA=EXP(17.106-2621/0./T)
      D5=0.5406-4*(T/273.15)**1.80
      D1=0.4926*D5
      D2=0.49328*D5
      D4=0.346603*D5
      PH2=1.-E
      A1=1.+3.25274*E
      W=WOBS
      XID=B1*W*T
      A0=XID/(D2*KA*1.414)
      IF(1.+4.*A0)44,44,45
   44 RETURN
   45 CONTINUE
      AL=(1.+SQRT(1.+4.*A0))/A0
      Z2=(3.0+2.0*AL)
      Z3=(4.0+2.0*AL)
      A5=1.0+(41.7271+22.8887*AL)*E/Z3
      C5=-(52.3507+23.5564*AL)/Z2
      G1=A1+(4.10773+0.55596*AL)*XID/(Z2/D1)
      G2=A1+(4.13624+0.55915*AL)*XID/(Z2/D2)
      G4=A1+(-1.7199-2.22606*AL)*XID/(Z2*D4)
      G5=A5-(1.0+C5)*XID/(D5*2.0)+E*Z2/Z3
      X1=G1*XID/D1
      X2=G2*XID/D2
      X4=G4*XID/D4
      X5=G5*XID/D5
      Y=(X4/(4.+2.*AL))**.25
      EQN51=X1*Y*SQRT(PH2)-K1*(E-X5)
      RETURN
      END
```

4C Derivation of the master equation for the InAs/HCl system

The following equations can be used to describe the transport of indium arsenide by hydrogen chloride gas over the temperature range 1090 - 715 K (see Chapter 4):

$$InAs(c) + HCl(g) \leftrightharpoons InCl(g) + 1/4As_4(g) + \tfrac{1}{2}H_2(g) \qquad (C.1)$$

$$As_4(g) \leftrightharpoons 2As_2(g) \qquad (C.2)$$

The equilibrium constants for reactions (C.1) and (C.2) are given by:

$$K_1 = \frac{p^\circ_{InCl}(p^\circ_{As_4})^{1/4}(p^\circ_{H_2})^{\frac{1}{2}}}{p^\circ_{HCl}} \qquad (C.3)$$

$$K_2 = (p^\circ_{As_2})^2/p^\circ_{As_4} \qquad (C.4)$$

Following exactly the same procedure as in 4B but substituting Cl for Br, the master equation obtained is:

$$K_1 = \frac{\gamma\bar{\xi}_{InCl}\left[\dfrac{\gamma\bar{\xi}_{As_4}}{4+2\alpha}\right]^{1/4}(p^\circ_{H_2})^{\frac{1}{2}}}{(\varepsilon - \gamma\bar{\xi}_{HCl})} \qquad (C.5)$$

Table 3 contains the subroutine EQN51 for this system. Here 1,2 and 3 refer to InBr, As_2 and As_4 respectively. The constant B1, which is affected by channel dimensions and molecular weight of sample, changes size in the InAs/HCl experiment using the silica bottle with the 1 mm diameter channel (see Appendix 1 for dimensions).

Table 3.

SUBROUTINE EQN51,InAs/HCl system (2mm channel).

```
      FUNCTION EQN51(WOBS,K1,T,E,F)
      REAL K1,KA
      B1=2.0689967*1.04169
      KA=EXP(17.106-26270./T)
      D5=0.498E-4*(T/273.15)**1.78
      D1=0.6446*D5
      D2=0.7349*D5
      D4=0.5196*D5
      PH2=1.-E
      A1=1.+5.3354*E
      W=WOBS
      XID=B1*W*T
      A0=XID/(D2*KA*1.414)
      IF(1.+4.*A0)44,44,45
   44 RETURN
   45 CONTINUE
      AL=(1.+SQRT(1.+4.*A0))/A0
      Z2=(3.0+2.0*AL)
      Z3=(4.0+2.0*AL)
      A5=1.0+(46.5048+25.2775*AL)*E/Z3
      C5=-(29.81498+12.48383*AL)/Z2
      G1=A1+(3.63841+0.428185*AL)*XID/(Z2*D1)
      G2=A1+(6.11883+1.65044*AL)*XID/(Z2*D2)
      G4=A1+(0.202285-1.264962*AL)*XID/(Z2*D4)
      G5=A5-(1.0+C5)*XID/(D5*2.0)+E*Z2/Z3
      X1=G1*XID/D1
      X2=G2*XID/D2
      X4=G4*XID/D4
      X5=G5*XID/D5
      Y=(X4/(4.+2.*AL))**.25
      EQN51=X1*Y*SQRT(PH2)-K1*(E-X5)
      RETURN
      END
```

4D Development of programmes (the three-equation case)

The object of the computer analysis on the three systems described above was to find those values for the enthalpy and entropy (ΔH and ΔS), for the reactions considered, which gave the best fit to the experimental rates of weight loss. The difference between $\dot{w}_{OBS}$, the experimental rate of weight loss, and $\dot{w}_{CALC}$, the computed $\dot{w}$, had to be minimised over the range of temperatures investigated.

For the master equation to be satisfied, F (the right-hand side minus the left-hand side of the master equation (A.37) must be zero, i.e. $F = f(\dot{w}) = 0$. This function was first investigated in order to discover the location of its roots and found to be a cubic in $\dot{w}$. For most choices of H and S only one real root appeared. Sometimes, however, there were two real values of $\dot{w}_{CALC.}$ close to $\dot{w}_{OBS.}$

A plotting programme (table 4) was first developed to find the position of the real roots. Values for the thermodynamic functions H and S were estimated using literature data. Three combinations of H_1, H_2, S_1 and S_2 close to the literature estimates were chosen and five temperatures within the experimental range. For each temperature and each combination of H and S, the value of F was plotted as a function of $\dot{w}$, yielding $\dot{w}_{CALC.}$ where $F = 0$. These values of $\dot{w}_{CALC.}$ were compared graphically with the $\dot{w}_{OBS.}$ results, then H and S were varied to obtain better agreement between $\dot{w}_{OBS.}$ and $\dot{w}_{CALC.}$

Table 4.

Plotting programme,3 reaction system (omitting SUBR. EQN51).

```
      PROGRAM FJT69(INPUT,OUTPUT,TAPE7=INPUT)
      DIMENSION X(4),WEXP(6),TEMP(6),Y(3,101)
      REAL K1,K3
      R=8.314
      E=0.0354
      DO 39 I=1,6
      READ(7,100)TEMP(I),WEXP(I)
  100 FORMAT(F10.4,E14.6)
      PRINT 200,TEMP(I),WEXP(I)
  200 FORMAT(*  TEMPERATURE = *,F10.4,*  WEIGHT = *,E14.6)
      DO 6 J=1,3
      READ(7,99)X(1),X(2),X(3),X(4)
   99 FORMAT(4F10.2)
      PRINT 201,X(1),X(2),X(3),X(4)
  201 FORMAT(*0 H= *,2F10.2,* S= *,2F10.2)
      WORS=WEXP(I)
      T=TEMP(I)
      K1=EXP((-X(1)/T+X(3))/R)
      K3=EXP((-X(2)/T+X(4))/R)
      JJ=0
      DO 60 II=1,101
      JJ=JJ+1
      W1=FLOAT(II)*1.00E-10
      CALL EQN51(W1,K1,K3,T,E,F1)
      Y(J,JJ)=F1
   60 CONTINUE
    6 CONTINUE
      CALL PLOT(Y)
   39 CONTINUE
      STOP
      END


      SUBROUTINE PLOT(Y)
      DIMENSION Y(3,101),TEXT(101)
      DO 2 I=1,101
    2 TEXT(I)=1H
      DO 1 I=1,101
      L1=INT(25.0*(Y(1,I)+2.0)+1.5)
      L2=INT(25.0*(Y(2,I)+2.0)+1.5)
      L3=INT(25.0*(Y(3,I)+2.0)+1.5)
      IF(L1.GT.101)L1=101
      IF(L1.LT.1)L1=1
      IF(L2.GT.101)L2=101
      IF(L2.LT.1)L2=1
      IF(L3.GT.101)L3=101
      IF(L3.LT.1)L3=1
      TEXT(1)=TEXT(51)=TEXT(101)=1HI
      TEXT(L1)=1H+
      TEXT(L2)=1H*
      TEXT(L3)=1H-
      PRINT 200,I,Y(1,I),Y(2,I),Y(3,I),(TEXT(J),J=1,101)
  200 FORMAT(I4,3F9.3,101A1)
      TEXT(L1)=1H
      TEXT(L2)=1H
      TEXT(L3)=1H
    1 CONTINUE
      PRINT 4,(1H-,J=1,101)
    4 FORMAT(31X,101A1)
      RETURN
      END
```

Two forms of minimisation function were explored:

$$SIG_1^2 = \Sigma (\dot{w}_{OBS.} - \dot{w}_{CALC.})^2/N \qquad (D.1)$$

and

$$SIG_2^2 = \Sigma \left[\ln \frac{\dot{w}_{OBS.}}{\dot{w}_{CALC.}}\right]^2/N \qquad (D.2)$$

where N is the number of points.

From the plotting programme, the range of H and S values within which realistic roots occurred was known. In this second programme (table 5) all combinations of three values for each thermodynamic function (making $3^4 = 81$ combinations) were covered. For each combination, values of $\dot{w}_{OBS}(T)$ were entered and SIG^2 calculated. Using equation (D.1) as the criterion of "goodness of fit", points with high values of $\dot{w}$ were effectively weighted more heavily than those with smaller $\dot{w}$ and, in consequence, the fit was good at high $\dot{w}$ but very poor at low $\dot{w}$ where the proportional error was in excess of 50%. Using the second expression (equation (D.2)) a better fit was obtained at all temperatures. The fit at very high temperatures is determined by the value of D^{o}_{HX,H_2} (the binary diffusion coefficient of hydrogen halide in hydrogen, at $0^{o}C$), see chapter 3. The best values of H_1, H_2, S_1 and S_2 are those which give the minimum SIG_2^2 for a given input set of $\dot{w}_{OBS.}(T)$. The shape of the minimum in F (H_1, H_2, S_1, S_2) was determined by plotting graphs of SIG_2^2 vs. (H_1, H_2, S_1, S_2). These cross-sections were constructed as follows:- a set of H_1, H_2, S_1 and S_2 was selected (enclosed by two vertical lines, see figures in chapters 4 and 5) and each of these quantities was then varied as shown on the x axis keeping the other three at their selected values.

Table 5.

Minimisation programme,GaAs/HBr system (omitting SUBR.EQN51).

```
      PROGRAM EJT61(INPUT,OUTPUT,TAPE7=INPUT)
      DIMENSION X(4),WEXP(25),TEMP(25)
      COMMON WEXP,TEMP,E
      E=0.0354
      DO 8 I=1,6
      READ(7,100)TEMP(I),WEXP(I)
  100 FORMAT(F10.4,E14.6)
      PRINT 200,TEMP(I),WEXP(I)
  200 FORMAT(*    T=   *,F10.4,*    W=    *,E14.6)
    8 CONTINUE
      READ(7,99)X(1),X(2),X(3),X(4)
   99 FORMAT(4F10.2)
      PRINT 201,X(1),X(2),X(3),X(4)
  201 FORMAT(*0 H=   *,2F10.2,*   S =   *,2F10.2)
      X1S=X(1)-3000.0
      X2S=X(2)-3000.0
      X3S=X(3)-3.0
      X4S=X(4)-3.0
      SS=1.0
      X4=X4S
      DO 1 I=1,5
      X4=X4+1.0
      X3=X3S
      DO 1 J=1,5
      X3=X3+1.0
      X2=X2S
      DO 1 K=1,5
      X2=X2+1000.0
      X1=X1S
      DO 1 L=1,5
      X1=X1+1000.0
      VAL=SIG(X1,X2,X3,X4)
      SS=AMIN1(SS,VAL)
    1 CONTINUE
      PRINT 506,SS
  506 FORMAT(*  SS =  *,E14.6)
      STOP
      END
```

Table 5 (continued).

```
      FUNCTION SIG(S1,S2,S3,S4)
      DIMENSION S(4),WEXP(25),TEMP(25)
      COMMON WEXP,TEMP,E
      REAL K1,K3,SIG
      R=8.314
      SIG=0.
      DO 39 J=1,6
      WOBS=WEXP(J)
      T=TEMP(J)
      K1=EXP((-S1/T+S3)/R)
      K3=EXP((-S2/T+S4)/R)
      W1=1.5*WOBS
      CALL EQN51(W1,K1,K3,T,E,F1)
      DO 60 I=1,50
      W2=W1
      F2=F1
      W1=W2-WOBS*0.1
      IF(W1)8,8,9
    8 PRINT 13,W1
   13 FORMAT(*  W1=  *,E14.6)
      GO TO 39
    9 CONTINUE
      CALL EQN51(W1,K1,K3,T,E,F1)
      IF(F1*F2)70,60,60
   60 CONTINUE
      PRINT 14
   14 FORMAT(*0NO ROOT*)
      RETURN
   70 XA=W1
      XB=W2
      FA=F1
      FB=F2
   58 DIFF=(XB-XA)*FA/(FA-FB)
      X=XA+DIFF
      CALL EQN51(X,K1,K3,T,E,FX)
      IF(FX*FA)15,30,20
   15 XB=X
      FB=FX
      GO TO 40
   20 XA=X
      FA=FX
   40 IF(ABS(DIFF/XA).LE..001.OR.ABS((XB-X)/XB).LE..001)GO TO 30
      GO TO 58
   30 CONTINUE
      SIG=SIG+(ALOG(WOBS)-ALOG(X))**2
      PRINT 507,WOBS,ALOG(WOBS),X,ALOG(X),FX
  507 FORMAT(5E14.6)
   39 CONTINUE
      SIG=SIG/6.0
      PRINT 10,S1,S2,S3,S4,SIG
   10 FORMAT(04F10.2,* SIG= *,E14.6)
      RETURN
      END
```

The final programme developed (table 6) was for use in the simpler two-reaction situation. Having estimated values for H_1 and S_1, a value for each was selected which fell well below the error limits for these parameters. A wide search was then carried out, calculating SIG_2^2 at all combinations of H_1 and S_1 at suitable intervals over the required range. Subsequent searches in the same programme, covered smaller ranges round the H_1 and S_1 values which had given the minimum SIG_2^2 in the previous search. Thus, using this iterative method, a minimum for SIG_2^2 was quickly approached.

References

1. D. Battat, M.M. Faktor, I. Garrett, R.H. Moss, J. Chem. Soc. Faraday Trans. 1, 70, 2302 (1974).

2. D. Battat, M.M. Faktor, I. Garrett, R.H. Moss, J. Chem. Soc. Faraday Trans. 1, 70, 2267 (1974).

Table 6.

Minimisation programme,2 reaction system (omitting FUNCT.EQN51).

```
      PROGRAM EJT78(INPUT,OUTPUT,TAPE7=INPUT)
      DIMENSION X(2),WEXP(100),TEMP(100)
      COMMON WEXP,TEMP,E
      REAL INCH,INCS
      E=0.0354
      DO 8 I=1,36
      READ(7,100)TEMP(I),WEXP(I)
  100 FORMAT(F10.4,E14.6)
      PRINT 200,TEMP(I),WEXP(I)
  200 FORMAT(*   T=  *,F10.4,*   W=   *,E14.6)
    8 CONTINUE
      READ(7,99)X(1),X(2)
   99 FORMAT(2F10.2)
      PRINT 201,X(1),X(2)
  201 FORMAT(*0 H=  *,F12.2,*   S  =   *,F12.2)
      H=X(1)
      S0=X(2)
      N=20
      M=10
      INCH=0.2E+4
      INCS=2.0
      DO 2 K=1,2
      HMIN=H
      SMIN=S0
      FMIN=SIG(H,S0,0)
      DO 10 I=1,N
      H=H+INCH
      S=S0
      DO 10 J=1,M
      S=S+INCS
      FTEST=SIG(H,S,0)
      IF(FTEST.GT.FMIN)GO TO 10
      FMIN=FTEST
      HMIN=H
      SMIN=S
   10 CONTINUE
      PRINT 3,K,FMIN,HMIN,SMIN
    3 FORMAT(*0 ITERATION NUMBER *,I2,* CURRENT ERROR = *,E15.7,* THE
     1CURRENT H VALUE = *,F12.3,* THE CURRENT S VALUE = *,F7.2)
      FDUMMY=SIG(HMIN,SMIN,1)
      H=HMIN-INCH
      S0=SMIN-INCS
      INCH=INCH*0.5
      INCS=INCS*0.5
      N=M=10
    2 CONTINUE
      STOP
      END
```

Table 6 (continued).

```
      FUNCTION SIG(S1,S2,IFLAG)
      DIMENSION S(2),WEXP(100),TEMP(100)
      COMMON WEXP,TEMP,E
      REAL K1
      R=8.314
      SIG=0.
      DO 39 J=1,36
      WOBS=WEXP(J)
      T=TEMP(J)
      K1=EXP((-S1/T+S2)/R)
      ANS0=WOBS
  195 VAL1=EQN51(ANS0,K1,T,E,F)
      WP1=1.00001*ANS0
      VAL2=EQN51(WP1,K1,T,E,F)
      WM1=0.99999*ANS0
      VAL3=EQN51(WM1,K1,T,E,F)
      ANS1=ANS0-VAL1/(VAL2-VAL3)*0.00002*ANS0
      IF(ABS((ANS1-ANS0)/ANS1).LT.1.0E-04)GO TO 200
      ANS0=ANS1
      GO TO 195
  200 X=ANS1
      SIG=SIG+(ALOG(WOBS)-ALOG(X))**2
      IF(IFLAG.EQ.0)GO TO 39
      PRINT 6,T,ALOG(WOBS),ALOG(X)
    6 FORMAT(3F10.4)
   39 CONTINUE
      SIG=SIG/36
      PRINT 7,SIG,S1,S2
    7 FORMAT(E14.6,2F20.4)
      RETURN
      END
```

APPENDIX 5

Experimental Results

Table 1 : GaAs/HBr, $\varepsilon = 0.0354$, $\varepsilon = 0.0591$ (2 mm diameter channel)

Table 2 : GaAs/HBr, $\varepsilon = 0.0354$ (3 mm diameter channel)

Table 3 : GaAs/HBr, $\varepsilon = 0.0354$, $\varepsilon = 0.0591$ (3 mm diameter channel)

Table 4 : GaAs/HBr, $\varepsilon = 0.0591$, $\varepsilon = 0.0354$ (1 mm diameter channel)

Table 5 : GaAs/HBr, $\varepsilon = 0.0591$, $\varepsilon = 0.0354$ (1 mm diameter channel)

Table 1

Transport of gallium arsenide in hydrogen bromide gas, using the silica bottle with the 2 mm diameter channel.

Rates of weight loss, $\dot{w}$, at temperatures T are listed chronologically.

$\varepsilon = 0.0354$

T/K	$10^{10}\dot{w}$/kg s^{-1}	T/K	$10^{10}\dot{w}$/kg s^{-1}
1021.40	25.359	894.55	9.581
1021.40	24.981	894.55	9.419
1215.55	43.182	933.95	12.245
1215.15	43.304	933.45	12.250
1214.35	43.636	772.95	3.700
1118.55	37.077	1256.00	43.644
1119.05	36.885	1256.00	43.644
1119.05	36.923	1181.65	40.500
1060.40	30.594	1180.85	40.583
1061.15	31.125	1180.45	40.375
820.15	6.400	1141.55	37.731
820.15	6.507	1140.75	37.846
999.15	21.674	1084.15	32.933
1000.85	21.889	1082.45	32.828
951.15	14.708	1081.65	32.633
951.15	14.600	843.05	7.170
870.95	8.392	843.05	7.067
870.95	8.332	913.15	10.562
1041.05	28.235	912.15	10.400
1041.05	28.000	803.75	5.356
971.15	17.351	983.85	19.500
971.15	17.404	983.85	19.160

Table 1 (continued)

$\varepsilon = 0.059$

T/K	$10^{10}\dot{w}$/kg s^{-1}	T/K	$10^{10}\dot{w}$/kg s^{-1}
982.45	25.684	789.05	7.832
981.15	24.974	789.05	7.925
930.85	17.096	1043.15	38.640
930.85	17.493	1041.90	38.039
1021.25	34.214	971.15	23.050
1021.25	33.552	970.15	23.082
893.25	14.104	1215.55	60.438
894.55	14.385	1215.55	60.125
954.15	20.379	1181.35	57.882
952.35	20.505	1180.15	57.765
839.15	10.944	1081.65	45.476
840.65	11.089	1080.90	45.619
910.55	15.388	1021.15	33.793
911.45	15.310	1020.40	33.759
819.55	9.717	921.15	16.226
1000.65	29.212	921.15	15.968
767.25	4.825	1003.15	29.364
871.15	12.594	1001.45	29.152
871.65	12.867	1119.75	51.158
805.15	8.435	1119.35	51.053
805.65	8.536	1144.40	54.571
864.25	12.516	1141.65	54.444
788.55	7.560	1139.65	53.838

Table 2

Transport of gallium arsenide in hydrogen bromide gas, using the silica bottle with the 3 mm diameter channel. Rates of weight loss, $\dot{w}$, at temperatures T are listed chronologically.

$\varepsilon = 0.0354$

T/K	$10^{10}\dot{w}$/kg s^{-1}	T/K	$10^{10}\dot{w}$/kg s^{-1}
939.15	30.375	844.95	13.160
937.40	29.485	878.05	17.836
979.15	43.955	877.55	17.655
977.15	42.261	795.15	7.089
899.55	20.830	957.15	35.000
899.55	20.689	957.15	34.714
821.65	10.733	886.15	18.307
824.65	11.165	886.15	18.158
917.05	24.175	865.05	15.648
915.65	24.200	866.35	15.680
844.15	13.200		

Table 3

Transport of gallium arsenide in hydrogen bromide gas using the silica bottle with the 3 mm diameter channel. Rates of weight loss, $\dot{w}$, at temperatures T are listed chronologically.

$\varepsilon = 0.0354$

T/K	$10^{10}\dot{w}$/kg s^{-1}	T/K	$10^{10}\dot{w}$/kg s^{-1}
935.65	31.097	922.55	27.286
933.95	31.310	886.15	21.622
873.25	20.505	885.15	21.103
873.25	19.959	901.65	22.810
855.05	17.943	900.40	23.129
855.05	18.673	1025.45	60.688
917.90	26.316	1025.15	61.000
915.15	25.947	1005.85	53.189
826.15	15.568	1005.40	52.865
825.35	15.639	903.65	23.176
825.35	15.664	904.15	22.965
955.25	36.111	795.15	11.097
954.45	35.630	795.65	11.247
975.55	43.022	905.35	23.177
975.15	42.553	905.35	23.515
923.05	27.686		

Table 3 (continued)

ε = 0.0591

T/K	$10^{10}\dot{w}$/kg s^{-1}	T/K	$10^{10}\dot{w}$/kg s^{-1}
905.85	35.074	954.55	46.300
905.35	34.357	904.65	34.679
936.05	41.660	903.85	34.357
935.65	41.489	924.05	38.792
915.95	35.778	923.15	38.600
915.15	35.741	844.15	25.333
826.15	22.022	844.55	25.161
825.85	22.612	964.25	52.000
886.15	31.400	964.25	51.892
885.65	31.161	899.15	32.800
853.45	26.786	899.15	33.113
853.45	26.952	946.65	44.884
868.35	28.057	945.45	44.409
867.45	27.714	808.85	16.517
867.15	27.971	808.85	17.422
794.55	15.231	945.65	32.333
795.55	15.760	944.65	33.207
795.55	15.984	1067.75	73.259
977.65	56.057	1066.90	75.040
976.40	54.500	844.75	16.000
954.55	46.191	844.75	14.939

Table 4

Transport of gallium arsenide in hydrogen bromide gas using the silica bottle with the 1 mm diameter channel. Rates of weight loss, $\dot{w}$, at temperatures T are listed chronologically

$\varepsilon = 0.0591$

T/K	$10^{10}\dot{w}$/kg s^{-1}	T/K	$10^{10}\dot{w}$/kg s^{-1}
1040.05	7.531	980.45	4.878
1039.15	7.585	980.15	4.809
1119.15	10.115	959.90	4.201
1020.90	6.785	959.90	4.141
1020.15	6.747	917.40	3.170
971.15	4.638	918.15	3.212
1083.05	9.195	1007.45	6.067
1082.85	9.055	1008.25	6.000
1140.85	10.478	988.15	5.188
1140.85	10.620	988.15	5.188
1062.15	8.491	939.05	3.567
1062.15	8.322	1041.45	7.257
951.65	3.980	1040.15	7.364
951.65	4.004	1041.45	7.425
1000.45	5.893	1039.85	7.508
1000.45	5.895	979.85	5.016
895.45	2.887	979.85	5.005
895.15	2.905	928.75	3.434
1000.65	5.904	1011.65	6.050
930.95	3.554	1010.85	6.030
910.95	3.160	879.55	2.700

Table 4 (continued)

$\varepsilon = 0.0591$

T/K	$10^{10}\dot{w}$/kg s^{-1}	T/K	$10^{10}\dot{w}$/kg s^{-1}
879.55	2.678	838.65	2.552
871.15	2.700	838.65	2.544
989.40	5.269	838.65	2.567
989.40	5.130	962.90	4.238
839.55	2.427	961.65	4.293
970.25	4.591	960.85	4.252
860.05	2.640	779.85	2.314
1000.15	5.556	779.85	2.341
999.15	5.646	970.55	4.776
816.15	2.338	971.05	4.722
928.65	3.500	819.95	2.515
899.65	2.984	819.95	2.581
869.95	2.725	944.85	3.936
1002.05	5.782	944.40	3.894
1000.15	5.794	759.25	2.165
939.15	3.693	759.25	2.133
938.90	3.760	759.25	2.173
859.35	2.637	1020.25	6.683
859.85	2.683	1019.90	6.683
950.40	4.063	920.25	3.300
949.95	4.029	920.25	3.302

Table 4 (continued)

$\varepsilon = 0.0591$		$\varepsilon = 0.0354$	
T/K	$10^{10}\dot{w}$/kg s^{-1}	T/K	$10^{10}\dot{w}$/kg s^{-1}
804.25	2.383	971.15	3.404
804.85	2.497	970.65	3.322
912.15	3.177	929.15	2.412
911.15	3.097	929.15	2.484
970.45	4.730	816.75	1.566
970.45	4.686	817.65	1.578
890.35	2.894	949.40	2.885
890.35	2.885	949.40	2.908
790.85	2.375	1060.40	6.232
790.85	2.492	1060.40	6.187
1101.15	9.660	1139.15	7.577
1100.05	9.880	1139.15	7.686
1099.55	9.800	1118.15	7.289
878.95	2.908	1118.45	7.207
878.95	2.882	1018.65	5.021
768.95	2.319	1018.95	4.905
769.95	2.267	889.55	1.933
		1000.15	4.307
		999.15	4.284
		908.85	2.103
		908.85	2.090
		789.15	1.377
		979.15	3.735
		979.15	3.727
		859.55	1.654
		859.55	1.684
		869.45	1.658

Table 5

Transport of gallium arsenide in hydrogen bromide gas using the silica bottle with the 1 mm diameter channel. Rates of weight loss, $\dot{w}$, at temperatures T are listed chronologically.

$\varepsilon = 0.0591$

T/K	$10^{10}\dot{w}$/kg s^{-1}	T/K	$10^{10}\dot{w}$/kg s^{-1}
971.65	4.814	1022.25	6.651
971.65	4.700	1021.45	6.690
1119.45	10.184	873.90	2.772
1119.45	10.198	873.90	2.793
1081.15	9.189	922.65	3.403
1081.15	9.111	922.45	3.414
932.45	3.569	823.95	2.515
932.45	3.549	823.95	2.503
1040.90	7.424	963.25	4.287
1040.90	7.508	962.90	4.342
1001.45	5.847	884.40	2.794
1002.25	5.782	884.40	2.373
951.25	3.992	913.15	3.046
952.15	4.008	913.15	3.079

Table 5 (continued)

$\varepsilon = 0.0591$		$\varepsilon = 0.0354$	
T/K	$10^{10}\dot{w}$/kg s^{-1}	T/K	$10^{10}\dot{w}$/kg s^{-1}
983.45	4.830	1042.05	5.788
983.15	4.751	1042.05	5.706
842.15	2.351	912.90	2.195
842.15	2.393	912.90	2.168
948.15	3.417	843.15	1.602
948.15	3.439	1084.65	6.641
841.65	2.383	1084.65	6.655
1063.65	8.529	1002.65	4.302
981.65	5.126	1002.65	4.532
982.15	5.132	873.55	1.807
946.45	3.855	873.55	1.758
946.45	3.916	952.97	2.957
1012.90	6.303	793.51	1.489
1012.15	6.367	793.51	1.495
842.35	2.573	972.88	3.362
1001.15	5.607	972.88	3.607
792.85	2.336	933.95	2.542

APPENDIX 6

Materials

Gases

Argon: Air Products, ultra high purity grade, 99.999%.

Helium: British Oxygen Company, CP. grade, 99.9992%.

Hydrogen: BOC, high purity grade, 99.99+%.

Hydrogen chloride: Matheson Gas Products, technical grade, 99.0+%.

Nitrogen: BOC, oxygen free, 99.9+%.

Liquids

Bromine: B.D.H., Aristar grade, 99.8+%.

Water: Deionised distilled.

Solids

Indium: Halewood Chemicals Ltd., indium shot, 99.999+%.

Zinc: Goodfellow Metals Ltd., zinc wire, 99.99+%.

Indium arsenide: MCP Electronics Ltd., polycrystalline, undoped, N-type material (crystal P.445).

Indium antimonide: MCP Electronics Ltd., polycrystalline, undoped, N-type material (lot No. 15148).

Gallium arsenide: MCP Electronics Ltd., polycrystalline, undoped, material (batch A1476).